CASCADING OUTAGES DETECTION AND MITIGATION TOOL TO PREVENT MAJOR BLACKOUTS

A Dissertation

by

AHAD ESMAEILIAN

Submitted to the Office of Graduate and Professional Studies of
Texas A&M University
in partial fulfillment of the requirements for the degree of

DOCTOR OF PHILOSOPHY

Chair of Committee,	Mladen Kezunovic
Committee Members,	Garng M. Huang
	Robert D. Nevels
	Erick Moreno-Centeno
Head of Department,	Miroslav Begovic

December 2017

Major Subject: Electrical Engineering

ABSTRACT

Due to a rise of deregulated electric market and deterioration of aged power system infrastructure, it become more difficult to deal with the grid operating contingencies. Several major blackouts in the last two decades has brought utilities to focus on development of Wide Area Monitoring, Protection and Control (WAMPAC) systems. Availability of common measurement time reference as the fundamental requirement of WAMPAC system is attained by introducing the Phasor Measurement Units, or PMUs that are taking synchronized measurements using the GPS clock signal. The PMUs can calculate time-synchronized phasor values of voltage and currents, frequency and rate of change of frequency. Such measurements, alternatively called synchrophasors, can be utilized in several applications including disturbance and islanding detection, and control schemes.

In this dissertation, an integrated synchrophasor-based scheme is proposed to detect, mitigate and prevent cascading outages and severe blackouts. This integrated scheme consists of several modules. First, a fault detector based on electromechanical wave oscillations at buses equipped with PMUs is proposed. Second, a system-wide vulnerability index analysis module based on voltage and current synchrophasor measurements is proposed. Third, an islanding prediction module which utilizes an offline islanding database and an online pattern recognition neural network is proposed. Finally, as the last resort to interrupt series of cascade outages, a controlled islanding module is developed which uses spectral clustering algorithm along with power system state variable and generator coherency information.

DEDICATION

To my wife:

Dr. Yasaman Motlaghzadeh

my parents:

Molud Nabizadeh & Ahmad Esmaeilian

and siblings:

Afsaneh, Amir & Farzaneh

for their love, patience, support, trust, and encouragement in every possible way during my Ph.D. study. I couldn't have made this far without you. I love you all.

ACKNOWLEDGEMENTS

I would like to express my sincere gratitude to my advisor Dr. Mladen Kezunovic for his support and guidance throughout my studies at Texas A&M University. His knowledge and experience contributed many of the inspiring ideas explored in this dissertation.

I gratefully thank my committee members Dr. Garng M. Huang, Dr. Robert D. Nevels, and Dr. Erick Moreno-Centeno for their time, comments and support.

CONTRIBUTORS AND FUNDING SOURCES

Contributors

This work was supported by a dissertation committee consisting of Professors Mladen Kezunovic, Garng M. Huang and Robert D. Nevels of the Department of Electrical and Computer Engineering and Professor Erick Moreno-Centeno of the Department of Industrial and Systems Engineering.

Funding Sources

This study is supported by the Advanced Research Projects Agency-Energy (ARPA-E) under the Green Electricity Network Integration (GENI) contract 0473-1510.

TABLE OF CONTENTS

Page

ABSTRACT ii

DEDICATION iii

ACKNOWLEDGEMENTS iv

CONTRIBUTORS AND FUNDING SOURCES iv

TABLE OF CONTENTS vi

LIST OF FIGURES ix

LIST OF TABLES xii

1. INTRODUCTION 1

1.1 Problem Formulation 1
1.2 Current Research Efforts 3
1.2.1 Cascading Outage Modeling 3
1.2.2 Cascade Outage Detection and Mitigation 4
1.3 Proposed Research 6
1.4 Organization of Dissertation 8

2. UNDERSTANDING OF CASCADING OUTAGES MECHANISM 8

2.1 Overview 8
2.2 Frequency of Large Blackouts 9
2.3 Analysis of August 14th 2003 Blackout 11
2.3.1 Timeline of Events 12
2.3.2 Observations 14
2.4 Other Cascading Outages Without Successful Mitigation 15
2.5 Successfully Mitigated Cascading Outage Cases 16
2.6 Mechanism of Cascading Outages 17
2.7 Conclusion 19

3. FUNDAMENTALS OF THE PROPOSED SYNCHROPHASOR BASED APPROACH 21

3.1 Overview 21

3.2 Application of Synchrophasor System in Power System 21
3.3 Application of Synchrophasor System in Blackout Prevention 23
3.3.1 Monitoring and Prediction Tools 23
3.3.2 Mitigation Tool 25
3.4 Interaction of the Proposed Tools 27
3.5 Conclusion 29

4. SYNCHROPHASOR BASED ONLINE MONITORING TOOLS 30

4.1 Introduction 30
4.2 Graph Representation of Power Systems 30
4.2.1 Graph Model of Power System Elements 31
4.2.1.1 Undirected Graph 31
4.2.1.2 Directed Graph 33
4.2.2 Betweenness Centrality Concept 34
4.3 Synchrophasor Based Vulnerability Analysis Module 36
4.3.1 Formulation 37
4.3.2 Case Study 42
4.4 Synchrophasor Based Online Fault Identification Module 46
4.4.1 Electromechanical Wave Propagation Phenomena 48
4.4.2 Fault Location Methodology 50
4.4.2.1 ToA and Fault Type Detection 51
4.4.2.2 Detection of Faulty Line 53
4.4.2.3 Fault Location Using Binary Search 57
4.4.3 Case Study 58
4.4.3.1 Testing with Different Fault Scenarios 60
4.4.3.2 Impact of PMU Bad Data 63
4.4.3.3 Impact of Topology Changes 65
4.4.3.4 Impact of Availability of PMUs 66
4.5 Conclusion 70

5. SYNCHROPHASOR BASED ISLANDING PREDICTION TOOL 71

5.1 Overview 71
5.2 Generation of the Offline Islanding Database 71
5.2.1 Observability Matrix 71
5.2.2 Constraints to Reduce the Size of Database 77
5.3 Adaptive Neural Network Module to Predict Islands 79
5.3.1 Application of Neural Networks in Power Systems 79
5.3.2 Formulation of the Proposed ANN Method 81
5.4 Case Study 84
5.4.1 Offline Analysis 84
5.4.1.1 Islanding Database 84
5.4.1.2 Employing the SOVI Tool 84

5.4.1.3 Training the ANN Module 86
5.4.2 Online Analysis 88
5.5 Conclusion 94

6. INTEGRATED CONTROLLED ISLANDING TOOL 95

6.1 Overview 95
6.2 Background on Controlled Islanding 95
6.3 Spectral Clustering 97
6.4 Proposed Constraint Optimization Method 100
6.4.1 Static Constraints 100
6.4.2 Dynamic Constraints 102
6.4.3 Constrained Spectral K-Embedded Clustering 103
6.5 Triggering Mechanism 109
6.6 Case Study 111
6.6.1 Cascade Outage Scenario Creation 111
6.6.2 Controlled Islanding Scheme 115
6.6.3 Computational Efficiency 117
6.7 Conclusion 118

7. TESTING METHODOLOGY USING LARGE NETWORK 119

7.1 Test System 119
7.2 Full Scale Synchrophasor Testbed 120
7.3 Test Results Before Utilization of the Proposed Tools 121
7.4 Test Results After Utilization of the Proposed Tools 124
7.5 Conclusion 127

8. CONCLUSIONS 128

8.1 Contributions 128
8.2 Advantages of the Proposed Methods 130
8.3 Suggestion for Future Research 131

REFERENCES 132

APPENDIX A - PUBLICATIONS 146

LIST OF FIGURES

Page

Figure 2.1 North American blackout size probability distribution from NERC disturbance analysis working group data [53] 10

Figure 2.2 The relative blackout frequency to blackout risk from large North America blackouts in various size categories [2] 10

Figure 2.3 Generation, demand, and interregional power flows on August 14, 2003, at 15:05 EDT [3] 11

Figure 2.4 Timeline of 2003 Northeastern blackout [3] 12

Figure 2.5 Different stages of cascading outages 18

Figure 3.1 PMUs distribution and synchrophasor data flows in the North American power grid, March 2015 [66]. 22

Figure 3.2 Overall architecture of synchrophasor system applications 23

Figure 3.3 Typical control actions to prevent cascading outages [67] 25

Figure 3.4 Flowchart of the proposed method for detection, prevention and mitigation of cascading outages 28

Figure 4.1 A graph with five vertices and seven edges 32

Figure 4.2 A graph with five vertices and seven edges 34

Figure 4.3 A directed graph with six vertices and seven edges 36

Figure 4.4 Overall structure of the SOVI tool 38

Figure 4.5 IEEE 39-bus test system 42

Figure 4.6 Vertex and edge betweenness distribution for IEEE 39-bus System 43

Figure 4.7 Overall structure of the SOFI tool 47

Figure 4.8 64-generator ring system 49

Figure 4.9 Bus angle modulation following a fault at bus 16 at t=0 50

Figure 4.10 The network structure of the back propagation neural network model 52

Figure 4.11 Illustration of theoretical and measured delay matrices 55
Figure 4.12 Illustration of the binary search used for fault location method 57
Figure 4.13 Testing SOFI tool with IEEE 118-bus test system 59
Figure 4.14 Phasor angle of PMU equipped buses of IEEE118 bus system 62
Figure 4.15 Fault location percent error under effect of PMU bad data 64
Figure 4.16 Effect of unavailability of PMUs on fault location accuracy 67
Figure 5.1 IEEE 9-bus test system 72
Figure 5.2 IEEE 9-bus test system 76
Figure 5.3 Illustration of infeasible islanding scenarios 78
Figure 5.4 Overall structure of SIP module 82
Figure 5.5 Testing SIP tool with IEEE 118-bus test system 85
Figure 5.6 Graphical diagram of the ANN method trained for the SIP tool 86
Figure 5.7 Error vs. epoch for training, validation and test data 87
Figure 5.8 Voltage magnitude at PMU locations in case 1 89
Figure 5.9 Voltage angle at PMU locations in case 1 90
Figure 5.10 Voltage magnitude at PMU locations in case 2 90
Figure 5.11 Voltage angle at PMU locations in case 2 91
Figure 5.12 Voltage magnitude at PMU locations in case 3 92
Figure 5.13 Voltage angle at PMU locations in case 3 92
Figure 5.14 Voltage magnitude at PMU locations in case 4 93
Figure 5.15 Voltage angle at PMU locations in case 4 93
Figure 6.1 Solving graph-cut problem using spectral clustering 99
Figure 6.2 Two types of objective function using active power flow 102
Figure 6.3 The proposed controlled islanding method 106

Figure 6.4 Verifying ICI tool using IEEE 9-bus 107

Figure 6.5 The proposed tools triggering mechanisms 109

Figure 6.6 Testing ICI tool with IEEE 118-bus test system 113

Figure 6.7 Bus voltage, bus angle and frequency of system during cascade outages without controlled islanding scheme 114

Figure 6.8 Bus voltage, bus angle and frequency of system equipped with controlled islanding scheme 116

Figure 7.1 1354-bus European high voltage transmission network 119

Figure 7.2 TAMU synchrophasor testbed 120

Figure 7.3 Voltage profile of area 1 without proposed tools 121

Figure 7.4 Voltage profile of area 2 without proposed tools 122

Figure 7.5 Voltage profile of area 3 without proposed tools 123

Figure 7.6 Voltage profile of area 4 without proposed tools 123

Figure 7.7 Voltage profile of area 1 with proposed tools 124

Figure 7.8 Voltage profile of area 2 with proposed tools 125

Figure 7.9 Voltage profile of area 3 with proposed tools 126

Figure 7.10 Voltage profile of area 4 with proposed tools 126

LIST OF TABLES

Page

Table 1 Summary of Several Major Blackouts 8

Table 2 List of Synchrophasor Based Applications in Power System 22

Table 3 SOVI Values under Different Load Conditions 44

Table 4 SOVI Values for N-1 Contingency Analysis 45

Table 5 SOVI Values for N-2 Contingency Analysis 46

Table 6 Fault Location Results under Different Fault Specification 60

Table 7 Fault Location Results on Different Regions 63

Table 8 Impact of Topology Changes and PMU Availability 65

Table 9 Impact of Topology Changes on Fault Location 69

Table 10 Iterations required to determine islanding scenarios 77

Table 11 Number of Islanding Scenarios in IEEE 118-bus Test System 84

Table 12 Description of Islanding Scenarios 88

Table 13 Summary of Simulated Cascade Outage Scenarios 117

Table 14 Proposed Method Execution Time 118

1. INTRODUCTION

1.1 Problem Formulation

Various disturbances occur in the power system due to reasons such as natural disasters, human errors, animal and vegetation contacts, malicious attacks and equipment malfunction, which may lead to the power network outages. In most cases, protective schemes along with proper control actions steer the system away from extreme outages. However, in certain situations a major disturbance may initiate successive outages over a large geographic area of the system known as "Cascading Outages" [1].

Many factors may contribute to cascading failures such as aging infrastructure, power system market conditions, inaccurate security analysis, inadequate relay setting and coordination, increased system complexity and lack of proper decision-making support tools and training for new operating conditions [2].

Large-scale cascading outages may result in considerable economic loss to utilities and many other companies, as well as catastrophic impact on people's life. Cascading failures often result in wide area blackouts which demand complicated troubleshooting and restoration process. It may take several hours up to few days to restore electric power in the affected areas due to the slow re-starting and re-synchronizing generators and loads, and re-energizing out of service transmission lines.

The North American Electric Reliability Council (NERC) introduced several standards on system planning and operation to assure the power systems' reliability based on the key concepts defined as below [3], [4]:

- Continuous active generation and load balance [5];

- Maintain voltage profile by balancing reactive generation and demand [6];
- Monitor thermal limits of transmission lines [7];
- Keep the system in stable condition [8];
- Design system to withstand the "N-1" contingency condition [9];
- Plan, design, and maintain the system to remain reliable [10];
- Prepare for emergencies [11].

Despite implementation of these key concepts, blackouts are yet inevitable which can be explicated by the following:

- The transmission lines capacity did not upgraded at the same pace as the load demand;
- In today's restructured market, market participants regularly respond to load demand by transferring power over longer distances which requires further transmission investments [12];
- Consequently, the grid may operate closer to its margin, which have been the contributing factor in number of power system blackouts [13].
- Interconnection of neighboring grids may contribute to propagation of cascading outages following the blackout in one section [14].

Since, it is infeasible to eliminate all random failures, it is crucial to execute methods to reduce the likelihood of such failures evolving into major blackouts. Many researchers devoted their efforts to model and analyze cascading failures, as well as detection, mitigation or prevention of such events. Due to the wide range of involved

components along with different time scales of the event dynamics, study of cascading outages is extremely complicated and still remains an ongoing researching challenge.

1.2 Current Research Efforts

Several methods aiming at understanding and finding ways for detecting, preventing, and mitigating the cascading events have been proposed so far [15]-[43]. An overview of existing major methods of cascading outages analysis is summarized as follows.

1.2.1 Cascading Outage Modeling

Considering complicated nature of the cascading outage, it is infeasible to model it with all possible combinations of failures since it would demand an enormous computational burden. Hence, several cascading outages modeling methods with simplification of different factors have been introduced in the literature.

Three different methods based on the self-organized criticality theory have been proposed. The Oak Ridge-PSerc-Alaska (OPA) model [15]-[19] describes expansion of cascading outages over a large area of power system by analyzing slow and fast dynamics behavior of the system in a long-term view. The CASCADE model [20] explains the probability relations between the blackout size and the initial disturbance of power system and captures the weakening of the system as the cascade proceeds. The Branching Process (BP) model [21]-[23] simplifies the mathematical modeling of CASCADE models to estimate the probability distribution of the final blackout size. The three models neglect

many of the steps in the cascading process leading to blackouts, as well as the consideration of the timing of the events.

The vulnerability of power system to cascading failures is studied in [24], [25] using a protection system reliability model. In these papers, the mechanism of protection schemes and system stability following a fault is studied to determine its contribution in cascading outages. Then, the stochastic properties of contingencies and protection system failures are studied using a Monte Carlo simulation.

1.2.2 Cascade Outage Detection and Mitigation

Several researchers studied different methods to protect power system against cascading outages. In [26]-[29], relay hidden failures are analyzed to decrease number of relay mis-operations which is the most influential factor impacting major blackouts.

In [30], wide area backup protection and artificial intelligence techniques are used to minimize impact of a disturbance on the network. The Backup Protection Expert System (BPES) identifies the faulted component, and avoids unnecessary trip by blocking trip signals coming from other conventional backup protection relays.

In [31], authors proposed a dynamic event tree method integrated with an event probability function to predict and mitigate cascading events. In [32], a pattern recognition method identifying typical patterns of cascading events has been introduced. However, these two methods require an excessive computational resources to consider different variations that may occur for a given cascading outage in a power system.

The introduction and installation of Phasor Measurement Units (PMUs) in power systems has opened a new avenue to explore methods improving power systems operation.

Wide area monitoring, protection and control (WAMPAC) methods [33]-[38] incorporate GPS synchronization into protection, monitoring and control methods to make decisions at both substation and control center levels based on local and remote information send through communication channels. In [39], an intelligent scheme based on synchrophasor measurements to predict and mitigate wide area system transient instabilities is proposed. The scheme incorporates artificial neural networks (ANN) to predict the system instabilities, and applies a remedial action scheme (RAS) by splitting the system into islands and initiating under frequency load shedding actions. The challenge is to determine if an initially trained network is valid once the system is in a different operating state. In [40], two islanding detection methods, "Frequency Standard Deviation" and "Relative Phase Angle Change Rate" based on PMU measurement are proposed and tested using historical synchrophasor data. The proposed method is simple and effective, but it fails to identify the exact boundaries of the islands.

A real-time event detection and feature extraction using PMU measurement data is proposed in [41]. The authors did not compare their algorithm with other event detection techniques, and failed to confirm whether it is applicable to large-scale interconnections, or not. A decentralized/hierarchical stabilizing control approach utilizing PMU measurements to improve dynamic performance of the Hydro-Quebec's power system is proposed in [42]. The approach has not consider communication time lag and remote control signal loss as two important factors. In [43], a fast PMU based approach is deployed to monitor the stress with regard to bulk power transfer across different areas in real time when multiple outages occur inside an area. The method utilizes constant weights

that are calculated from the base case DC load flow, which decrease the overall accuracy of it.

1.3 Proposed Research

The introduction of PMUs into power system in the early eighties has exhibited great superiority in enhancing system situational awareness [37]-[39]. PMUs made it possible to measure voltages and currents phasor at different locations in the power grid all having the angle difference calculated related to a given location with a reference angle. As these measurements are synchronized using Global Positioning System (GPS), they can be used to assess and correlate system conditions in real-time.

In this dissertation, several new tools based on availability of synchrophasor measurements have been developed to detect, prevent and mitigate the cascading outages. The main objectives of this dissertation are: a) investigation of cascading outages' mechanisms to effectively design proposed techniques, b) development, implementation and testing of the tools to detect, prevent and mitigate cascading outages. The methodology of this research is as follows:

- Investigate the mechanism of cascading outages;
- Develop a synchrophasor based fault identification tool based on propagation of electromechanical wave oscillations, along with a vulnerability analysis tool for the early detection of cascading outages based on the steady state progress character of cascading outages;
- Develop an islanding prediction tool to prevent progression of cascading outages from steady state to fast transient state;

- Develop an intentional islanding tool to mitigate cascading outages at the fast transient state and prevent it from unfolding to a major blackout;
- Implement, integrate and evaluate the performance of the proposed control schemes.
- The proposed approach has some major advantages over the previously proposed techniques, such as:
- Identifying vulnerable areas and reducing maintenance time by notifying operator about the type and location of disturbance;
- Detecting areas which are prone to uncontrolled islanding and preventing occurrence of such islands;
- Introducing an automated controlled islanding strategy which minimize the cascade outage damage due to fast and optimized decision making process.

2. UNDERSTANDING OF CASCADING OUTAGES MECHANISM

2.1 Overview

Table 1 lists several major blackouts in the past decades which affected millions of people [3], [44]-[47]. A simple observation verifies that the number of major blackouts has increased in the recent years which draws special attention to the cascading outages.

TABLE 1 SUMMARY OF SEVERAL MAJOR BLACKOUTS

no	Location	Date	MW Loss	Affected People (10^6)	Collapse Time	Restoration Time (Hr)
1	US-Northeastern	11/09/1965	20000	30	13 mins	13
2	New York	7/13/1977	6000	9	1 hr	26
3	Thailand	03/18/1978	-	40	-	9
4	France	12/19/1978	29000	-	26 mins	5
5	Sweden	12/27/1983	> 7000	4,5	53 secs	5
6	Tokyo (Japan)	07/23/1987	8200	2.8	20 mins	1.25
7	US-Western	07/02/1996	11850	2	36 secs	-
8	US-Western	08/10/1996	30500	7.5	>6 mins	9
9	Brazil	03/11/1999	25000	75	30 secs	4
10	India	01/02/2001	12000	220		13
11	US- Northeastern	08/14/2003	61800	50	> 1hr	Up to 4 days
12	Denmark/Sweden	09/23/2003	6550	4.85	7 mins	2 to 4.3
13	Italy	09/28/2003	27700	57	27 mins	2.5 to 19.5
14	Moscow/Russia	05/24/2005	2500	4	> 6 hr	-
15	US-EI	08/04/2007	4261	-	6 mins	-
16	Brazil	11/10/2009	18000	60		>3
17	US-San Diego	09/08/2011	6982	2.7	11 mins	1.5 to 12
18	South Korea	09/15/2011	240	2.1	2 hr	> 3
19	Chile	09/25/2011	-	9	-	> 2
20	India	07/30/2012	>36000	300	2.5 hr	13.5
21	India	07/31/2012	>48000	670	5 min	2 to 8
22	Bangladesh	11/01/2014	445	150	-	10
23	Pakistan	01/26/2015	>8400	140	-	<1 day
24	Turkey	03/31/2015	-	70	-	10

2.2 Frequency of Large Blackouts

It has been a common concern to estimate the frequency of large-scale blackouts in comparison with the small ones. Researchers suggested that the probability distribution of blackouts with a similar size as the 2003 North American one can be approximately modeled by a power law region with an exponent between -1 and -2 [48]-[52]. Figure 2.1 illustrates the example of the empirical probability distribution of the North American blackout size obtained on a logarithmic scale [53]. Figure 2.2 is another numerical proof of the power law properties which has been obtained by analysis of historical blackouts in North America [53]. In this figure, the frequencies of blackouts in various size categorize in terms of the total amount of demand interrupted is calculated, which obeys the mentioned power law region (see Figure 2.2). The identical power law properties have been obtained from analysis of historical blackouts in China [54], Sweden [55], Norway [56], etc.

The power law property indicates that the possibility of large-scale blackouts is much greater than it was expected earlier. This situation can be described considering dependency of outages during a blackout. As the number of outages increases in a given cascading outage scenario, the power system becomes more stressed. The weakened power system elevates the possibility of succeeding outages, which will evolves to the large-scale blackout.

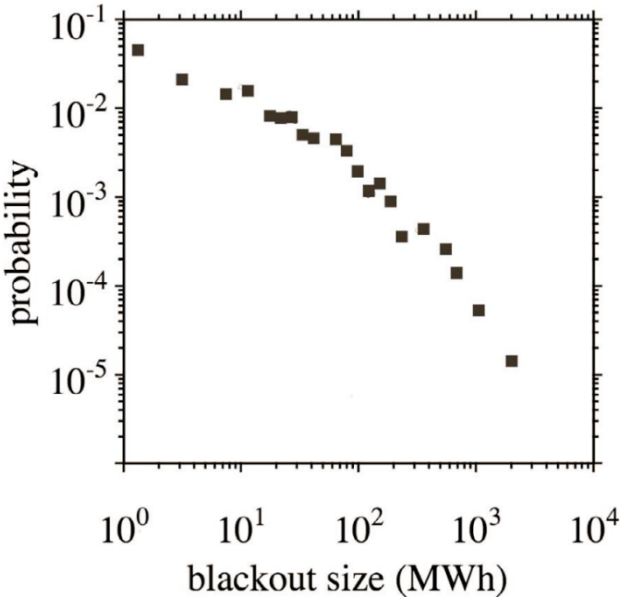

Figure 2.1 North American blackout size probability distribution from NERC disturbance analysis working group data [53]

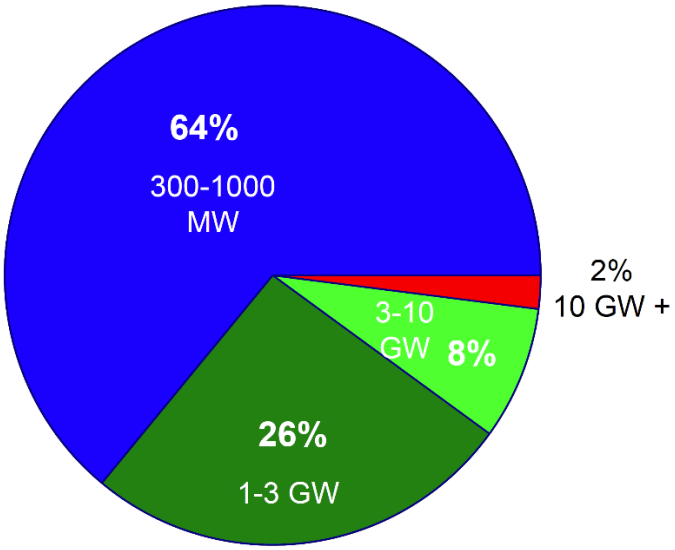

Figure 2.2 The relative blackout frequency to blackout risk from large North America blackouts in various size categories [2]

2.3 Analysis of August 14th 2003 Blackout

On August 14, 2003, large area of the Northeast United States and Province of Ontario, Canada, experienced a major blackout (case 11 of Table 1). The aftermath reports estimated that nearly 50 million people were affected due to the 61.8 GW electric load loss caused by the blackout. Figure 2.3 shows generation, demand, and interregional power flows before the blackout [3].

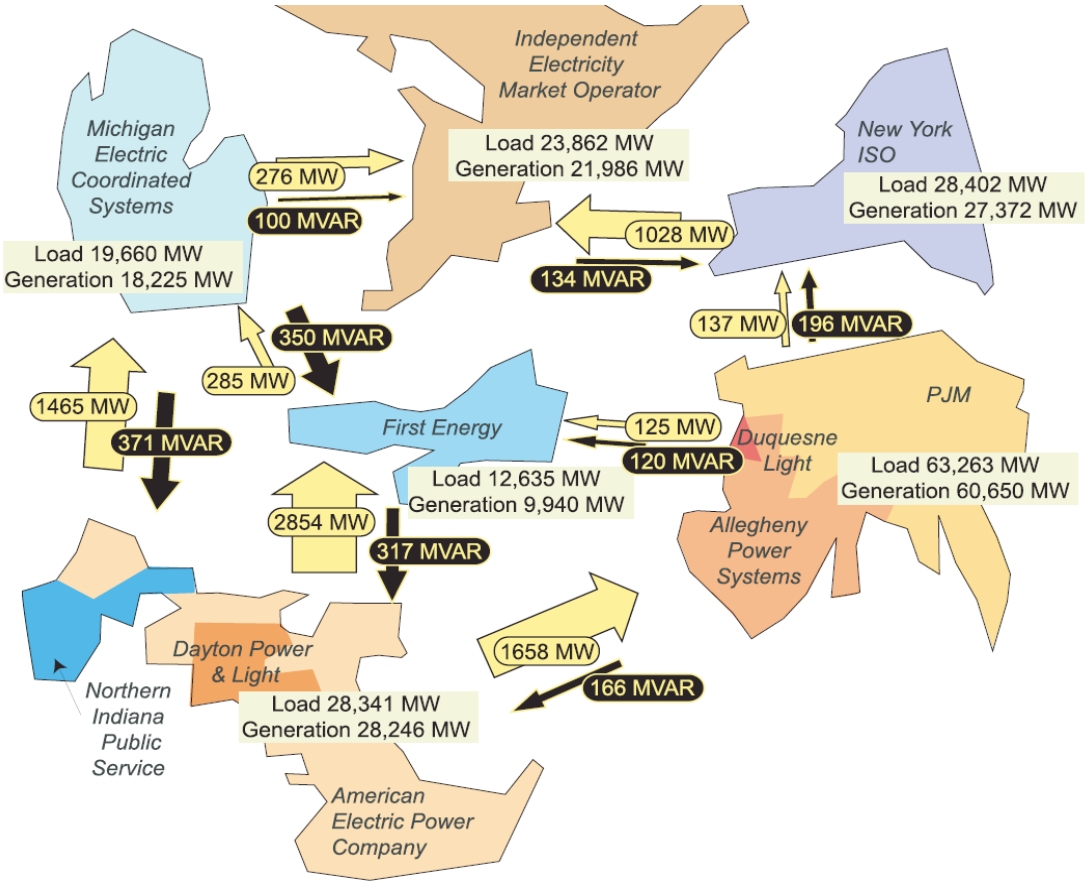

Figure 2.3 Generation, demand, and interregional power flows on August 14, 2003, at 15:05 EDT [3]

2.3.1 Timeline of Events

Analysis revealed that similar to many other blackouts, this one could also be divided into two main stages. In the first stage, the system went from a normal operating state into a period of abnormal but yet likely manageable state. Then, at the second stage, an uncontrollable sequence of events in the northern Ohio spread the outages into other areas and led to the major blackout. Figure 2.4 shows the sequence of events [3].

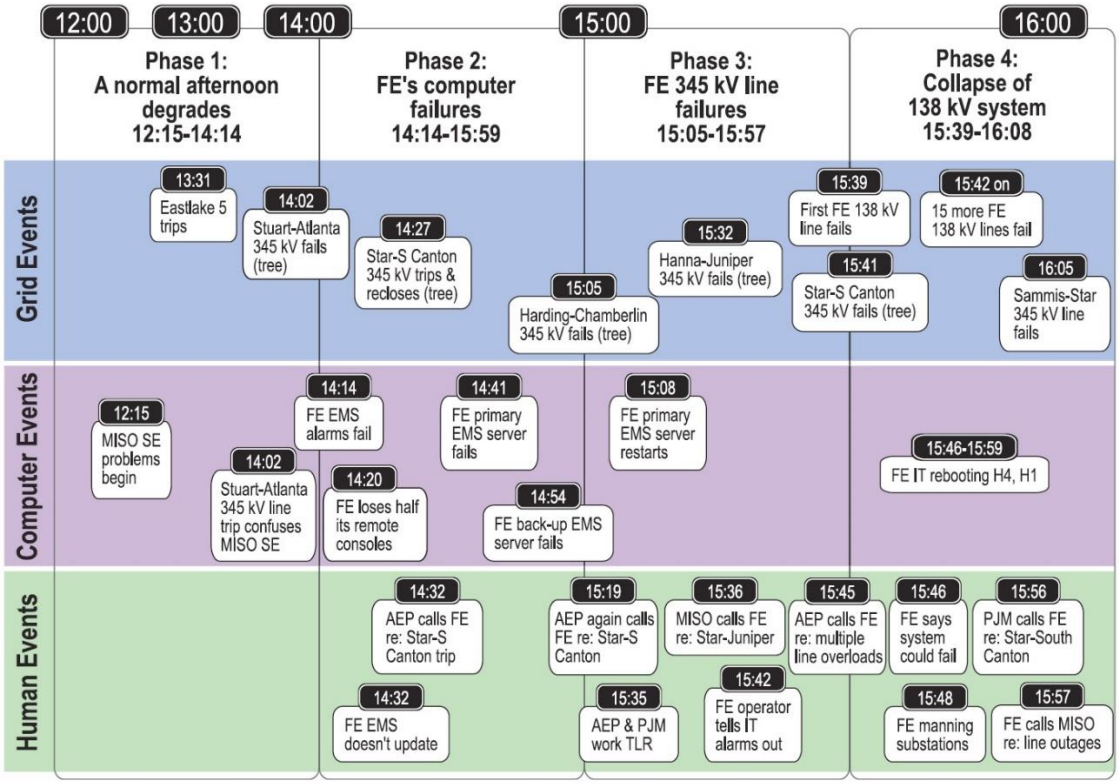

Figure 2.4 Timeline of 2003 Northeastern blackout [3]

The MISO's state estimator failed to update its status following the losses of the Eastlake 5 unit and Stuart-Atlanta 345-kV transmission line. As a result, MISO failed to perform contingency analysis, and realize that several transmission lines were heavily loaded. The state estimator and contingency analysis failure started 12:15 EDT and failed to get restored till 16:04 EDT, about two minutes before the start of the second stage of the cascade outages [57].

From 15:05 EDT to 15:42 EDT, three FirstEnergy (FE) 345-kV transmission lines in the Cleveland area went out of service due to heavily loaded conductors which sagged into overgrown trees. This caused outages that further increased the overloading problem on the remaining lines and decreased voltage level of the system which resulted in the collapse of 138-kV transmission system in Northern Ohio in less than half an hour [57].

Tripping of the Sammis-Star 345-kV transmission line due to a zone-3 impedance relay operation became a turning point which initiated the fast transient stability loss stage of cascading outages, which resulted in the blackout across the northeast United States and Ontario. In a time span of 5 minutes, thirteen 345-kV or 138-kV transmission lines in Ohio and Michigan states tripped due to zone 2 or 3 operation of distance relays. The excessive voltage drop caused the intrusion of impedance characteristic into zone 2 or 3 and it appear to the protective relays as a remote fault on the system. As oscillations continued getting stronger; the voltages were also declining faster, and the system was losing power plants one after each other. Many events occurred on the grid between 16:10:36 EDT and 16:13 EDT due to automatic equipment operations, which formed

several islands in northeast U.S. and Canada, including Ohio, Michigan, Pennsylvania, New York, Vermont, Massachusetts, Connecticut, New Jersey and Ontario [57].

2.3.2 Observations

The first post event observation revealed that during blackout the grid was split into two sections, one that experienced a blackout, and the other one that recovered without further propagation of the cascade outages. In the Midwest area, the amount of reserved reactive power was relatively small which left the system little margin to deal with low voltage conditions. In contrast, in the Northeast area, availability of more reactive reserves helped the operators to buffer their areas against potential voltage collapse without widespread generation trips.

The second observation revealed that the proper load shedding by Under Frequency Load Shedding (UFLS) and Under Voltage Load Shedding (UVLS) relays before the loss of the Sammis-Star line might have prevented further cascade outages and massive blackout. However, in the second cascade stage when the fast dynamic transients were spreading throughout the system, even the proper action of UFLS and UVLS relays would have not prevent the successive outages.

The third observation revealed the reason behind the tripping of large number of generators. According to [3], more than 508 individual generating units in 265 power plants shut down in this blackout. In the first stage, protective relays responded to overloaded transmission lines and tripped 29 (6%) generators. Due to the system configuration change during formation of islands, loss of synchronism and excitation system failures, another fifty generators (10%) tripped. After the formation of islands, 431

generators (84%) tripped mainly concurrent with under-frequency load-shedding relay operation. Several generators tripped in response to over-speed or over-voltage protection relays trip command initiated due to the major loss of their loads. On the other hand, in several islands, generators faced a sudden huge increase of loads and tripped by UFLS and UVLS protection relays.

The fourth observation is the successive tripping of three 345-kV transmission lines which were below their emergency rating and could have withstand the situation. Due to overgrown trees in their path and lack of proper tree trimming, the conductors sagged into the vegetation following the continuous overload condition. Degradation of the system following these outages resulted in voltage drops across vulnerable areas and triggered the mis-operation of zone 2 and zone 3 of impedance relays.

The last observation suggests that the Quebec system in Canada survived the blackout due to being tied to Eastern Interconnection through high voltage DC (HVDC) transmission lines. Therefore, the practice of using DC links to tie areas to each other can act as a shield against frequency swings under such circumstances.

2.4 Other Cascading Outages without Successful Mitigation

In 2012, a massive blackout occurred in India [58] which affected nearly 700 million customers (case 21 of Table 1). Tripping of the tie lines due to load encroachment following largely unscheduled power interchanges, power swing and UFLS/UVLS protective relays tripping commands were among the main reasons which eventually led to the blackout.

In September 2011, the loss of a single 500 kV transmission line which was a major transmission corridor from generators in Arizona to the San Diego area, initiated an 11-minute cascading outages leading to a blackout. Nearly 2.7 million customers were affected in parts of Arizona, Southern California, and Baja California, Mexico for up to 12 hours [59]. After loss of the 500kV line, power flows significantly increased through lower voltage systems. As a consequence, some sizeable voltage deviations and equipment overloads occurred throughout the system, as well as significant overloading occurred on three 230/92 kV transformers. The flow redistributions, voltage deviations, and resulting overloads had a ripple effect, as transformers, transmission lines, and generating units were tripped by relays, which initiated the automatic load shedding throughout the region in a relatively short time span. Just seconds before the blackout, Path 44 of WECC carried all flows into the San Diego area as well as parts of Arizona and Mexico. Eventually, the excessive loading on Path 44 initiated a RAS scheme at San Onofre Nuclear Generating Station (SONG) which led to the loss of the SONGS nuclear units, and eventually resulted in the complete blackout [60].

2.5 Successfully Mitigated Cascading Outage Cases

In 2008, on the UK network, two large size generators tripped within 2 minutes resulted in further tripping of embedded generation in the distribution system, which caused frequency to drop to 48.795 Hz [61]. This frequency drop was stopped by shedding of 1.5% of demand load to restore system frequency and later the dropped loads restored within a range of 20-40 minutes. In this case, successful coordination between the Transmission System Operator (TSO) and the Distribution Network Operators (DNOs) in

the load shedding process prevented the progress of cascading outages and system collapse.

In 2006, a planned outage by E.ON Netz[1] (TSO Company) which were failed to be properly evaluated for the N-1 security caused a major disturbance in Europe [62]. Tripping of a tie-line (connecting two TSOs) with different protection settings on each end has initiated cascades throughout the UCTE[2] system. Next, the trip commands of over-current distance protection and out of synchronism relays caused the UCTE system to split into three areas. Within 20 minutes, two of these areas were restored from an under-frequency situation owing to the sufficient generation reserve and proper load shedding. However, lack of coordination between TSOs and DNOs resulted in longer restoration time in the over-frequency area.

2.6 Mechanism of Cascading Outages

The sequence of cascading failures varies widely from event to event, and whether they have similarities among them is an important topic to explore. So far, by reviewing the major blackouts in the world, the background of cascading outages have been introduced. Figure 2.5 shows the structure of a generalized sequence of cascading events and associated power system operations [63]. Before the system falls under extreme condition, operator might yet have enough time to initiate remedial actions to mitigate the progression of cascading events. A real time automated cascade event mitigation tools

[1] The company was founded in 1927 and is based in Bayreuth, Germany.
[2] Union for the Coordination of Transmission of Electricity.

may significantly decrease the risk of progression of such events into a large-scale blackout since they will help operators to deal with the cascade mitigation timely.

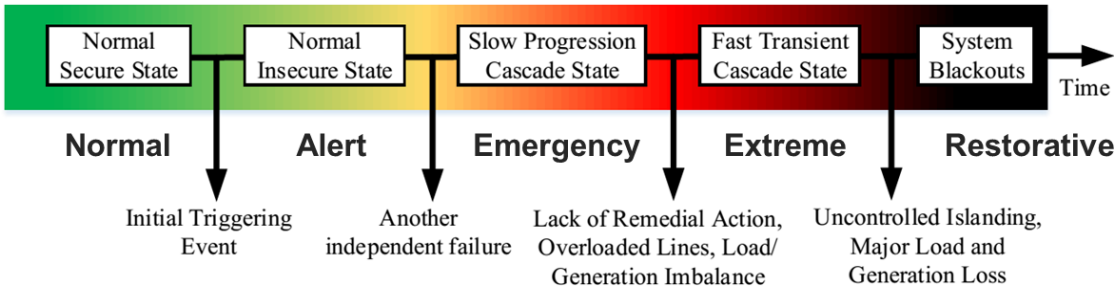

Figure 2.5 Different stages of cascading outages

Most of cascading outages have following stages of progression:

- The initial triggering event may occur anytime in power system due to reasons such as tripping a line or generator following a fault or maintenance order.
- Another independent failure or unexpected change in operating conditions following the previous control action may coincidently or sequentially occur while system is in normal insecure state. At this point, depending on the system loading condition, power system may enter to the state of slow progression of cascading outages. In a time span of few minutes to several hours, some lines might be taken out due to tripping commands from overcurrent, distance and thermal protection units.

- Without proper remedial actions, power system will enter to an unstable state with major load/generation imbalance, voltage and frequency instability, followed by an uncontrolled islanding and finally a blackout.

The time interval between an initial triggering event in the normal state and series of outages in cascade state may varies significantly. For instance, the time interval between a fault and a trip caused by relay mis-operation can be less than a second. However, an overload and/or generator over-excitation situation caused by tripped line due to a fault may cause subsequent outages which may occur minutes or even hours later.

Large-scale blackouts start for different reasons, but once they evolve into the cascading events, they reveal similar mechanisms. The following mechanisms were detected among most of historical cascading outages [64]:

- Over-current and distance relays disconnect highly overloaded lines
- Thermal failures of highly overloaded lines
- Relay mis-operation due to hidden failures
- Voltage and frequency instability
- Small-disturbance and transient angular instability
- Lack of coordination between operators, planners and protection engineers in terms of protection settings, real time exchanges, system studies and planning in key areas

2.7 Conclusion

Studies have revealed the devastating impacts of cascading outages on economic and social life. In this section, fundamentals of cascading outages have been introduced

by exploring several major blackouts in recent decades. By investigation of the mechanisms of cascading outages, it has been determined that if a real time automated tool is developed to arrest cascade outage at its early progression stages, it can avoid further propagation of outages. In the next section, the fundamental of an integrated real time synchrophasor based solution to achieve this goal will be discussed.

2.8 Organization of Dissertation

This dissertation is organized as follows. Section 2 discusses the mechanism of cascading outages by reviewing several historical outages. The fundamentals of the proposed approach are provided in Section 3. The proposed synchrophasor based monitoring tools are presented in Section 4. An islanding prediction tool to predict areas of system which are prone to unwanted islanding formation is proposed in section 5. In section 6, a controlled islanding tool is proposed to split system into islands and prevent propagation of cascading outages. The initial test results follow in section 7. The expected contribution and conclusions of the dissertation are discussed in section 8. References, as well as published papers related to this work are listed in the end.

3. FUNDAMENTALS OF THE PROPOSED SYNCHROPHASOR BASED APPROACH

3.1 Overview

In this dissertation, a set of tools to support power system operator's decision-making process is proposed which includes online monitoring tools, islanding prediction tool, and intentional islanding tool. Based on these proposed tools, this dissertation provides an interactive scheme solution for the fast detection and mitigation of cascading outages in power system.

3.2 Application of Synchrophasor System in Power system

Nowadays, PMUs are the latest technology advancement in the measuring instruments in the power system which offer synchronized voltage/current phasor measurements across different locations of the system. Based on a comprehensive literature survey, a broad range of PMU-based applications in power systems has been identified. A list of synchrophasor based applications in power system is shown in Table 2 [65].

In recent years, synchrophasor systems have been widely used by utilities around the world to monitor and analyze power system behavior. With the availability of fast processing CPUs and a reliable high-speed communication infrastructure to transfer all measurements, synchrophasors are now being deployed to address a variety of power system protection, automation, and control problems, as well.

TABLE 2 LIST OF SYNCHROPHASOR BASED APPLICATIONS IN POWER SYSTEM

Offline Applications	Online Applications
Post-Event Analysis	Enhanced State-estimation
System Parameterization	Oscillation Monitoring & Control
Dynamic Model Validation	Voltage Security Assessment & Control
System Protection & Control Planning	System Protection & Real-time Control
	Fault Location & Detection
	Intelligent Islanding & Resynchronization

Figure 3.1 shows the placement of PMUs in the North American power grid by March 2015. The blue points are PMUs' locations and red lines show the path of data transfer from local PMUs to regional data concentrator locations.

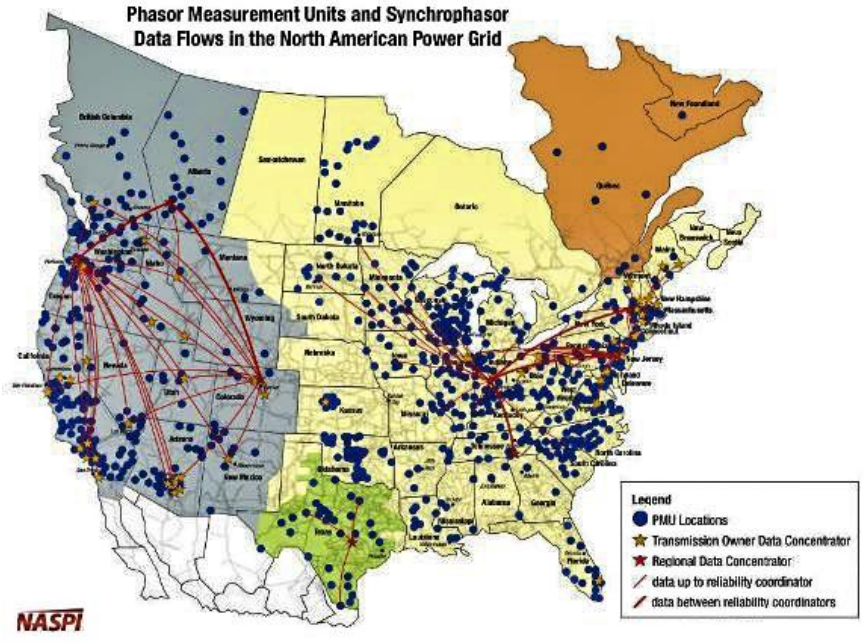

Figure 3.1 PMUs distribution and synchrophasor data flows in the North American power grid, March 2015 [66].

3.3 Application of Synchrophasor System in Blackout Prevention

3.3.1 Monitoring and Prediction Tools

Local protective devices operate mainly based on local measurements, and may fail to observe the effect of their decision-making process on the entire system. For instance, operation of a local protection unit to secure an asset in case of a thermal overload condition, may trigger a series of cascade failures due to thermal overloads of other assets.

With the availability of synchrophasor systems, time-stamped measurements could be collected from remote locations to form real time snapshots of power systems with a resolution up to 30, 60, 120 or 240 frames per second. Thus, it can provide a unique opportunity to monitor the power system at a wide area level. These measurements could be further used to develop monitoring applications to improve security and dependency of the power system protection. Figure 3.2 shows a typical architecture of synchrophasor system which is used to implement different power system applications.

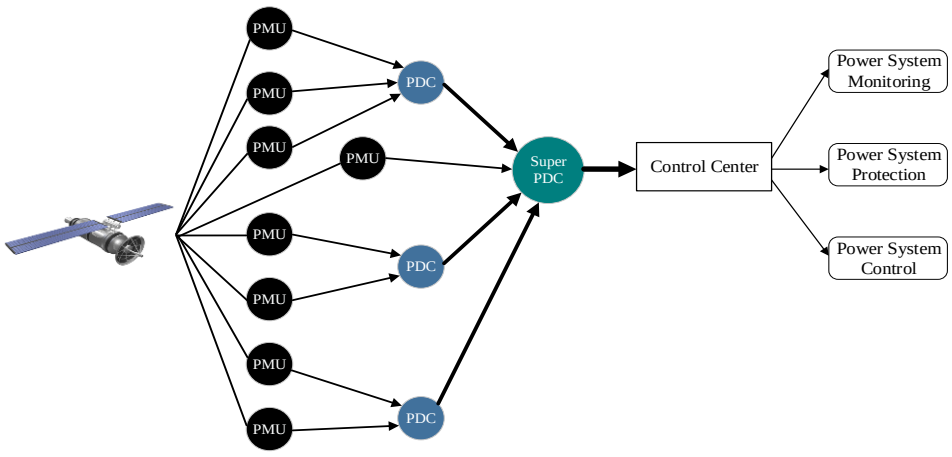

Figure 3.2 Overall architecture of synchrophasor system applications

In the example of overloaded asset, a wide area synchrophasor based monitoring scheme could halt the local protection action by monitoring the evolving threat to the system security. Thus, it can provide additional time for control center operator to mitigate the overload condition and maintain system security.

It should also be noted that the complexity of wide area disturbances and the short restoration time requires an automatic decision-making mechanism to speed up the process rather than human-based one, which may be too slow. These automatic monitoring tools can be developed using synchrophasor measurements to avoid human errors which may drag the system into insecure state and a possible blackout.

In this dissertation, three synchrophasor based tools are developed to monitor the power system in real time and predict possibility of unwanted islanding formation. These tools work together to provide a full resolution of the system condition in normal and slow progression cascade stages. The first tool monitors the power system by computing vulnerability indices defined based on synchrophasor measurements. These synchrophasor based indices can provide a precise quantitative measure of system vulnerability and security condition by continuously monitoring of the system. These indices can be calculated for different regions to identify vulnerable parts of the system (if any), and notify operators to take the suitable control action to prevent further outages. The second monitoring tool uses synchrophasor measurements to identify location of a fault within the grid. The methodology used to develop the fault identification tool is based on detection of electromechanical waves which propagate in the network following a fault.

The third tool uses the output of vulnerability analysis tool along with an islanding database which is created in offline analysis to predict areas prone to formation of unwanted islands. This tool can inform the operator regarding the chance of un-wanted island formation as well as a list of possible outages that may lead to a system unwanted separation.

3.3.2 Mitigation Tool

The typical control actions to prevent cascading outages are shown in Figure 3.3 [67]. Certain mechanisms such as optimizing active and reactive power generation, tripping generators and transmission lines or load shedding trigged by under voltage or under frequency load shedding relays (UVLS/UFLS) are used to prevent or mitigate contingencies. However, these techniques may fail to mitigate cascading outages due to the complex nature of the cascading outages as described in section 2.

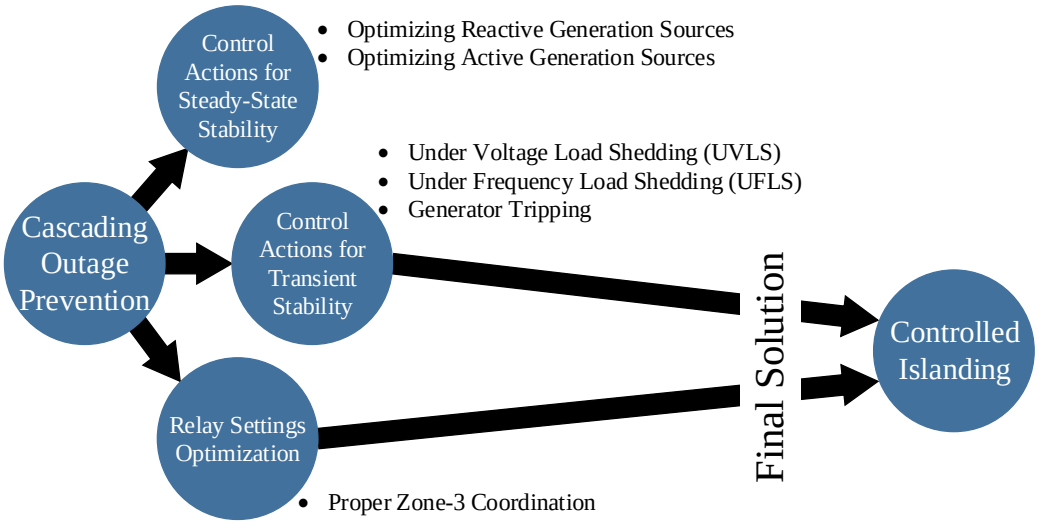

Figure 3.3 Typical control actions to prevent cascading outages [67]

Today's modern power systems operate closer to their stability margins, and are more subjected to large disturbances which make the conventional mitigation mechanisms less effective. In case of a large disturbance created by a series of cascading outages, operation of local distance or overcurrent relays, as well as load shedding triggered by UFLS and UVLS relays system may not be sufficient, and the system can eventually split into several islands. In this condition, a controlled islanding scheme could be used as a final solution to prevent the propagation of cascading outage and minimize load and generation losses.

In this dissertation a controlled islanding method to prevent system from further outages and losses is proposed. If the monitoring and prediction tools fail to prevent progression of cascading outages, the proposed controlled islanding tool will be triggered using information obtained through synchrophasor measurements. Then, the controlled islanding tool intentionally separates the power system into several load-generation balanced islands to prevent the propagation of cascading outages with an optimal minimum loss of load and generation. Once a disturbance occurs, depending on the topology and nature of the system, generators will swing together in different groups. These groups of generators swinging together can be determined using the slow coherency characteristics of the system [68]. The proposed controlled islanding tool determines the cutsets with minimum loss of load and generation while keeping the coherent generators within same islands. This way, the generators within each intentionally created island will swing together, while the islands' boundaries are optimized to have load-generation balance.

3.4 Interaction of the Proposed Tools

Figure 3.4 shows the integrated framework of the proposed tools, which covers different stages of cascading outages described in Figure 2.5. The key algorithms of the proposed solution are as follows:

- In the normal stage (secure or insecure), the two proposed methods, namely, Synchrophasor based Online Vulnerability Index (SOVI) and Synchrophasor based Online Fault Identification (SOFI) modules operate together to monitor the state of power systems. If the sequence of events is such that the system is drifting towards the stage of slow progression cascading outage, an alarm is sent to the operator and the other proposed mechanisms to prevent progression of cascading outages. The SOFI module determines the type and location of disturbances, and consequently, the network parameters are updated.
- In the stage of slowly progressing cascading outages, a Synchrophasor based Islanding Predication (SIP) module is proposed to determine parts of the system which have tendency to be separated from the rest of it. The SIP module runs in real-time, and if an area prone to form of an unwanted island is detected, an alarm is sent to the operator to apply proper RAS actions. The SIP module consists of two parts, an offline islanding scenario database, and an online intelligent method which uses the output of SOFI module to determine whether a specific area is prone to form an island.

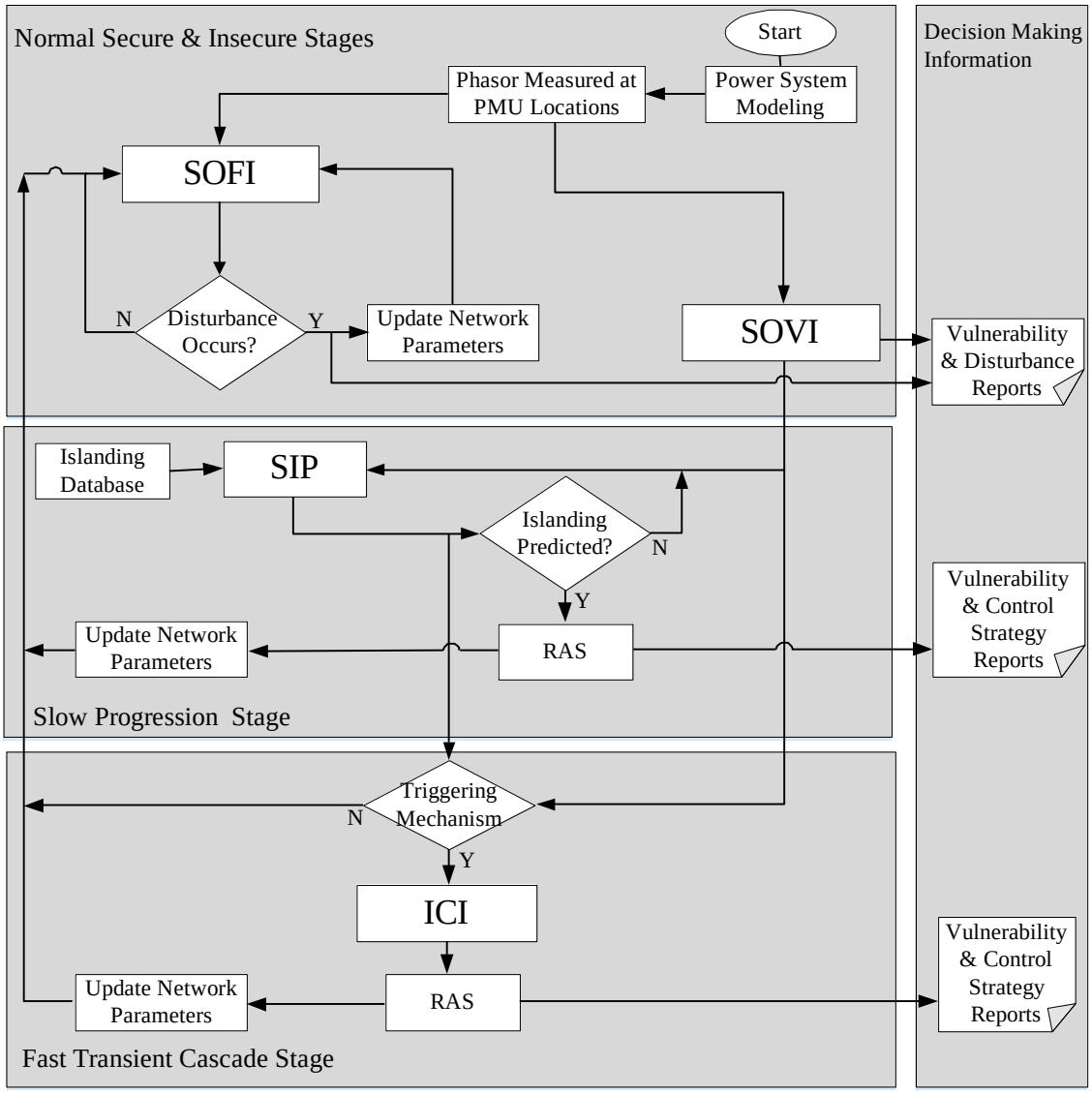

Figure 3.4 Flowchart of the proposed method for detection, prevention and mitigation of cascading outages

- If the RAS module fails to restore the system into the normal stage, and cascading outages continue to unfold, the system enters to the stage of fast transient cascading outage. In this stage, an Integrated Controlled Islanding (ICI) module is proposed

to rescue the system from a total blackout. The ICI module utilizes the graph representation of the power system, power flow analysis, location of PMUs and generator coherency information to solve a constrained optimization problem. The ICI module runs in real-time to determine the switching sequences required to create intentional islands.

3.5 Conclusion

The power system cascading outages are complex because many factors can cause cascading outages. Synchrophasor systems can provide a unique opportunity to detect, prevent and mitigate cascading outages. In this section, an overview of the proposed synchrophasor based tools to be deployed at different system condition to detect, prevent, and mitigate cascading outages is presented. These tools will be thoroughly discussed and tested in the remaining sections.

4. SYNCHROPHASOR BASED ONLINE MONITORING TOOLS*

4.1 Introduction

In the normal condition, power systems are designed to withstand "N-1" contingency. In many cases, a system is able to withstand more than one contingency, while its stability margins shrinks. Under these circumstances, it is pivotal to design a monitoring tool to continually monitor the power system, and notify the operator when areas of the system becomes vulnerable. In this section, two synchrophasor based tools are introduced to monitor the power system in the normal stage. These methods utilize the base power flow and network topology data along with available PMU measurements to determine the vulnerability of different areas of the power system, as well as disturbance locations. Section 4.2 reviews the applications of graph theory in the proposed power system monitoring tools. The Synchrophasor based Vulnerability Index (SOVI) and Synchrophasor based Online Fault Identification (SOFI) modules are presented in Sections 4.3 & 4.4, respectively. Summary is given in Section 4.5.

4.2 Graph Representation of Power Systems

Graph theory is one of the fast-growing areas of modern mathematics which has been extensively utilized in many areas, such as mathematics, computer programming and networking, economics and communications [69]-[76]. Graph theory is a practical mean to simplify the complicated problems into a set of edges and vertices. Electric power

* Part of this section is reprinted with permission from "Fault Location Using Sparse Synchrophasor Measurement of Electromechanical-Wave Oscillations" by A. Esmaeilian and M. Kezunovic, Aug. 2016. *IEEE Transactions on Power Delivery*, vol. 31, no. 4, pp. 1787-1796, ©2016 IEEE, with permission from IEEE.

system composed of thousands of generators, transformers, transmission lines, and loads, can be modeled and analyzed as a graph network.

In [77], Lee, et al. proposed an economic dispatch model based on graph theory. In [78], graph theory is used to describe the grid as a function of its electrical topology rather than physical one. In [79], authors applied graphs theory to demonstrate that the heterogeneous nature of the power system makes it vulnerable to malicious attacks which may trigger a large-scale cascade outages.

A state estimation observability analysis based on hybrid topological-numerical approach is proposed in [80]. The authors used a graph partitioning method to split system into observable and unobservable areas. A multiple criteria decision-making (MCDM) method based on the definition of the attack graph is presented in [81]. Authors used the MCDM method to address issues related to the security analysis of power control process. A model-based fault identification and location scheme based on graph structural analysis is presented in [82]. The proposed method provides an automatic residual generation strategy using the analytical redundancy inherent in the system structure.

In this section, graph theory is used to identify the vulnerable parts of the power system.

4.2.1 Graph Model of Power System Elements

4.2.1.1 Undirected Graph

Suppose $G=(V, E)$ is a graph network with v nodes (vertices) and e links (edges) where V and E are the sets of vertices, and connecting edges between those vertices, respectively. An important matrix, widely used to study graphs is known as adjacency

matrix which is a measure of connectivity of graphs' vertices. The adjacency matrix A is a symmetric matrix with all its diagonal elements equal to 1, which indicates each vertex is connected to itself. The element a_{ij} of adjacency matrix A is equal to 1 if there is an edge between v_i and v_j, otherwise is equal to zero.

$$A_{v\times v} = \{a_{ij}\} \qquad a_{ij} = \begin{cases} 1 & if\ there\ is\ an\ edge\ between\ v_i\ and\ v_j \\ 0 & otherwise \end{cases} \tag{4.1}$$

For instance, for a graph with five vertices and seven edges shown in Figure 4.1, the incidence matrix A can be obtained based on (4.1):

$$A = \begin{bmatrix} 1 & 1 & 1 & 0 & 0 \\ 1 & 1 & 1 & 1 & 0 \\ 1 & 1 & 1 & 1 & 1 \\ 0 & 1 & 1 & 1 & 1 \\ 0 & 0 & 1 & 1 & 1 \end{bmatrix}$$

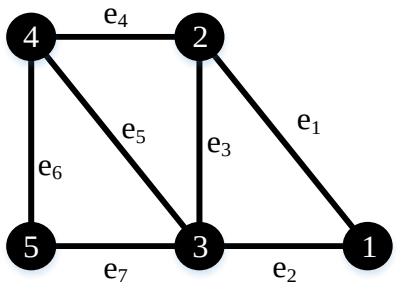

Figure 4.1 A graph with five vertices and seven edges

In this dissertation, to represent the topological model of power system as a graph, substations (composed of generators, bus bars and loads) and transmission lines are modeled as the nodes and links of the graph, respectively. Thus the undirected graph model of the power system is easily obtained.

4.2.1.2 Directed Graph

In power engineering, the power flow study is always an important tool involving numerical analysis applied to a power system. It has been demonstrated that in steady state condition, a power system could be modeled as a directed graph network [63], since the directions of power flow in the modeled network can be measured in any given steady state condition.

For the directed graph, the definition of incidence matrix is different than the one in undirected graph. For a directed graph G, the incidence matrix *A* implies the connectivity of the vertices with regard to edges' directions. Similarly, all diagonal elements of the adjacency matrix *A* are equal to 1, which indicates each vertex is connected to itself. The element a_{ij} of incidence matrix *A* is equal to 1 if there is a directed edge from v_i to v_j, otherwise is equal to zero.

$$A_{v\times v} = \{a_{ij}\} \qquad a_{ij} = \begin{cases} 1 & if\ there\ is\ a\ directed\ edge\ from\ v_i\ to\ v_j \\ 0 & otherwise \end{cases} \tag{4.2}$$

For instance, for a directed graph with five vertices and seven edges shown in Figure 4.2, the incidence matrix *A* can be obtained based on (4.2):

$$A = \begin{bmatrix} 1 & 1 & 1 & 0 & 0 \\ 0 & 1 & 0 & 1 & 0 \\ 0 & 1 & 1 & 1 & 0 \\ 0 & 0 & 0 & 1 & 1 \\ 0 & 0 & 1 & 1 & 1 \end{bmatrix}$$

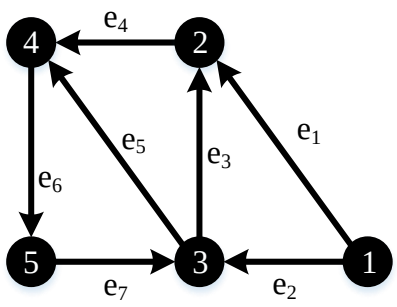

Figure 4.2 A graph with five vertices and seven edges

4.2.2 Betweenness Centrality Concept

The betweenness centrality was first introduced by Freeman [83] as part of his study to obtain influential level of a person or group in a social network. In graph theory, betweenness centrality index can be defined for each vertex and edge based on definition of shortest paths. Betweenness centrality has a wide application in network theory. For instance, in a telecommunications network, a node with higher betweenness centrality would have more control over the network, because more information will pass through that node.

For the given graph *G=(V, E)*, the vertex betweenness centrality *BC(v)* of a vertex $v \in V$ is the sum over all pairs of vertices $u,w \in V$, of the fraction of shortest paths between *u* and *w* that pass through vertex *v*, which is shown as:

$$BC(v) = \sum_{\substack{u,w \in V \\ u \neq w \neq v}} \frac{\sigma_{uw}(v)}{\sigma_{uw}} \tag{4.3}$$

where $\sigma_{uw}(v)$ denotes the total number of shortest path between vertex *u* and *w* that pass through *v*, and σ_{uw} denotes the total number of shortest paths between *u* and *w*.

Similar to the vertex betweenness centrality, the edge betweenness centrality *BC(e)* of a edge $e \in E$ *is* defined as the sum over all pairs of vertices $u,w \in V$, of the fraction of shortest paths between *u* and *w* that pass through edge *e*, which is shown as:

$$BC(e) = \sum_{\substack{u,w \in V \\ u \neq w}} \frac{\sigma_{uw}(e)}{\sigma_{uw}} \tag{4.4}$$

where $\sigma_{uw}(e)$ denotes the total number of shortest path between vertex *u* and *w* that pass through *e*, and σ_{uw} denotes the total number of shortest paths between *u* and *w*.

For instance, consider a graph with six vertices and seven edges shown in Figure 4.3. The vertex betweenness centrality of node *b* is calculated as:

$$BC(b) = \sum_{\substack{u,w \in V \\ u \neq w \neq v}} \frac{\sigma_{uw}(b)}{\sigma_{uw}} = \sigma_{ac}(b)/\sigma_{ac} + \sigma_{ad}(b)/\sigma_{ad} + \sigma_{ae}(b)/\sigma_{ae} + \sigma_{af}(b)/\sigma_{af}$$
$$= 1 + 1 + 1 + 1 = 4$$

Similarly, the edge betweenness centrality of edge *ab* is calculated as:

$$BC(ab) = \sum_{\substack{u,w \in V \\ u \neq w}} \frac{\sigma_{uw}(ab)}{\sigma_{uw}}$$

$$= \sigma_{ab}(ab)/\sigma_{ab} + \sigma_{ac}(ab)/\sigma_{ac} + \sigma_{ad}(ab)/\sigma_{ad} + \sigma_{ae}(ab)/\sigma_{ae} + \sigma_{af}(ab)/\sigma_{af}$$

=1+1+1+1=4

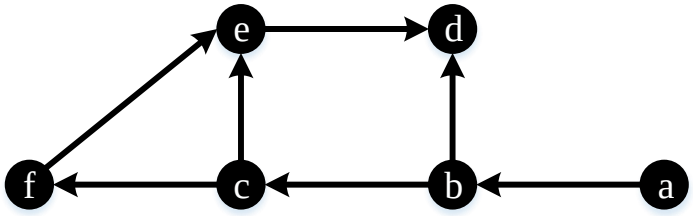

Figure 4.3 A directed graph with six vertices and seven edges

4.3 Synchrophasor Based Vulnerability Analysis Module

Song has proposed the concepts of Vulnerability Index (VI) and Margin Index (MI) [1] for the main elements in power system including generators, buses, and branches. The system-wide vulnerability and security of individual elements can be evaluated by the different VI and MI values computed for various system conditions. Pang improved the concept of VI and MI by inducing a method to calculate the weight values for each VI and MI [2] using the concept of vertex and edge betweenness centralities. His approach provided a combined consideration of both electrical characteristics of power system and

topology parameters in the graph representation of the electrical network. But, those VIs and MIs are only considered in the steady state condition when the power flow result is available through state estimation, and therefore may not be useful for cascade outage detection.

The vulnerability monitoring method, if developed as an online module, can swiftly and effectively determine which parts of the system are prone to cascading outage. This way, the cascading outages could be avoided ahead of the time by applying proper remedial actions to restore the stability margin of the system.

4.3.1 Formulation

In this dissertation, PMU measurements are used to obtain VIs of the power system in real-time at system-wide level. As shown in Figure 4.4, the proposed SOVI module operates within the following steps:

- The synchrophasor streams measured by PMUs (or other PMU enabled devices such as digital protective relays (DPRs) or digital fault recorders (DFRs)) at different substations are collected by substation Phasor Data Concentrators (PDCs) and transferred through communication links to the control center PDC and stored at synchrophasor PI historian database.
- The SOVI module utilizes voltage and current phasors measured captured at PMUs location in real-time to define three different types of VIs associated with buses, lines and generators, respectively.
- VIs associated with buses reflect changes in buses voltage or load from scheduled values and is defined as:

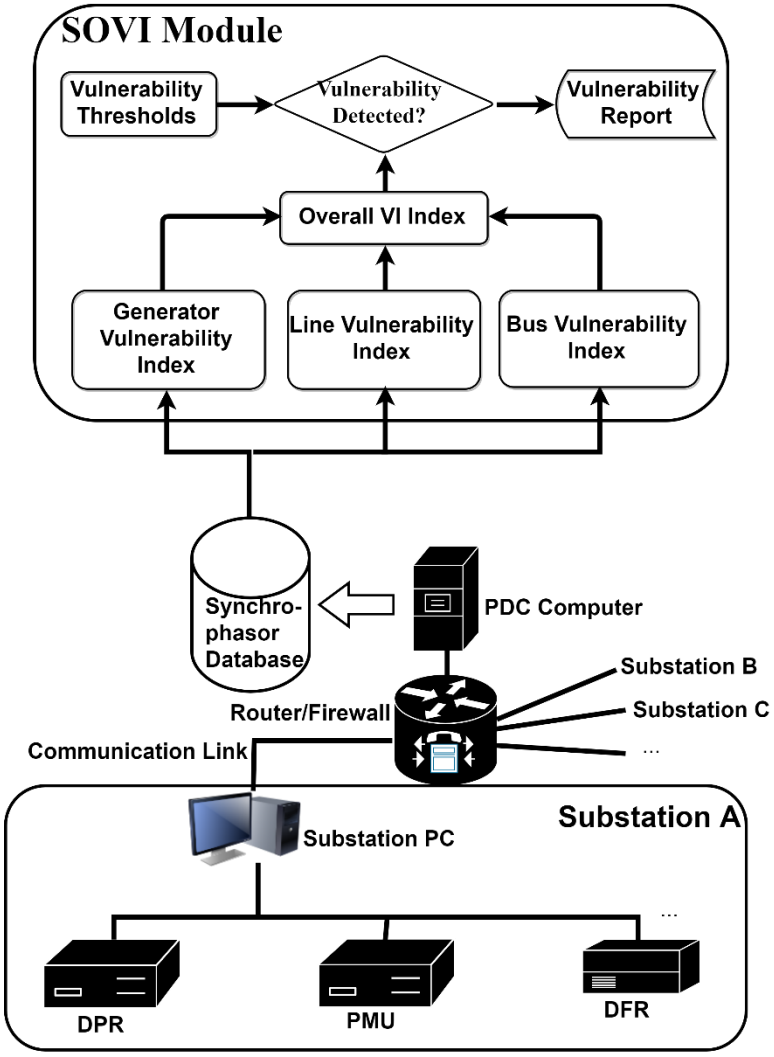

Figure 4.4 Overall structure of the SOVI tool

$$SVI_{Bus,i} = \frac{W_{V,i}}{2}\left[\left(\frac{V_i - \Delta V_i^{sch}}{\Delta V_i^{lim}}\right)^2 + r_i\right] \tag{4.5}$$

$W_{V,i}$: Weight of individual bus voltage influence

V_i: Individual bus voltage magnitude

ΔV_i^{sch}: Individual bus scheduled voltage magnitude

ΔV_i^{lim}: Individual bus voltage variance limit

r_i: load loss ratio, 0~1, 0: no loss; 1: completely loss

- VIs associated with lines reflect changes in active or reactive power flows through lines, as well as status of the lines (in-service or out-of-service).

$$SVI_{line,j} = \frac{W_{line,j}}{2}\left[\left(\frac{P_{f,j}}{S_j^{max}}\right)^2 + \left(\frac{Q_{f,j}}{S_j^{max}}\right)^2 + k_{line-j}\right] \quad (4.6)$$

$W_{line,j}$: Weight of individual line influence

$P_{f,j}$: Individual line real power

$Q_{f,j}$: Individual line reactive power

S_j^{max}: Individual line transmission limit, which can be either thermal limit or transfer limit due to security constraints

k_{line-j}: 1 when line is out-of-service, 0 when line is in-service

- VIs associated with generators reflect changes in active or reactive power generation.

$$SVI_{Gen,l} = \frac{W_{Pg,l}}{2}\left[\left(\frac{P_{g,l}}{P_{g,l}^{max}}\right)^2 + \left(\frac{Q_{g,l}}{Q_{g,l}^{max}}\right)^2 + k_{gen-l}\right] \quad (4.7)$$

$W_{Pg,l}$: Weight of individual generator

$P_{g,l}$: Individual generator real power output

$Q_{g,l}$: Individual generator reactive power output

$P_{g,l}^{max}$: Maximum real power output of generator

$Q_{g,l}^{max}$: Maximum reactive power output of generator when $Q_{g,l}$ is positive; minimum reactive power output of generator when $Q_{g,l}$ is negative

k_{gen-l}: 1 when generator is off, 0 when generator is on

- The aggregation of VIs calculated for the buses, lines and generators are used to determine the vulnerable elements/areas of the power system.

$$SVI_{Total} = \sum SVI_{Bus,i} + \sum SVI_{Line,j} + \sum SVI_{Gen,l} \tag{4.8}$$

As mentioned in section 4.2.2, the edge and vertex betweenness centrality can be used as measures to rank their influence in a given graph network. The higher betweenness centrality value of an element implies its relatively higher importance comparing to other elements within the graph. Considering the power system as a graph network (section 4.2.1), the betweenness centrality indices can be calculated for all buses and transmission lines to identify their impact on the system. Thus, these indices could be utilized as weights for the proposed SOVI module formulated within (4.5) to (4.8).

Since transmission lines are modeled as edges of the graph network, $W_{line,j}$ values are calculated based on vertex betweenness centrality ($BC(v)$). While generators and buses are represented as nodes of the graph, $W_{Pg,l}$ and $W_{V,i}$ values are obtained based on edge betweenness centrality ($BC(e)$). By growing the size of power system, the normalized edge and vertex betweenness centrality indices are defined to avoid large values.

$$BC_{norm}(v) = \frac{BC(v)}{(n-1)(n-2)} \tag{4.9}$$

$$BC_{norm}(e) = \frac{BC(e)}{(n-1)(n-2)} \tag{4.10}$$

where n is the total number of nodes in the power system. Finally, the weights associated with the elements of SOVI module formulated in (4.5) to (4.8) are obtained as follows:

- Obtaining power flow direction from power flow analysis;
- Building the directed graph representation of the power system;
- Obtaining shortest paths between each pairs of vertices;
- Determining sum of all fractions of shortest paths that pass through the vertex in question for all pairs of vertices to obtain betweenness centrality index for that vertex;
- Extending this calculation to all the vertices and edges to get the betweenness centralities of whole network using (4.3) and (4.4);
- Normalizing betweenness centralities indices using (4.9) and (4.10);

4.3.2 Case Study

The IEEE 39-bus test system is used to demonstrate the performance of proposed SOVI tool. Figure 4.5 shows the IEEE 39-bus system configuration. The detailed system configuration and base power flow data can be found in [84]. The power flow results obtained using MATPOWER package [85] is used along with system topology data to derive the directed graph model of the IEEE 39-bus test system. Once the adjacency matrix is calculated using (4.2), the vertex and edge betweenness centrality indices are calculated to rank the influence of each bus and transmission line, respectively. Figure 4.6.a and Figure 4.6.b depict the distributions of vertex and edge betweenness centrality for all buses and transmission lines, respectively.

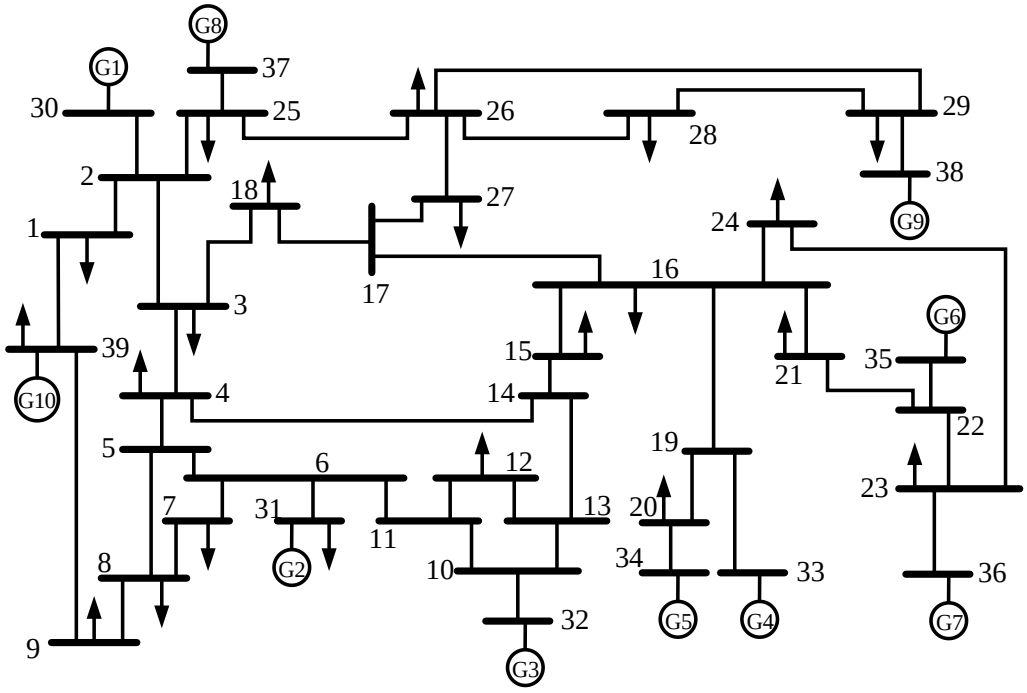

Figure 4.5 IEEE 39-bus test system

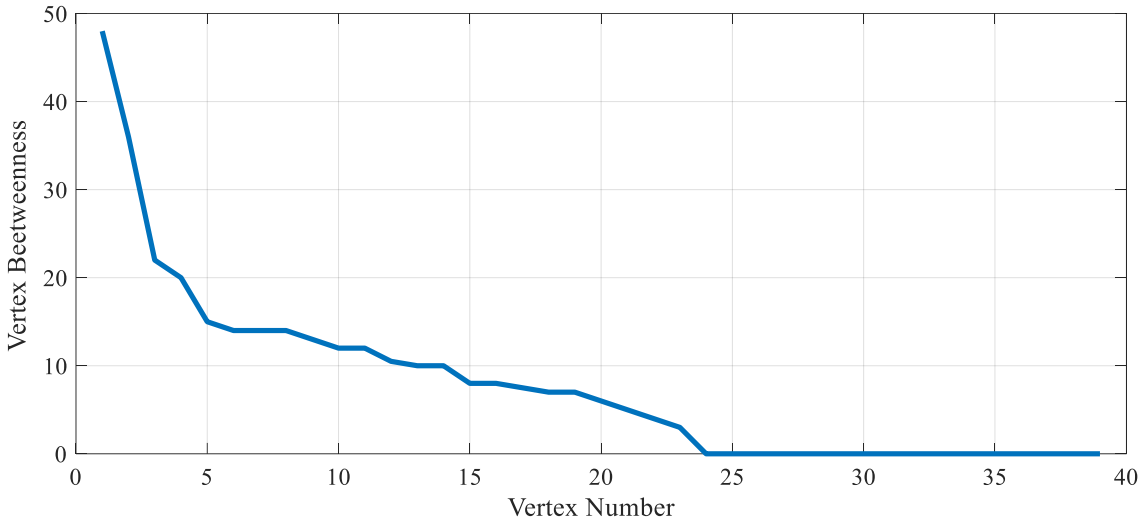

(a)

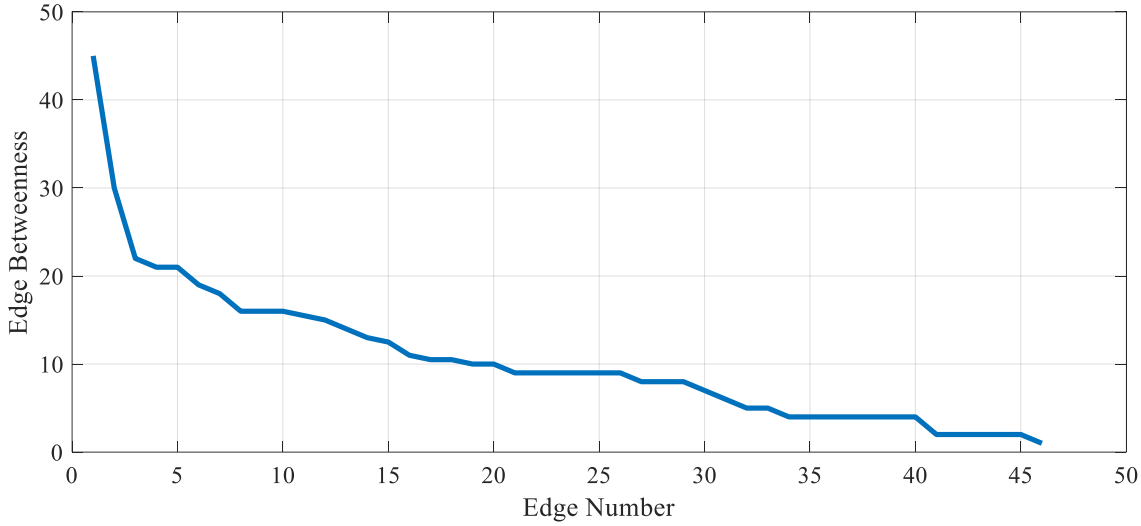

(b)

Figure 4.6 Vertex and edge betweenness distribution for IEEE 39-bus System

Analysis of Figure 4.6 demonstrates that few buses and transmission lines have higher betweenness centrality values, which means they have significantly higher importance compared to the remaining parts of the system. The betweenness centrality values calculated for larger systems proved that the above statement holds for a real size system, too. In this example, buses 16 and 17 and the transmission line between them have the highest betweenness centrality values which could be observed from their topological positions in the system shown in Figure 4.5.

Table 3 shows the output of the SOVI tool for the three cases under different load conditions. In Case 1, the simulation is performed using base load. In Cases 2 and 3, all active and reactive loads were multiplied by ratios of 1.1 and 1.25, respectively. Simulations have been performed using OPAL-RT real time simulator by modeling system within RT-LAB software environment. In each case, the SOVI tool outputs were selected after the system reached to the steady state condition. Table 3 shows the results of individual SOVI elements including SVI_{Bus}, SVI_{Gen} and SVI_{line}, as well as SVI_{Total}.

It can be seen from Table 3 that the output of SOVI tool increases as the load level is increased which indicates that the power system becomes more vulnerable.

TABLE 3 SOVI VALUES UNDER DIFFERENT LOAD CONDITIONS

Case no.	SVI_{Bus}	SVI_{Gen}	SVI_{line}	SVI_{Total}
1	0.9567	4.2090	6.0933	11.2590
2	1.0728	6.6529	8.2157	15.9414
3	1.3841	10.0448	11.7686	23.1975

The results of simulations for several N-1 and N-2 static contingency analysis are listed in Table 4 and Table 5, respectively. For the sake of simplicity, only those transmission line outages which results in non-islanding contingency scenarios are considered. As it was expected, the SOVI values in all contingency cases of both tables are higher than the normal condition (case 1 in Table 3) which means that the entire power system is more vulnerable under the contingency scenarios compare to normal situation. It can be also observed that the SOVI values in Table 5 are relatively higher than those in Table 4, which indicate that the system is more vulnerable under "N-2" contingency condition. These case studies prove the effectiveness of the proposed SOVI tool in detection of system vulnerability to assess the system security under different contingency and loading scenarios.

For a large power system, the SOVI tool can be developed for different areas of the system in order to detect its vulnerable areas with more precision. Additional testing of the SOVI tool using a larger network is performed in section 7.

Table 4 SOVI Values for N-1 Contingency Analysis

Case no.	**Line ID**	SVI_{Bus}	SVI_{Gen}	SVI_{line}	SVI_{Total}
1	L26 (16-17)	1.4856	18.1091	16.4219	36.0166
2	L16 (8-9)	1.3942	14.3360	13.4896	29.2198
3	L7 (3-18)	1.3907	15.5508	10.2731	27.2146

TABLE 5 SOVI VALUES FOR N-2 CONTINGENCY ANALYSIS

Case no.	Line ID	SVI_{Bus}	SVI_{Gen}	SVI_{line}	SVI_{Total}
1	L13 (6-11) L6 (3-4)	2.2534	25.3691	27.0581	54.6806
2	L26 (16-17) L11 (5-8)	2.3217	26.5410	23.7194	52.5821
3	L42 (26-27) L28 (16-21)	1.8914	21.7269	18.1137	41.7320

4.4 Synchrophasor Based Online Fault Identification Module

Electromechanical wave oscillations originated following a disturbance propagate through power system with speed much lower than electromagnetic travelling waves [86]-[89]. Electromechanical waveforms are characterized by phase angle modulation of voltages and currents with much lower frequency (0.1–10.0 Hz) than electromagnetic transients (>100 kHz) [90], [91]. Therefore, they could be detected by looking into phasor measurement captured by PMUs or other IEDs which can report phasors. Since these waves propagate through different paths in power system, they reach the remote buses with distinct time delays which solely depend on the paths' length and propagation speed of wave through each path. As shown in Figure 4.7, the proposed SOFI module which uses the synchrophasor measurements collected at the control center operates within the following steps [92]:

- The system topology and location of PMUs are used to run one-time offline computation using Dijkstra's shortest path algorithm [93] to build the "shortest Path Database".

- The synchrophasor streams measured by PMUs (or other PMU enabled devices such as digital protective relays (DPRs) or digital fault recorders (DFRs)) at different substations are collected by substation Phasor Data Concentrators (PDCs) and transferred through communication links to the control center PDC and stored at synchrophasor PI historian database.

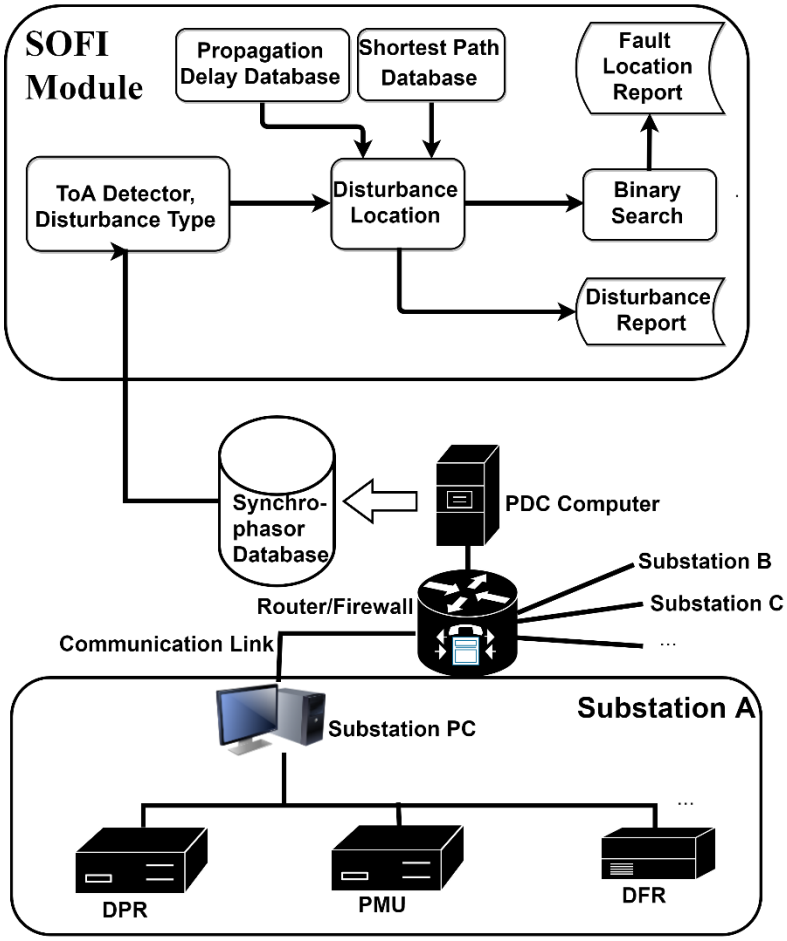

Figure 4.7 Overall structure of the SOFI tool

- The phasor angle measured by PMUs are extracted from PI database and continuously monitored. If any disturbance occurs in the system, the Time of Arrival (ToA) of electromechanical wave from the disturbance location to each PMU location is determined.
- An optimization method is used to minimize the difference between measured ToA and the "shortest path database". The outcome of optimization module is either the location of bus where load/generation outages occurred or the two-end buses of the faulty line.
- If the disturbance type is determined as fault, the binary search algorithm will be used to pinpoint the location of fault within the faulty line.

4.4.1 Electromechanical Wave Propagation Phenomena

When a disturbance occurs on a transmission line, electrical power flow changes in the network. This leads to a mismatch between electrical and mechanical torque of generators located in the vicinity. Therefore, each generator rotor angle changes to compensate the mismatch. Following the generators' rotor angle changes, the adjacent generator buses also encounter changes in their generators' rotor angle which again causes a mismatch in the electrical torque of other adjacent generators. In this fashion, the oscillation known as the electromechanical wave propagation is "seen" throughout the entire network. Electromechanical oscillations could be detected by monitoring phasor angle of bus voltages and characterized with much lower frequency (0.1–10.0Hz) than electromagnetic transients (>100 kHz) [86]. To illustrate the concept, a simple power-

system model in the form of a ring is used. Figure 4.8 shows the 64-generator ring system introduced in [86], which comprises 64 identical serially connected generators through identical transmission lines, forming a ring. The initial bus angles are evenly distributed from 0 to 360 degrees by steps equal to 360/64=5.625 degrees. Due to homogeneity and ring shape of the 64-bus system, it is well-suited to study basic aspects of electromechanical wave propagation phenomena [94], [95].

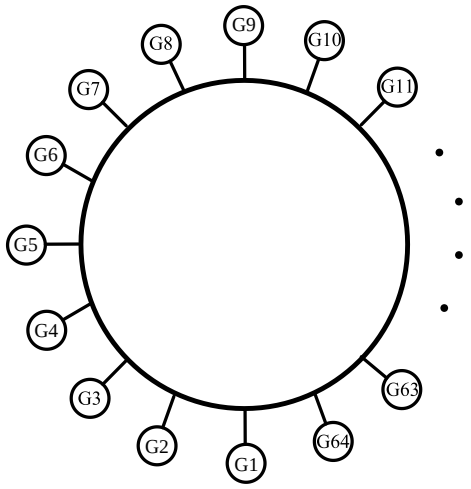

Figure 4.8 64-generator ring system

Figure 4.9 shows the phasor angle of 64-buses (in radian) with respect to time of a given disturbance occurring at bus 16 at t=0. Following the change in the angle of bus 16th shown by the dashed line in Figure 4.9, the other generators react in a similar fashion, but with a certain time delay. Plotting all the bus angles together, this time delay can be

represented as a wave modulated on voltage phase angle of buses, which travels away from the disturbance source into the network at a finite speed.

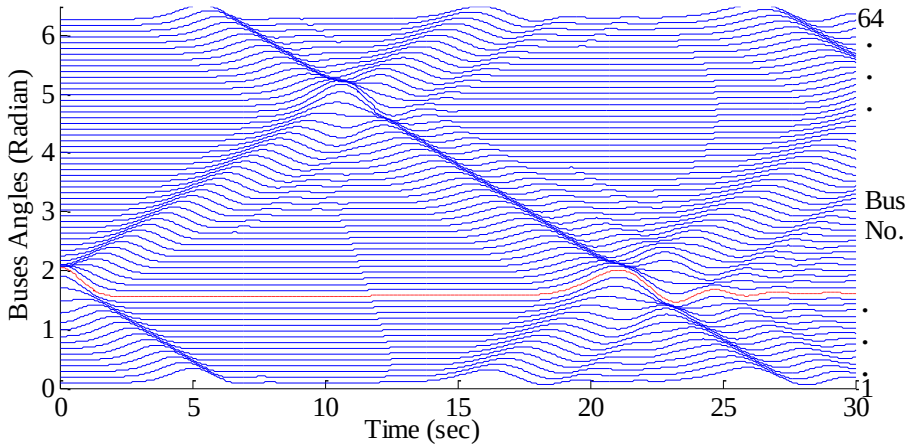

Figure 4.9 Bus angle modulation following a fault at bus 16 at t=0

4.4.2 Fault Location Methodology

As mentioned earlier, electromechanical wave originated following a disturbance travels with finite velocity in a given network. Since these waves propagate through different paths, they reach remote buses with distinct time delays which depend on each path length and propagation speed of wave through that path. Therefore, one can determine the fault location by using ToA measurements at various locations along with supporting information to determine each path's length and speed of propagation through that path.

The proposed method detects ToA of electromechanical waves modulated on phasor angle of voltage at selected buses where PMUs are available. Then the well-known Dijkstra's shortest path algorithm [93] is deployed combined with several mathematical steps to detect the faulty line. Finally location of the fault will be determined inside faulty line using binary search method. Details of the method are explained next.

4.4.2.1 ToA and Fault Type Detection

An Artificial Neural Network (ANN) method has been developed to detect ToA of electromechanical wave modulated on phase angle of voltage based on analyzing the first swing of the phase angle at buses where PMUs are installed. The proposed ANN method has been selected due to an initial assessment that this method provides higher accuracy and faster decision making outcome when compared to other pattern recognition methods which have been studied. Other methods should be explored in the future. One time calculation utilizing numerous training data sets on ANN implemented using MATLAB ANN toolbox led to an accurate ToA detector.

To develop the ToA detector, supervised training is used to train the ANN module. Figure 4.10 shows the overall structure of deployed ANN module. To differentiate between faults and other disturbances as well as different types of fault, three types of input signals were defined in the input layer. The phase angles of each three phase voltages, as well as their first and second time derivatives were selected as inputs. The inputs and desired outputs were compared in a hidden layer and errors are then propagated back through the system. The performance of system is calculated in terms of number of neurons in the hidden layer, and 4 neurons are selected as it provides the best result. The

back propagation algorithm causes the ANN system to tweak weights which control the neural network [96]. This process occurs continually till the weights are adjusted within a defined threshold.

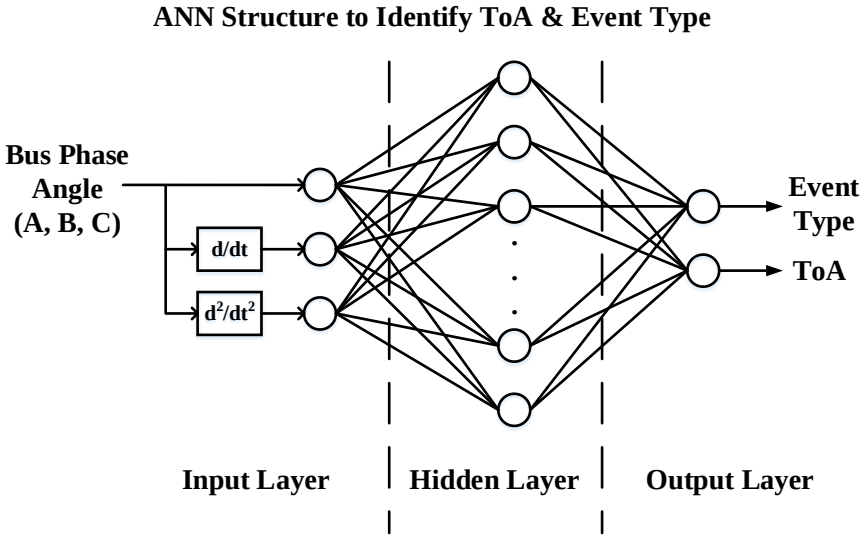

Figure 4.10 The network structure of the back propagation neural network model

The multilayer perceptron neural network with back propagation algorithm used in this study is one of most common ANN method applied in power system. The desired output of the ANN is the event type and ToA of the electromechanical wave modulated on voltage phase angle.

In the ANN training process, a set of 2000 events were created within IEEE 118 bus test system [97]. In the training process, all lines are considered to be in service. Training scenarios include generator and load outages, various types of faults with

different fault resistance at different locations. Then, another set of 500 previously unseen randomly generated event scenarios (ratio of unseen test cases to trained cases is equal to 0.25) were created to test and validate ANN-based ToA and fault type detector. Since the nature of electromechanical wave oscillation propagation and its related phase angle modulation is same for different networks, the ANN based ToA detector can be used for any given network as it has been demonstrated in section 7.

4.4.2.2 Detection of Faulty Line

Once the ToA of electromechanical wave oscillation is obtained at selected buses where PMUs are installed, it can be used to determine the faulty line. Several mathematic steps as described below must be deployed before the faulty line could be detected.

Computation of line propagation delay*:* The speed of electromechanical wave propagation is quite lower compared to electromagnetic one, which is close to speed of light. The researchers proved that applying continuum approach, the speed of electromechanical wave propagation through the network solely depends on system parameters and can be obtained as follows [86].

$$v = \sqrt{\frac{\omega \, sin\theta}{2h|z|}} \tag{4.11}$$

where ω is the nominal system frequency, θ is the line impedance angle (~90°), h is the inertia constant of generator and $|z|$ is the line impedance. Therefore, the propagation delay of each line in the network can be calculated by:

$$T_{delay-L} = \frac{x_L}{\sqrt{\frac{\omega \sin\theta}{2h|z|}}} \tag{4.12}$$

where L=1,…,k represents each transmission line in the network and xL is the total length of line L. Assuming that length and impedance of transmission lines are known, electromechanical wave propagation delay through each transmission line can be calculated using (4.12).

Calculation of measured ToA matrix: Figure 4.11 is used to explain computation of the shortest time delay matrix. As shown in Figure 4.11, for the given network assume that PMU measurements are available at buses A, B, C and D, while a fault occurs at an unknown bus k (this assumption will be removed later). The propagation delay of electromechanical wave to reach bus A after fault occurs at bus k can be obtained by:

$$t_{Ak} = t_A - t_k \tag{4.13}$$

where t_k represents fault initiation time at bus k, t_A represents ToA of electromechanical wave at bus A and t_{Ak} is the propagation delay of electromechanical wave to arrive at bus A. Since the fault initiation time t_k is unknown, it is impossible to obtain t_{Ak}. Suppose that bus A is the first to receive the propagated wave. It can be used as the time reference.

Therefore, the wave propagation delay from bus k to bus B with respect to ToA of electromechanical wave at bus A (t_A) can be defined as:

$$t_{BA} = t_{Bk} - t_{Ak} = (t_B - t_k) - (t_A - t_k) = t_B - t_A \tag{4.14}$$

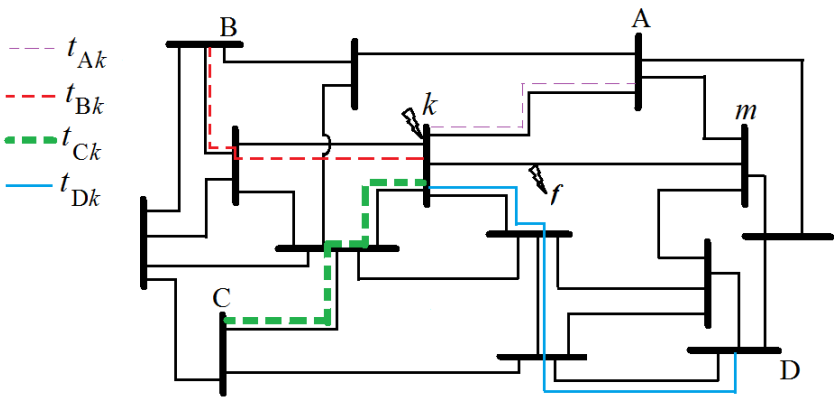

Figure 4.11 Illustration of theoretical and measured delay matrices

It should be noted that (4.14) is always correct due to the fact that the electromechanical waves propagate along the transmission lines is always following the shortest path rule.

The electromechanical wave propagation delay from bus k to other buses with respect to ToA of electromechanical wave at bus A (t_A) can be defined similar to (4.14). Hence, the measured propagation time delay matrix can be defined as:

$$T_m = [t_{BA} \quad t_{CA} \quad t_{DA}] \tag{4.15}$$

Calculation of theoretical time delay matrix: Since the propagation delay of each transmission line is known by (4.12), vector of time differences resulting from the shortest propagation delay could be computed as follows.

$$T_{sp-x} = [\tau_{Bx} - \tau_{Ax} \quad \tau_{Cx} - \tau_{Ax} \quad \tau_{Dx} - \tau_{Ax}] \tag{4.16}$$

where τ_{Ax}, τ_{Bx}, τ_{Cx} and τ_{Dx} are the theoretical shortest propagation time delay from buses A, B, C and D to any arbitrary bus x, respectively. It can be rewritten as:

$$T_{sp-x} = [\tau_{BAx} \quad \tau_{CAx} \quad \tau_{DAx}] \tag{4.17}$$

The shortest time delay path for each bus pair is computed utilizing the Dijkstra's algorithm. One time computation of (4.17) with Dijkstra's algorithm is valid for a given topology before any line switching takes place. After any topology changes, the calculation must be repeated to update the matrix elements.

Definition of minimum error function: As shown in Figure 4.11, if the fault occurs at unknown bus k, the calculated T_{sp-k} should identically match T_m captured by ToA detectors. Therefore, one can define P_x as follows and then check it for all buses to find the bus that corresponds to the minimum (zero) P_x value.

$$P_x = Min\left(\left\|T_{sp-x} - T_m\right\|\right) \qquad x = 1, \dots, n \tag{4.18}$$

where $x = 1, \dots, n$ is the total number of buses and P_x is the minimum norm linked with bus x.

As previously stated, we assumed that faults only take place at buses, which is not realistic in actual power system. Consequently, the methodology must be revised, so that the method can be applied for any arbitrary fault located along transmission lines.

As shown in Figure 4.11, if the fault occurs at an arbitrary point *f*, two buses corresponding to the minimum two values obtained from (4.18) will be selected. The

network topology will be checked to see if this pair of buses has a direct link to each other. If so, the line connecting these two buses will be declared as faulty line.

If there is no direct link between the two buses, then each line connected to the two buses will be considered as the faulty line candidate. Hence, fault location calculation must be repeated for all possible candidates which can be tolerated due to limited number of lines connected to the pair of suspect buses.

4.4.2.3 Fault Location Using Binary Search

Once the faulty line is determined, the exact location of fault can be derived by adding fictitious buses and dividing the faulty line into two line segments using binary search approach [96]. As shown in Figure 4.12, the first fictitious bus divides the faulty line $(m-k)$ into two equal sections $(a_1-m$ and $a_1-k)$. Then, (4.18) will be recalculated for $x=a_1$, m and k. Then, the two buses which correspond to lowest P_x values will be treated as faulty section. Similarly, the second fictitious bus divides the faulty section (a_1-k in Figure 4.12) into equal sections (a_1-k and a_2-k) and so on.

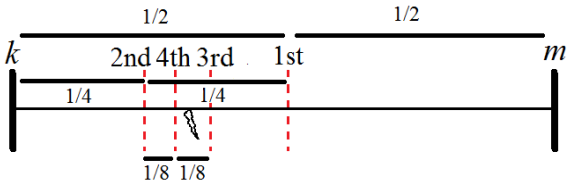

Figure 4.12 Illustration of the binary search used for fault location method

If this process occurs over and over, mathematically, after adding i^{th} fictitious bus, the location of fault will be determined within the following error:

$$E = \left(\frac{1}{2^i}\right) \times 100 \tag{4.19}$$

In this study, we considered adding 5 fictitious buses to reach accuracy greater than 99%.

4.4.3 Case Study

In this section, the proposed SOFI method is tested using IEEE118 bus test system (Figure 4.13) [98]. The proposed methodology does not require optimal PMU placement. To avoid an arbitrary placement of PMUs, suggested optimal PMU placement studied in [99] is used to demonstrate the effectiveness of the proposed method for a given PMU optimal placement driven by other applications. Designing an optimal PMU placement considering electromechanical wave propagation based fault location as a driving reason for the PMU placement decision could be a future work of this study.

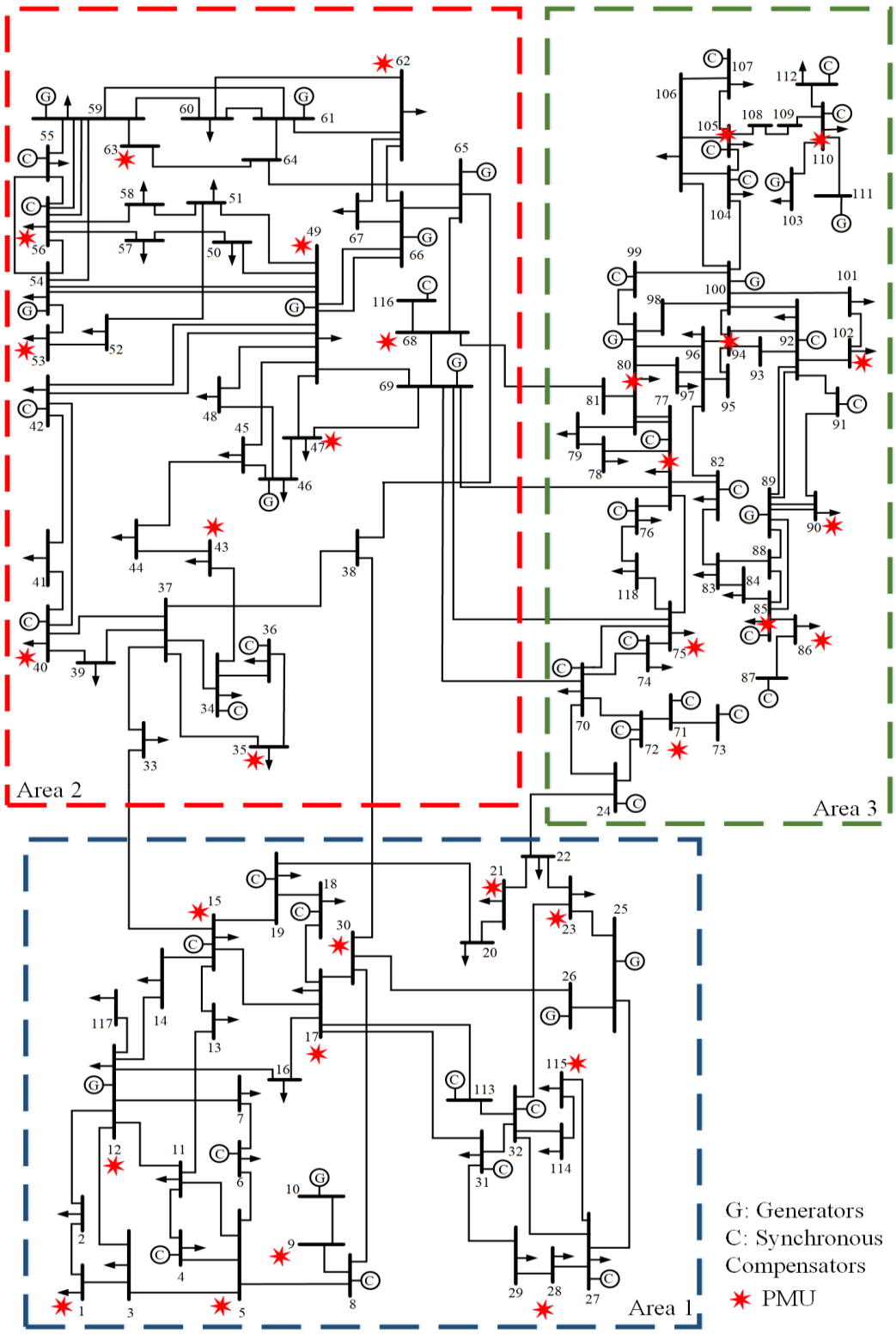

Figure 4.13 Testing SOFI tool with IEEE 118-bus test system

4.4.3.1 Testing with Different Fault Scenarios

In this subsection, the proposed method is tested by changing fault parameters (fault resistance, fault distance, fault type and faulty line). Table 6 brings summary of results for a few test cases. In all cases, the proposed method correctly detects fault type using proposed ANN module and then identifies faulty lines.

TABLE 6 FAULT LOCATION RESULTS UNDER DIFFERENT FAULT SPECIFICATION

Case no.	Faulty line	Fault type	Fault resistance (Ω)	Fault distance (p.u.)	Fault location error (%)
1	19-20	a-g	1	0.1	0.73
2				0.5	0.59
3				0.9	0.34
4			20	0.1	1.23
5				0.5	0.92
6				0.9	0.74
7		ab-g	1	0.1	0.56
8				0.5	0.51
9				0.9	0.49
10			20	0.1	0.84
11				0.5	0.83
12				0.9	0.77
13	100-106	ab	1	0.1	0.44
14				0.5	0.47
15				0.9	0.62
16			20	0.1	0.75
17				0.5	0.67
18				0.9	0.93
19		abc-g	1	0.1	0.17
20				0.5	0.14
21				0.9	0.15
22			20	0.1	1.11
23				0.5	0.96
24				0.9	1.04

Furthermore, the associated fault location error for each case demonstrates that the proposed method is able to accurately locate faults (in most cases error is within 1%).

Figure 4.14 represents the phasor angle captured by PMUs related to cases 6, 13 and 20 from Table 6 (only 4 phasor angles from PMUs with smallest ToAs were plotted to avoid confusion).

In Figure 4.14.a, the electromechanical wave oscillation following the fault (a-g with 20Ω at 0.9 pu from bus 19) on line 19-20 is first detected at bus 21 at t=5.43 sec and then detected at buses 15, 23 and 17, respectively.

In Figure 4.14.b, the electromechanical wave following the fault (ab with 1Ω at 0.1 pu from bus 19) on line 19-20 is first detected at bus 21 at t=5.97 sec and then detected at buses 15, 17 and 30, respectively.

In Figure 4.14.c, the electromechanical wave following the fault (abc-g with 1Ω at 0.5 pu from bus 100) on line 100-106 is first detected at bus 94 at t=5.66 sec and then detected at buses 105, 110 and 80, respectively. In each case, after detection of ToAs of electromechanical wave oscillations at PMU locations, T_m and P_x will be calculated from (13) and (16), respectively.

The location of faults for these three examples are calculated using proposed binary search method with error equal to 0.74%, 0.44% and 0.14%, respectively.

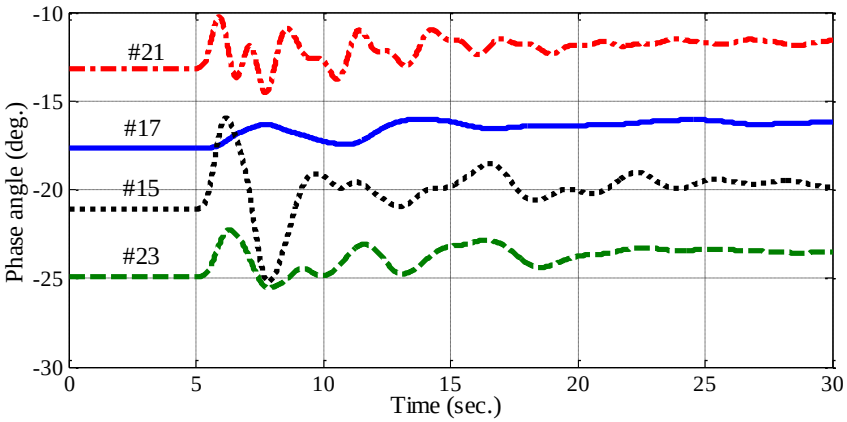

(a) Case 6

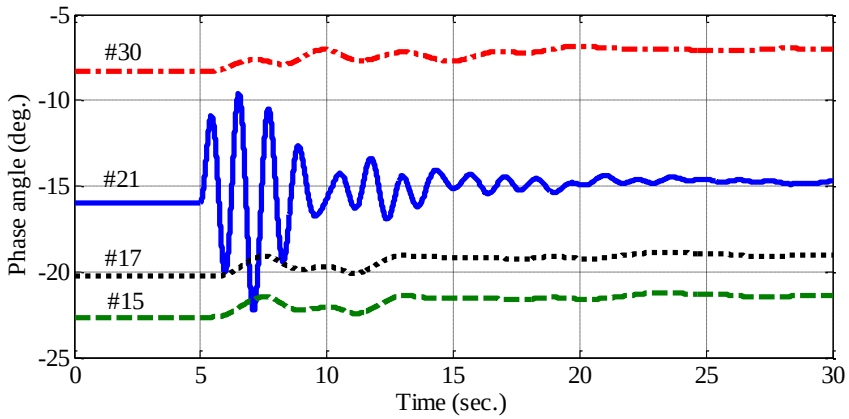

(b) Case 13

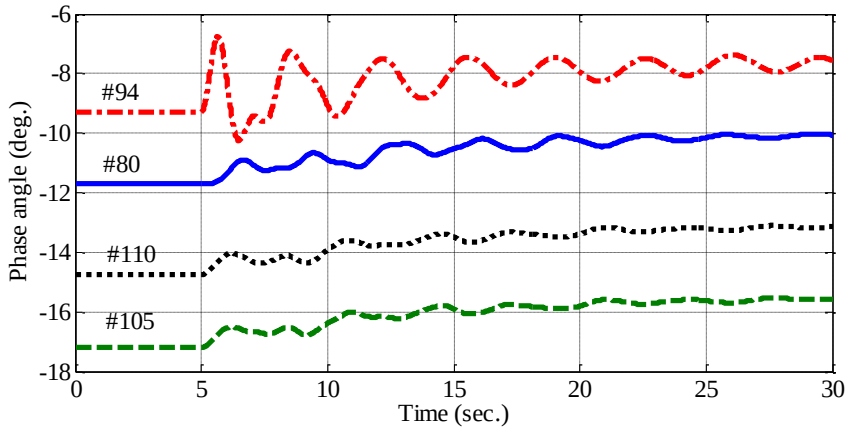

(c) Case 20

Figure 4.14 Phasor angle of PMU equipped buses of IEEE118 bus system

Table 7 shows the average error percentage of the proposed fault location method under numerous test cases. As depicted in Figure 4.13, IEEE 118 bus system can be divided into three areas with almost same number of PMUs. We considered 9 points to insert faults (0.1pu to 0.9pu with span of 0.1pu) on every single line in these three areas. It can be concluded from results in Table 7 that area 1 which has higher ratio of PMU to line (0.216) is linked with least average error. However, area 2 which has lower ratio of PMU to line (0.147) has the highest average error.

TABLE 7 FAULT LOCATION RESULTS ON DIFFERENT REGIONS

Area	**Number of lines**	**Number of PMUs**	**PMU/Line ratio**	**Fault location error (%)**
Area 1	51	11	0.216	0.352
Area 2	68	10	0.147	0.978
Area 3	67	11	0.164	0.754
Total	**186**	**32**	**0.172**	**0.724**

4.4.3.2 Impact of PMU Bad Data

One of the main concerns for applications based on wide area measurements is the accuracy and calibration of PMUs. Since PMU measurements might be affected by inaccuracy of algorithms, or by being out of calibration, different test cases were simulated by artificially adding error to phasor angle measurements.

Figure 4.15 shows the average percent error of proposed fault location method under three main scenarios. In scenario 1, first column represents the average percent error

corresponding to 20 fault cases simulated in area 1 (see Figure 4.13), while the manipulated PMU measurements are among PMUs within area 1. Similarly, the second and third columns show the average percent errors corresponding to same faults in area 1, while the manipulated PMU measurements are within area 2 and 3, respectively. It can be seen that the effect of PMU bad data is felt when the affected PMUs are in the same area where the faults are located. The same can be concluded from the second and third scenarios where faults occurred in area 2 and area 3, respectively. Finally, from the results one can conclude that PMU bad data will affect the accuracy of proposed fault location. However, the methodology is still able to operate within acceptable error (less than 2%).

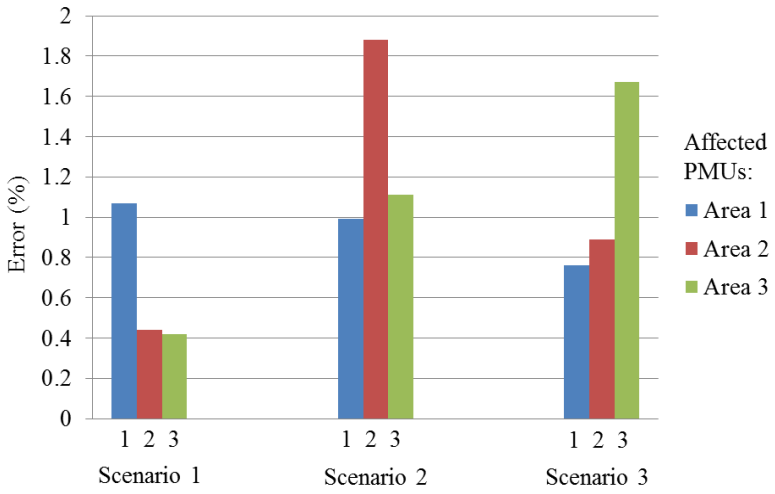

Figure 4.15 Fault location percent error under effect of PMU bad data

4.4.3.3 Impact of Topology Changes

Following a topology change, two situations could be considered for the proposed fault location method. First, the shortest path database of proposed method will be recalculated considering updated information on system current topology. Second, due to unrelated reasons, current topology of system may not be updated. Table 8 shows the result of simulations which have been carried out by switching off lines and simulating faults to address the impact of topology change on the fault location method.

TABLE 8 IMPACT OF TOPOLOGY CHANGES AND PMU AVAILABILITY

Case no.	Faulty line	Two Switched lines	Two Unavailable PMUs Location	Error before changes (%)	Error after changes (%)
Switched lines do not contribute in shortest path					
1	1-2	55-59, 24-70	49, 71	0.32	0.32
2	1-2	55-59, 24-70	9, 21	0.32	0.41
3	41-42	3-5, 78-79	1, 110	0.86	0.86
4	41-42	3-5, 78-79	35, 56	0.86	1.07
5	76-118	5-6, 37-39	17, 40	0.49	0.49
6	76-118	5-6, 37-39	71, 94	0.49	0.70
Switched lines contributes in shortest path but located far from fault point					
7	1-2	20-21, 28-29	49, 71	0.32	0.32
8	1-2	20-21, 28-29	9, 21	0.32	0.46
9	41-42	15-17, 69-77	1, 110	0.86	0.86
10	41-42	15-17, 69-77	35, 56	0.86	1.11
11	76-118	22-23, 47-69	17, 40	0.49	0.49
12	76-118	22-23, 47-69	71, 94	0.49	0.71
Switched lines contributes in shortest path and located close to fault point					
13	1-2	5-8, 2-12	49, 71	0.32	0.76
14	1-2	5-8, 2-12	9, 21	0.32	1.48
15	41-42	34-43, 47-49	1, 110	0.86	1.44
16	41-42	34-43, 47-49	35, 56	0.86	2.89
17	76-118	76-77, 94-96	17, 40	0.49	1.63
18	76-118	76-77, 94-96	71, 94	0.49	2.01

The simulation results illustrate that fault location method would be affected only in certain cases where the line being switched off is contributing in the shortest path of electromechanical wave propagation from fault to buses with PMUs. The fault location error is acceptable if the switched line is far from the faulty line. As described in previous subsection, PMUs which are far from faulty line cannot dramatically affect output of the proposed method. To detect a topology change, a pre-defined signal (ping) could be generated at one of the PMU equipped buses and ToAs are measured at other PMU locations. If there is any difference between one of the measured ToAs and corresponding calculated ToAs, a topology change across the shortest path among corresponding two buses is determined.

4.4.3.4 Impact of Availability of PMUs

The other concern associated with wide area measurements based applications is unavailability of PMUs due to various reasons such as communication failure, device failure, etc. In such cases, applications must be robust enough to tolerate missing measurements from one or more PMUs.

Figure 4.16 depicts the average percent error of fault location algorithm versus the total number of PMUs assumed to be out of service. After taking each PMU out of service, 20 faults are simulated and average percent error is calculated to plot Figure 4.16. Similar to previous subsection, three main scenarios were simulated considering three areas in Figure 4.13. In Figure 4.16.a, faults are simulated in area 1, while dash, dash-dot and dotted lines are related to the cases where out of service PMUs are within areas 1, 2 and 3, respectively.

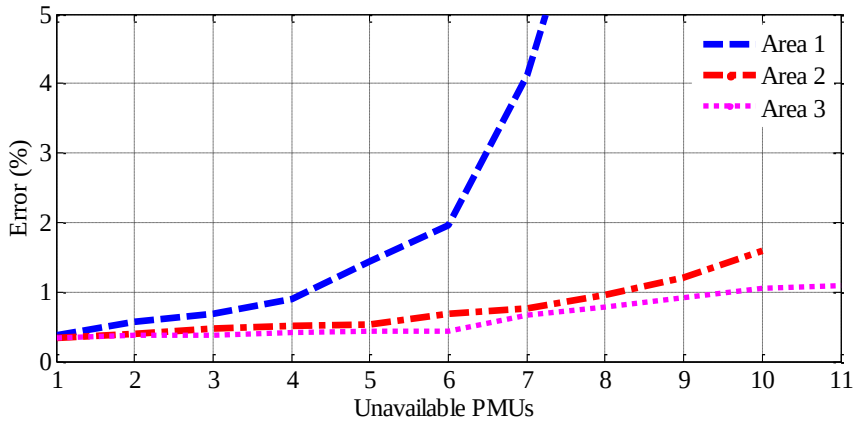

(a)

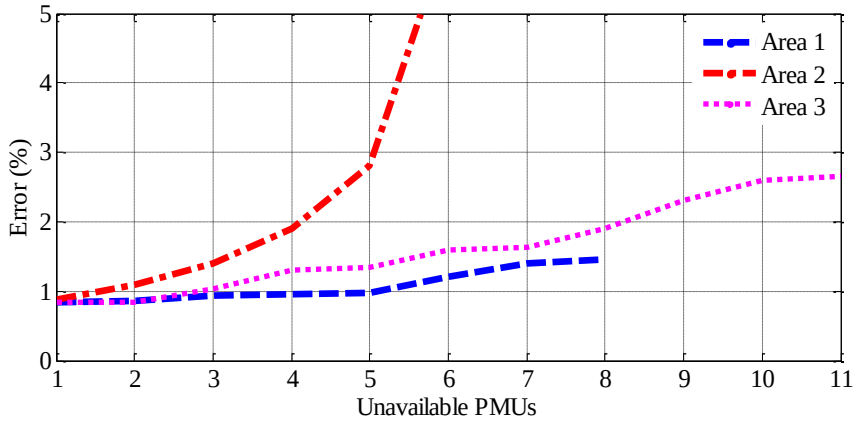

(b)

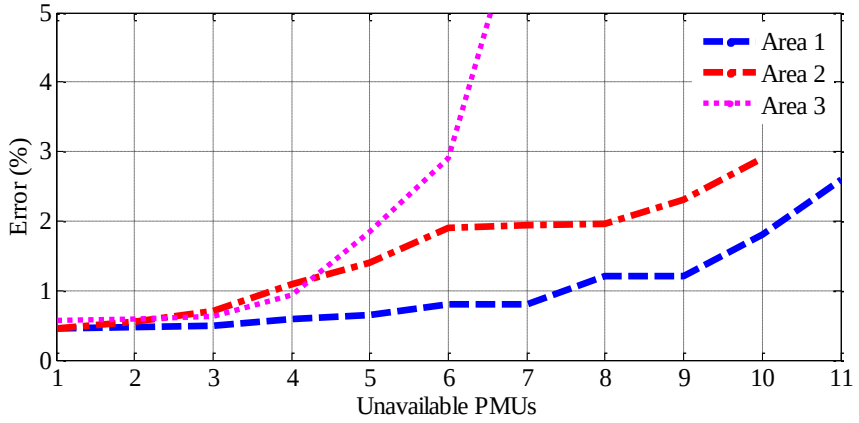

(c)

Figure 4.16 Effect of unavailability of PMUs on fault location accuracy

As it can be seen, the average percent error is less than 2% (dashed line) even after removing first 6 PMUs from area 1. It can be concluded that even under availability of 5 PMUs in area 1, the method operates with acceptable accuracy. The error remains under 2% even after removing all PMUs in areas 2 and 3, respectively. The same observation could be obtained by looking into Figure 4.16.b and Figure 4.16.c. It can be concluded that fault location method on each of the three areas is robust to unavailability of PMUs in other two areas. Since optimal fault location results may be sensitive to placement of PMUs and location of fault occurrence, one can conclude that the proposed method can operate within acceptable error (< 3%) with quite lower number of PMUs than what is needed to satisfy the observability requirement suggested by an optimal PMU placement.

The last scenario is designed to consider the impact of combination of topology changes and PMU availability on the accuracy of fault location method. Table 9 shows the result of fault location method by inserting faults at three different lines while two lines and two PMUs are taken out.

In cases 1 and 2, faults occurred on line 1-2 (area 1) while lines (55-59 and 24-70) are taken out but are not contributing to the shortest path to PMUs. In case 1 where the two out of service PMUs (49, 71) are not located in the same area as fault, the fault location error remains the same. In case 2 where the two out of service PMUs (49, 71) are located in the same area as fault, the fault location error slightly increases from 0.32% to 0.41%.

In cases 7 and 8, all simulation parameters are the same except switched lines which are selected from those that contribute to the shortest path but are located far from the fault point. Similarly, in cases 13 and 14, all simulation parameters are the same except

the switched lines are selected from those that contribute to the shortest path and are located close to the fault point.

From Table 9, it can be concluded that the fault location accuracy would not be affected if PMUs or lines out of service are away from the fault point. The errors would be tolerable even if the out of service PMUs and lines are in the same area where the fault has occurred.

TABLE 9 IMPACT OF TOPOLOGY CHANGES ON FAULT LOCATION

Case no.	**Faulty line**	**Switched off line**	**Error before topology change (%)**	**Error after topology change (%)**
Switched line does not contribute in shortest path				
1	1-2	55-59	0.32	0.32
2	25-27	34-37	0.44	0.44
3	41-42	78-79	0.86	0.86
4	76-118	37-39	0.49	0.49
5	110-112	12-117	0.97	0.97
Switched line contributes in shortest path but located far from fault point				
6	1-2	20-21	0.32	0.47
7	25-27	63-64	0.44	0.61
8	41-42	15-17	0.86	0.89
9	76-118	47-69	0.49	0.93
10	110-112	68-81	0.97	0.99
Switched line contributes in shortest path and located close to fault point				
11	1-2	3-5	0.32	-
12	25-27	27-28	0.44	5.98
13	41-42	40-41	0.86	7.41
14	76-118	77-82	0.49	4.75
15	110-112	94-100	0.97	3.64

4.5 Conclusion

In this section, two synchrophasor based tools have been proposed, one to monitor the system in real time, and the other one to alarm operators and corresponding automated control schemes to initiate remedial actions, once a series of outages is detected. The SOVI tool provides vital information regarding vulnerability of the different areas of the system which will be later used as decision making variables to trigger other tools to prevent un-wanted islands and blackouts. The SOFI tool detects disturbances, and provides immediate topology update. So the error caused by divergence of conventional state estimator under some contingency scenarios could be avoided.

These tools have been tested against various scenarios and their reliable performance was demonstrated.

5. SYNCHROPHASOR BASED ISLANDING PREDICTION TOOL

5.1 Overview

The steady state progression stage of cascading outages is an important period, since the system operators may have enough time to evaluate the system condition, identify some vulnerable contingencies, and take some control actions to increase the security level. In this section, a two-step islanding prediction method to inform the operator regarding possibility of un-wanted island formation, namely SIP tool, is studied.

5.2 Generation of the Offline Islanding Database

5.2.1 Observability Matrix

The proposed two step SIP method starts with creation of an islanding database which later can be used to generate the training dataset for the proposed Adaptive Neural Network (ANN) module. Due to the limited number of the actual islanding cases occurring in a given power system, it is vital to generate accurate simulated islanding scenarios in order to train the ANN module.

In power systems, the term “observability” is defined as the possibility of accessing one bus from any other bus in the system [100]. Also, the term “depth of observability” of a system is referred to as the maximum length of the shortest path between any two buses in that system. Next, we describe that how the incidence matrix which has been introduced in section 4 can be used to obtain *observability matrix* and *depth of observability* of a system.

For instance, consider the IEEE 9-bus system shown in Figure 5.1. It can be easily seen from the figure that:

- The system is observable, since there is a way to access any given bus in the system from any other buses in the system;
- The depth of observability is equal to 4, meaning that any given bus in this system can be accessed from any other buses within 4 steps or less.

In this case, it was easy to determine the system observability and its depth, but for a larger system, it won't be feasible to manually obtain the depth of observability.

To systematically determine the system observability and its depth, we first explain how the incidence matrix which has been introduced in section 4 can be used to define the observability matrix [101].

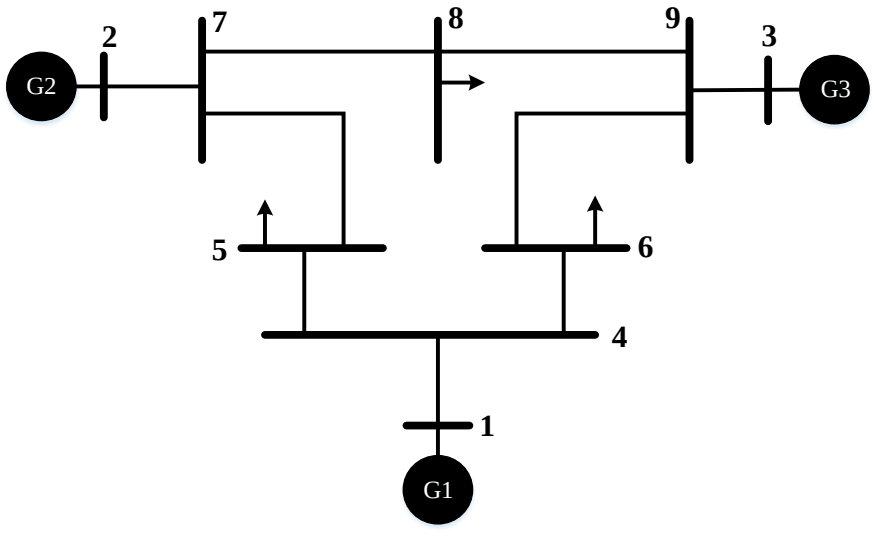

Figure 5.1 IEEE 9-bus test system

The k[th] depth observability matrix is defined as below:

$$C_{n\times n}^{k} = \{c_{ij}\} \quad c_{ij} = \begin{cases} 1 & if\ the\ shortest\ path\ between\ buses\ i\ and\ j\ is \leq k \\ 0 & otherwise \end{cases} \tag{5.1}$$

With this definition, one can realize that the 1[st] depth observability matrix is equal to the incidence matrix. The k[th] depth observability matrix can be obtained by computing the k[th] power of the system incidence matrix and change all non-zero elements to 1. All diagonal elements of the observability matrix are equal to 1, which imply each bus is observable by itself.

For example, the 1[st] depth observability matrix of the system in Figure 5.1 can be obtained using definition of incidence matrix in (4.1).

$$C^1 = A = \begin{bmatrix} 1 & 0 & 0 & 1 & 0 & 0 & 0 & 0 & 0 \\ 0 & 1 & 0 & 0 & 0 & 0 & 1 & 0 & 0 \\ 0 & 0 & 1 & 0 & 0 & 0 & 0 & 0 & 1 \\ 1 & 0 & 0 & 1 & 1 & 1 & 0 & 0 & 0 \\ 0 & 0 & 0 & 1 & 1 & 0 & 1 & 0 & 0 \\ 0 & 0 & 0 & 1 & 0 & 1 & 0 & 0 & 1 \\ 0 & 1 & 0 & 0 & 1 & 0 & 1 & 1 & 0 \\ 0 & 0 & 0 & 0 & 0 & 0 & 1 & 1 & 1 \\ 0 & 0 & 1 & 0 & 0 & 1 & 0 & 1 & 1 \end{bmatrix}$$

The 2[nd] depth observability matrix is calculated by computing (A×A) and replacing all non-zero elements with 1.

$$C^2 = \begin{bmatrix} 1 & 0 & 0 & 1 & 1 & 1 & 0 & 0 & 0 \\ 0 & 1 & 0 & 0 & 1 & 0 & 1 & 1 & 0 \\ 0 & 0 & 1 & 0 & 0 & 1 & 0 & 1 & 1 \\ 1 & 0 & 0 & 1 & 1 & 1 & 1 & 0 & 1 \\ 1 & 1 & 0 & 1 & 1 & 1 & 1 & 1 & 0 \\ 1 & 0 & 1 & 1 & 1 & 1 & 0 & 1 & 1 \\ 0 & 1 & 0 & 1 & 1 & 0 & 1 & 1 & 1 \\ 0 & 1 & 1 & 0 & 1 & 1 & 1 & 1 & 1 \\ 0 & 0 & 1 & 1 & 0 & 1 & 1 & 1 & 1 \end{bmatrix}$$

The elements of 2nd depth observability matrix is equal to one if the shortest path between the two corresponding buses is ≤ 2. For example, the shortest paths between bus 1 and buses 4, 5 and 6 are equal to 1, 2 and 2, respectively. Consequently, the associated elements of C^2 are ($C^2(1,4)$, $C^2(1,5)$, $C^2(1,6)$, $C^2(4,1)$, $C^2(5,1)$, $C^2(6,1)$) equal to 1.

Similarly, the 3rd and 4th depth system observability matrices can be obtained as below:

$$C^3 = \begin{bmatrix} 1 & 0 & 0 & 1 & 1 & 1 & 1 & 0 & 1 \\ 0 & 1 & 0 & 1 & 1 & 0 & 1 & 1 & 1 \\ 0 & 0 & 1 & 1 & 0 & 1 & 1 & 1 & 1 \\ 1 & 1 & 1 & 1 & 1 & 1 & 1 & 1 & 1 \\ 1 & 1 & 0 & 1 & 1 & 1 & 1 & 1 & 1 \\ 1 & 0 & 1 & 1 & 1 & 1 & 1 & 1 & 1 \\ 1 & 1 & 1 & 1 & 1 & 1 & 1 & 1 & 1 \\ 0 & 1 & 1 & 1 & 1 & 1 & 1 & 1 & 1 \\ 1 & 1 & 1 & 1 & 1 & 1 & 1 & 1 & 1 \end{bmatrix} \qquad C^4 = \begin{bmatrix} 1 & 1 & 1 & 1 & 1 & 1 & 1 & 1 & 1 \\ 1 & 1 & 1 & 1 & 1 & 1 & 1 & 1 & 1 \\ 1 & 1 & 1 & 1 & 1 & 1 & 1 & 1 & 1 \\ 1 & 1 & 1 & 1 & 1 & 1 & 1 & 1 & 1 \\ 1 & 1 & 1 & 1 & 1 & 1 & 1 & 1 & 1 \\ 1 & 1 & 1 & 1 & 1 & 1 & 1 & 1 & 1 \\ 1 & 1 & 1 & 1 & 1 & 1 & 1 & 1 & 1 \\ 1 & 1 & 1 & 1 & 1 & 1 & 1 & 1 & 1 \\ 1 & 1 & 1 & 1 & 1 & 1 & 1 & 1 & 1 \end{bmatrix}$$

It can be seen that all elements of 4th depth system observability matrix is equal to 1, which verifies the earlier conclusion obtained by manual investigation.

Now that the concept of observability matrix has been explained, we use another example to show how it can be used to create islanding database for the purpose of training the ANN method which will be discussed later in this section.

In Figure 5.2, the IEEE 9-bus system is modified by switching off the lines (5-7) and (6-9). The 1st, 2nd, 3rd and 4th depth observability matrices of the modified system are equal to:

$$C^1 = \begin{bmatrix} 1 & 0 & 0 & 1 & 0 & 0 & 0 & 0 & 0 \\ 0 & 1 & 0 & 0 & 0 & 0 & 1 & 0 & 0 \\ 0 & 0 & 1 & 0 & 0 & 0 & 0 & 0 & 1 \\ 1 & 0 & 0 & 1 & 1 & 1 & 0 & 0 & 0 \\ 0 & 0 & 0 & 1 & 1 & 0 & 0 & 0 & 0 \\ 0 & 0 & 0 & 1 & 0 & 1 & 0 & 0 & 0 \\ 0 & 1 & 0 & 0 & 0 & 0 & 1 & 1 & 0 \\ 0 & 0 & 0 & 0 & 0 & 0 & 1 & 1 & 1 \\ 0 & 0 & 1 & 0 & 0 & 0 & 0 & 1 & 1 \end{bmatrix} \quad C^2 = \begin{bmatrix} 1 & 0 & 0 & 1 & 1 & 1 & 0 & 0 & 0 \\ 0 & 1 & 0 & 0 & 0 & 0 & 1 & 1 & 0 \\ 0 & 0 & 1 & 0 & 0 & 0 & 0 & 1 & 1 \\ 1 & 0 & 0 & 1 & 1 & 1 & 0 & 0 & 0 \\ 1 & 0 & 0 & 1 & 1 & 1 & 0 & 0 & 0 \\ 1 & 0 & 0 & 1 & 1 & 1 & 0 & 0 & 0 \\ 0 & 1 & 0 & 0 & 0 & 0 & 1 & 1 & 1 \\ 0 & 1 & 1 & 0 & 0 & 0 & 1 & 1 & 1 \\ 0 & 0 & 1 & 0 & 0 & 0 & 1 & 1 & 1 \end{bmatrix}$$

$$C^3 = \begin{bmatrix} 1 & 0 & 0 & 1 & 1 & 1 & 0 & 0 & 0 \\ 0 & 1 & 0 & 0 & 0 & 0 & 1 & 1 & 1 \\ 0 & 0 & 1 & 0 & 0 & 0 & 1 & 1 & 1 \\ 1 & 0 & 0 & 1 & 1 & 1 & 0 & 0 & 0 \\ 1 & 0 & 0 & 1 & 1 & 1 & 0 & 0 & 0 \\ 1 & 0 & 0 & 1 & 1 & 1 & 0 & 0 & 0 \\ 0 & 1 & 1 & 0 & 0 & 0 & 1 & 1 & 1 \\ 0 & 1 & 1 & 0 & 0 & 0 & 1 & 1 & 1 \\ 0 & 1 & 1 & 0 & 0 & 0 & 1 & 1 & 1 \end{bmatrix} \quad C^4 = \begin{bmatrix} 1 & 0 & 0 & 1 & 1 & 1 & 0 & 0 & 0 \\ 0 & 1 & 0 & 0 & 0 & 0 & 1 & 1 & 1 \\ 0 & 0 & 1 & 0 & 0 & 0 & 1 & 1 & 1 \\ 1 & 0 & 0 & 1 & 1 & 1 & 0 & 0 & 0 \\ 1 & 0 & 0 & 1 & 1 & 1 & 0 & 0 & 0 \\ 1 & 0 & 0 & 1 & 1 & 1 & 0 & 0 & 0 \\ 0 & 1 & 1 & 0 & 0 & 0 & 1 & 1 & 1 \\ 0 & 1 & 1 & 0 & 0 & 0 & 1 & 1 & 1 \\ 0 & 1 & 1 & 0 & 0 & 0 & 1 & 1 & 1 \end{bmatrix}$$

It can be seen that the C^3 and C^4 are equal to each other, which means that the final depth matrix is C^3. Despite the first example, in this case all elements of the final depth observability matrix are not equal to 1. By digging into C^3 as shown below, one can realize that five diagonal blocks are formed (bus 1, bus 2, bus 3, buses 4-6, buses 7-9).

$$C^3 = \begin{bmatrix} 1 & 0 & 0 & 1 & 1 & 1 & 0 & 0 & 0 \\ 0 & 1 & 0 & 0 & 0 & 0 & 1 & 1 & 1 \\ 0 & 0 & 1 & 0 & 0 & 0 & 1 & 1 & 1 \\ 1 & 0 & 0 & 1 & 1 & 1 & 0 & 0 & 0 \\ 1 & 0 & 0 & 1 & 1 & 1 & 0 & 0 & 0 \\ 1 & 0 & 0 & 1 & 1 & 1 & 0 & 0 & 0 \\ 0 & 1 & 1 & 0 & 0 & 0 & 1 & 1 & 1 \\ 0 & 1 & 1 & 0 & 0 & 0 & 1 & 1 & 1 \\ 0 & 1 & 1 & 0 & 0 & 0 & 1 & 1 & 1 \end{bmatrix}$$

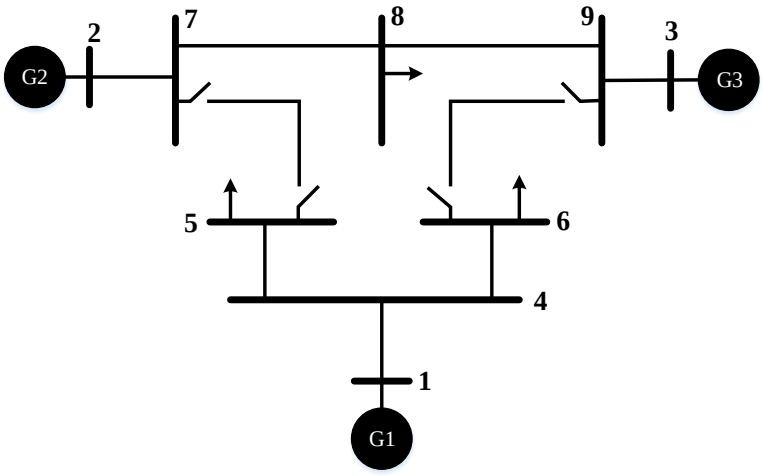

Figure 5.2 IEEE 9-bus test system

Furthermore, the off-diagonal blocks show the relationships between each diagonal bus group such that if elements are equal to 1, the blocks are in the same island. In this example, blocks 1 and 4 which includes buses (1, 4, 5 and 6) are in one island, and blocks 2, 3 and 5 which includes buses (2, 3, 7, 8 and 6) are in the other island. This can be visually confirmed by looking at Figure 5.2.

In summary, if all elements of the final observability depth matrix of a system are equal to 1, the entire system is connected. If not, the total number of islands as well as buses within each of them can be obtained only based on the final observability depth matrix. One can use the incidence matrix of a power system to determine all possible islanding scenarios in the system. This can be achieved by tripping one line (replacing associated 1s with 0s in the incidence matrix) and calculating the final observability depth matrix. This process can be expanded by tripping multiple lines and repeating the same procedure.

5.2.2 Constraints to Reduce the Size of Database

The complete testing combinations for tripping up to 3 lines in the IEEE 9-bus test system with 9 bus and 9 lines is equal to 129. Therefore, the matrix multiplication procedure (as described in section 5.2.1) to obtain final observability depth matrix should be repeated 129 times.

$$\text{Iterations} = \binom{9}{1} + \binom{9}{2} + \binom{9}{3} = 9+36+84=129 \tag{5.2}$$

Table 10 compares the total number of iterations for different test systems and different number of tripped lines without adding any constraints. The number of iterations will quickly grow as the size of system and number of tripped lines increases.

TABLE 10 ITERATIONS REQUIRED TO DETERMINE ISLANDING SCENARIOS

		Test systems			
		IEEE9-bus	IEEE118-bus	IEEE300-bus	European 1354-bus
No. Tripped lines	1	9	179	306	1751
	2	45	16,110	46,971	1,533,876
	3	129	956,039	4,775,691	894,762,751
	4	255	42,312,915	362,976,231	~3.91e+11

Given the fact that for larger systems the size of incidence matrix will also increases (which means higher computation burden), the process of islanding database creation without defining a proper constraint is infeasible. Numerous unrealistic combinations including many infeasible islanding scenarios are taken into account. For

instance, if line 1 in Figure 5.3 is tripped, the system will be separated into two islands. The same islands will be formed if any of lines 2, 3 and 4 is also tripped along with line 1. However, tripping line 1 with lines 3 and 4 will result in an infeasible islanding scenario due to their geographical and electrical distance to line 1.

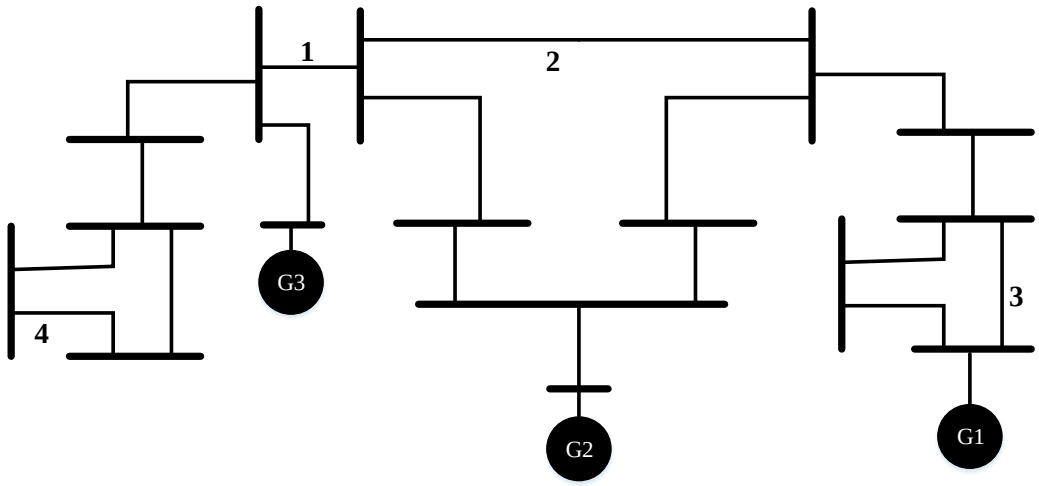

Figure 5.3 Illustration of infeasible islanding scenarios

Since the concept of observation depth is closely aligned with the geographical and electrical distances, it can be used to limit the search area in creation of the island scenarios. The certain geographical and electrical distance could be equivalently converted by certain observation depth n. Changing the value of n indicates involving larger/smaller area geographically and/or implementing a longer/shorter hidden failure chain [100].

Using observability depth as the constraint can tremendously reduce the computational burden by eliminating those unrealistic cases. For instance, by setting the depth of observation to k=5, the number combinations for up to 3 tripped lines in the 1354-bus system in Table 10 will be limited to less than 40,000. Therefore, the number of combinations will be less than 0.00005 of total one.

5.3 Adaptive Neural Network Module to Predict Islands

The underlying hypothesis in this method is to perform a data mining process based on measurements provided by PMUs to predict islanding before it occurs. A series of dynamic simulations of various islanding scenarios is used to train a neural network model in offline mode. Once the model has been tested and validated in offline mode, it can be used in real time to predict islanding scenarios in the system.

5.3.1 Application of Neural Networks in Power Systems

The neural network consist of a number of neurons at different layers which have different types of interactions together. The processing time and complexity of the neural network model including the number of layers or neurons are closely related to proper selection of the optimization process and the minimization goal of the layers [102].

In recent decades, the neural network has been widely used for various power system applications, and in many cases offered superior performance over the prior methods. These ANN methods were able to perform complex mapping and incorporating several input values to obtain a single system response which is the desired output for many power system applications.

In [103], an ANN model is defined as a topology recognition tool to find irregular topologies. The developed ANN model consists of 3 layers and four neurons which receives power line flow as input and generates the bus switch state as output. In [104], an ANN model to analyze reliability of power systems is proposed which were proved to have an accuracy of 99%. Authors claimed that the proposed method could be used in online reliability analysis due to its fast performance.

An ANN based method to enhance steady state security of the power system by optimizing the amount and location of reactive power banks is proposed in [105]. The maximum load, and reactive generation reserve are used as inputs to a multilayer perceptron neural network model. The outputs are defined as best, good, average, and poor, which represent the effectiveness of reactive power banks placement for the system steady state security.

In [106], an ANN model as a pattern classifier for operation of distance relay in transmission lines is defined. The post fault voltage and current measurements are used as input, and the output is defined as the trip command to the circuit breakers. A power system restoration method based on ANN concept is proposed in [107]. The method contains few island restoration schemes and determines restoration plan based on offline trainings. Authors argued that the proposed requires small amount data storage capacity and processing time.

In [108], authors defined a multi layered feed forward neural network method for the short term load forecasting in the power system. In [109] and [110] multi-layer

perceptron with back propagation ANN methods are used for precise security system prediction and assessment of power systems.

5.3.2 Formulation of the Proposed ANN Method

In this study, the proposed ANN pattern recognition method has been selected due to its flexibility in finding various connections between inputs and output values which is the key concern in development of SIP module. In addition, the supervised learning feature allows the training of the ANN module using offline simulations carried out based on islanding database. In this section, details of the proposed ANN method are demonstrated. The SIP module determines the transient behavior of the system and alarms the operator in case of an un-wanted islanding scenario. In the offline mode, the islanding database and the SOVI tool proposed in section 4 are used to train the ANN module. Once trained and tested offline, the SIP module can be used in real time to predict possible islanding scenarios. It should be noted that the major computational burden of the SIP method is associated with the offline part which includes creation of the islanding database, islanding scenario simulation and the ANN module training and testing.

The overall scheme of the proposed islanding prediction method is shown in Figure 5.4. The proposed SIP module is divided into offline and online stages and operates in the following steps:

- In the offline mode, the system incidence matrix A is created. The incidence matrix is a reversible symmetrical matrix that indicates the connectivity within a power network. It has all its diagonal elements (bus elements) equal to 1, which means the bus is connected to the system. For each two buses i, j ($i \neq j$) which have

transmission line connecting them, the corresponding elements in the A matrix are also 1. The rest of matrix elements are 0.

- The N-th observability of incidence matrix A is obtained by calculating A^N where the index N is defined to create realistic islanding scenarios. The index N represents the electrical distance of islanding scenarios.
- Once the islanding scenario database is created, simulations are performed for each scenario and measurements are captured at PMU locations.

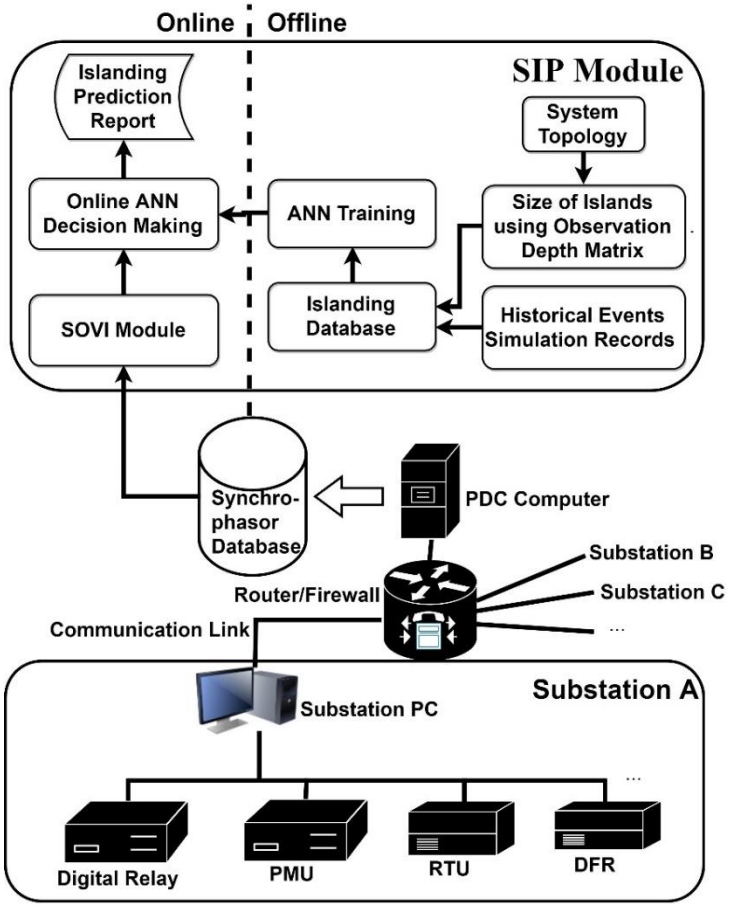

Figure 5.4 Overall structure of SIP module

- The power system is divided into M regions (M depends on the size of the system and number of available PMUs), and the proposed SOVI module is deployed to obtain vulnerability indices in each region. Outputs of SOVI modules for each scenario are used as the input to train the ANN method.
- The supervised learning is used to train the ANN module using the islanding database and SOVI modules' output. The first output of the ANN method is defined as a signal in the range of 0 to 1 which shows the possibility of formation of at least an islanding scenario. The second output list the critical lines that their outage can lead to formation of the islands (to limit the size of simulations, contingencies are limited to "N-3").
- The synchrophasor streams measured by PMUs (or other PMU enabled devices such as digital protective relays (DPRs) or digital fault recorders (DFRs)) at different substations are collected by substation Phasor Data Concentrators (PDCs) and transferred through communication links to the control center PDC and stored at synchrophasor PI historian database.
- In the online mode, the trained ANN module is used to monitor the power system in real-time and determine areas prone to un-wanted islanding formation.

5.4 Case Study

5.4.1 Offline Analysis

5.4.1.1 Islanding Database

The proposed islanding database creation method has been applied to IEEE 118-bus test system. The computation results are shown in Table 11. The total numbers of islanding cases by setting the maximum observability depth to 4 and tripping up to 2 and 3 lines are 182 and 684, respectively.

TABLE 11 NUMBER OF ISLANDING SCENARIOS IN IEEE 118-BUS TEST SYSTEM

IEEE 118-bus Test System		**Depth of Observability**		
		2	3	4
No. Tripped lines	Up to 2	49	97	182
	Up to 3	216	472	684

5.4.1.2 Employing the SOVI Tool

The IEEE 118-bus test system is divided into 9 regions as depicted in Figure 5.5. Each area contains few PMUs which are assumed to send measurements to their regional control center.

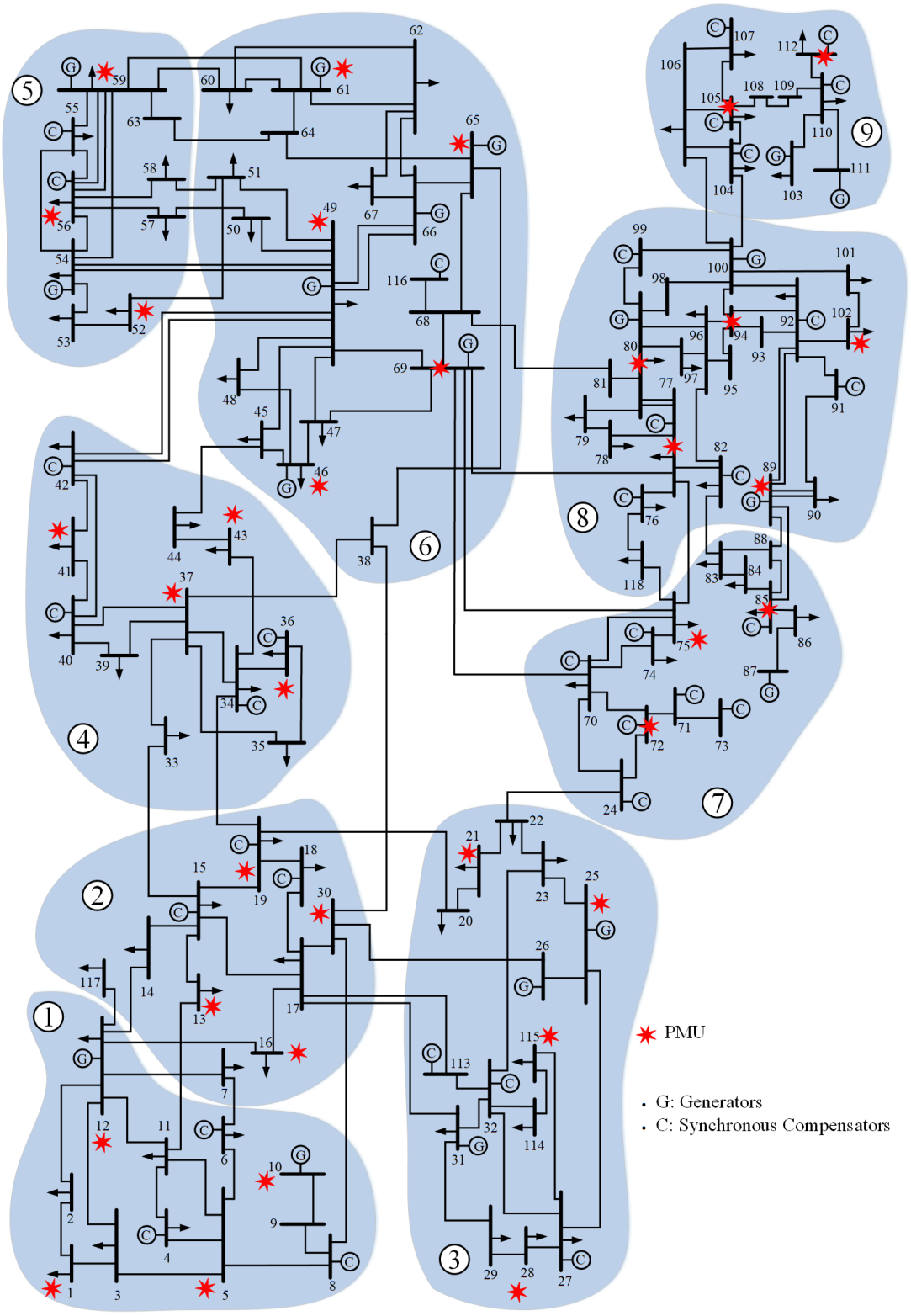

Figure 5.5 Testing SIP tool with IEEE 118-bus test system

The SOVI tool is developed at each regional control center using PMU measurements and procedures explained in section 4.

5.4.1.3 Training the ANN Module

Each SOVI's output is used as an input to the ANN method. Therefore, the ANN input layer consists of 9 nodes as shown in Figure 5.6. The output layer is defined with 9 nodes where each node is associated with a region shown in Figure 5.5. A zero value at an output node indicates that no islanding condition at its corresponding region is predicted. While a value of 1 at an output node indicates that an un-wanted islanding condition at its corresponding region is predicted. The hidden layer used in this training process contains 6 neurons.

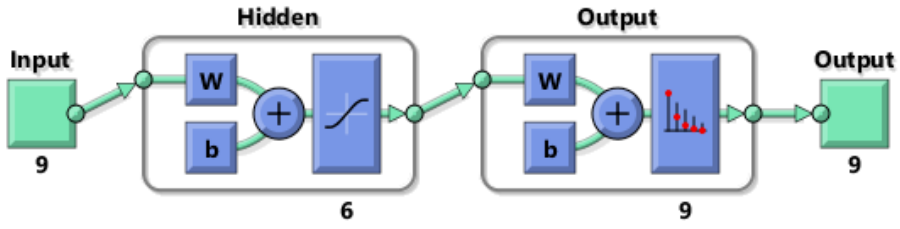

Figure 5.6 Graphical diagram of the ANN method trained for the SIP tool

The training dataset consists of all 684 islanding scenarios obtained in Table 11 and 1100 non-islanding cases. A script is developed to randomly generate "N-1" contingencies, as well as 5-20% overload condition scenarios in different regions. 70% of the dataset is used to train the ANN module and the rest is equally allocated to validation

and testing parts. Simulations have been carried out in RT-LAB software environment using OPAL-RT real time simulator [111]. Virtual PMUs are modeled within the model at the given buses as shown in Figure 5.5 and measurements are transferred to control center using PDCs. The SOVI module calculates the vulnerability indices at each of 9 regions. Each SOVI's output value is selected 10 seconds after the scenario has been occurred in order to eliminate the effect of transients on calculations.

Figure 5.7 indicates the iteration at which the validation performance reached a minimum. In the default setup, the training stops after six consecutive increases in validation error, and the best performance is taken from the epoch with the lowest validation error.

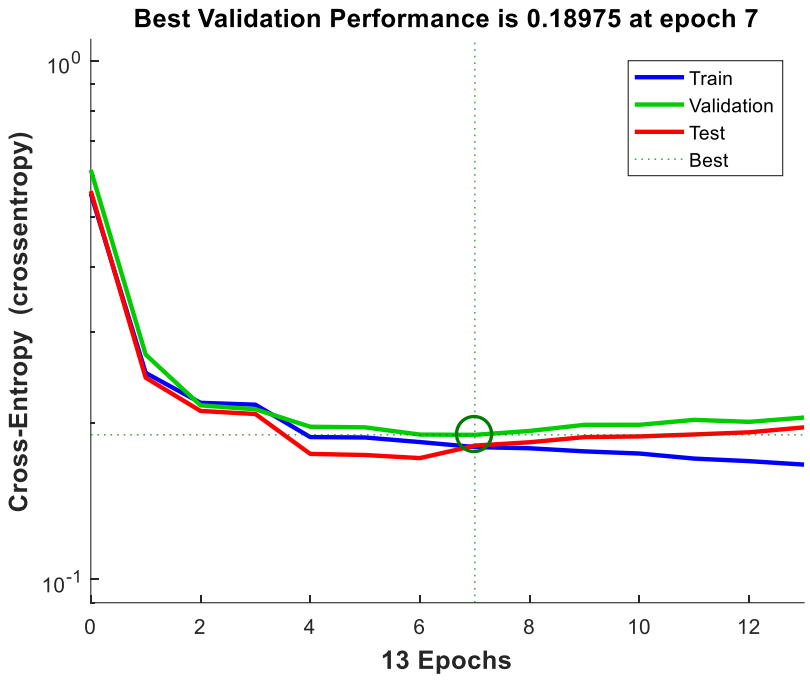

Figure 5.7 Error vs. epoch for training, validation and test data

This figure does not indicate any major problems with the training. The validation and test curves are very similar. If the test curve had increased significantly before the validation curve increased, then it was possible that some over fitting might have occurred. Generally, the error reduces after more epochs of training, but might start to increase on the validation data set as the network starts over fitting the training data.

5.4.2 Online Analysis

Once islanding database is created and offline simulations are performed to train the ANN module, the SIP tool can be deployed online to predict areas prone to formation of islands in real time. In order to test the SIP tool in real time, few islanding scenarios are simulated as described in Table 12.

TABLE 12 DESCRIPTION OF ISLANDING SCENARIOS

Case no.	Islanded areas	Details of Events	SIP Tool Output
1	Island 1: regions 1, 2, 3 Island 2: Rest of the System	• Line 44 (15-33) is tripped at t=10 sec • Line 45 (19-34) is tripped at t=20 sec • Line 30 (22-24) is tripped at t=30 sec • Line 54 (30-38) is tripped at t=40 sec	• Regions 1, 2 and 3 are detected to form an island at t= 33.5 sec
2	Island 1: Region 9 Island 2: Rest of the System	• Line 163 (100-103) is tripped at t=10 sec • Line 164 (100-104) is tripped at t=20 sec • Line 167 (100-106) is tripped at t=30 sec	• Region 9 is detected to form an island at t=22.8 sec
3	Island 1: Part of Region 3 Island 2: Rest of the System	• Line 41 (23-32) is tripped at t=10 sec • Line 33 (25-27) is tripped at t=20 sec • Line 178 (17-113) is tripped at t=30 sec • Line 39 (17-31) is tripped at t=40 sec	• Region 3 is detected to form an island at t=30.2 sec
4	Island 1: Region 1 and Part of Region 3 Island 2: Rest of the System	• Line 8 (5-8) is tripped at t=10 sec • Line 20 (12-16) is tripped at t=20 sec • Line 18 (13-15) is tripped at t=30 sec • Line 19 (14-15) is tripped at t=40 sec	• Regions 1 and 3 are detected to form an island at t=42.3 sec

For the sake of simplicity, only line outages are considered as contingencies to create islanding scenarios in Table 12. A delay of 10 sec is applied among contingencies to better understand the transient behavior of the system as well as the SIP method response. Next, simulation results of each cases from Table 12 is explained.

Case 1: Figure 5.8 shows voltage magnitudes captured at PMU locations. The impact of outages can be seen on voltage profiles especially after the fourth contingencies. The voltage drop across regions 1, 2 and 3 is more severe due to overload condition in the island. The phasor angles captured at PMU locations are also shown in Figure 5.9. Both islands remain stable after the contingency, however, the generators in the island 1 (regions 1, 2 and 3) go out of synchronism compare to generators in island 2 (main grid). The SIP module detects regions 1, 2 and 3 to form an island at t= 33.5 sec.

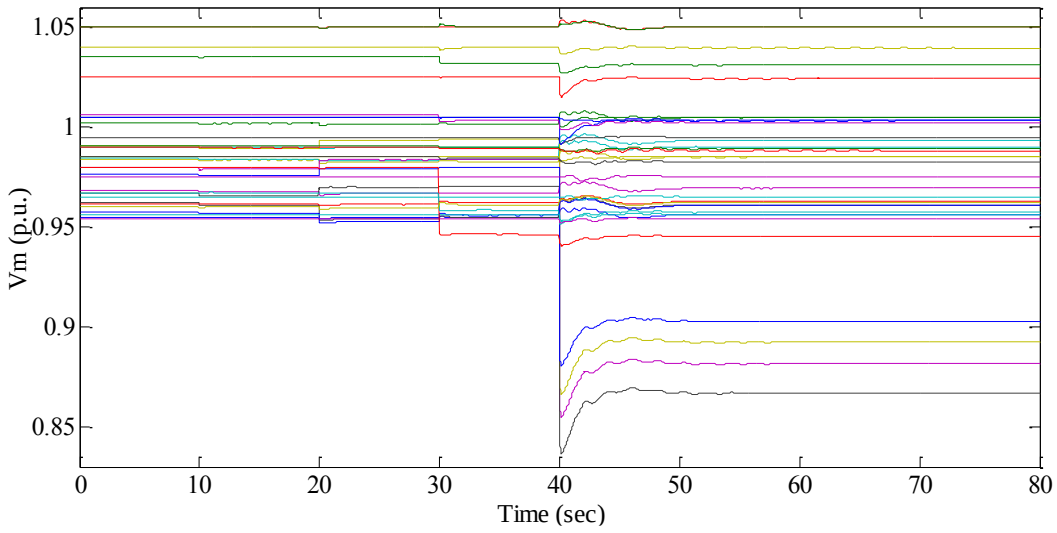

Figure 5.8 Voltage magnitude at PMU locations in case 1

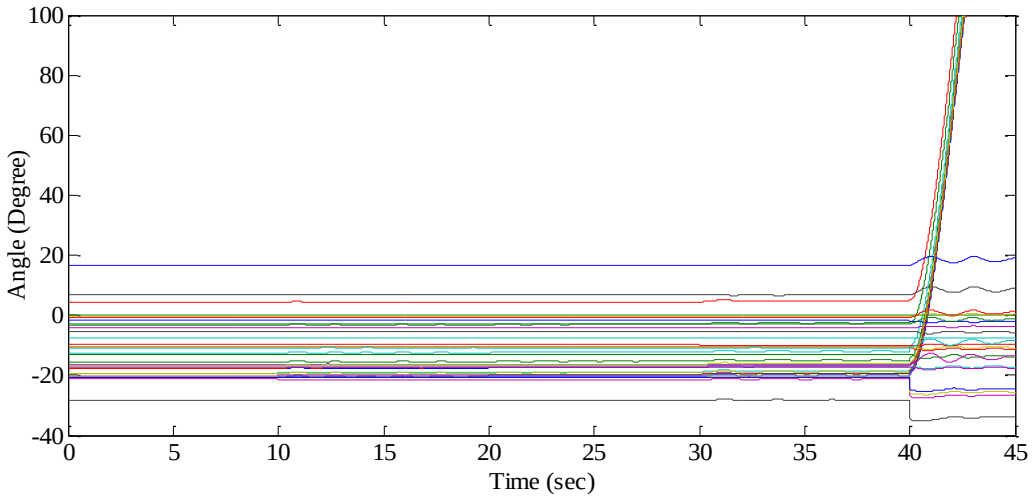

Figure 5.9 Voltage angle at PMU locations in case 1

Case 2: Figure 5.10 shows voltage magnitudes captured at PMU locations. The voltages oscillations after the second contingency indicates the impact of outages on both islands. As expected, bigger oscillations are related to the PMUs in island 1 (region 9).

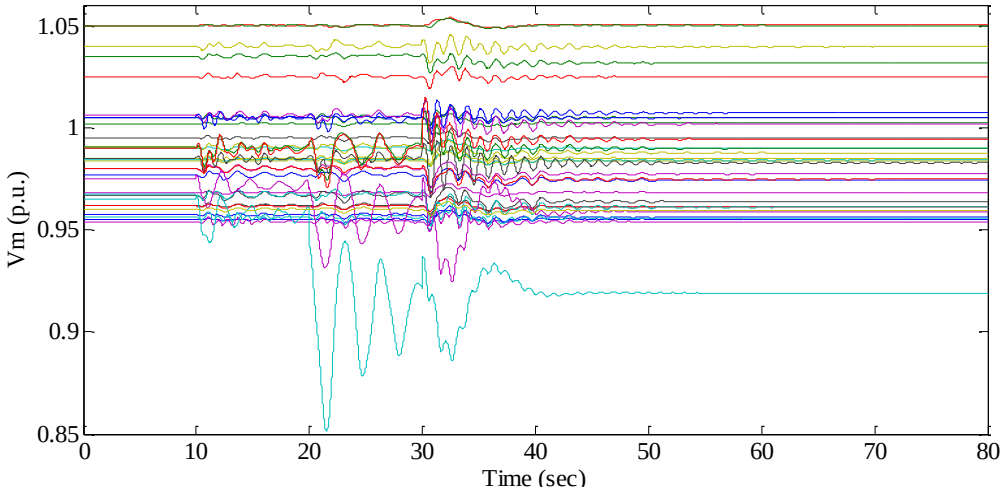

Figure 5.10 Voltage magnitude at PMU locations in case 2

The phasor angles captured at PMU locations are shown in Figure 5.11. Both islands remain stable and the islanded machine angles go along with the main grid. The SIP module detects region 9 to form an island at t= 22.8 sec.

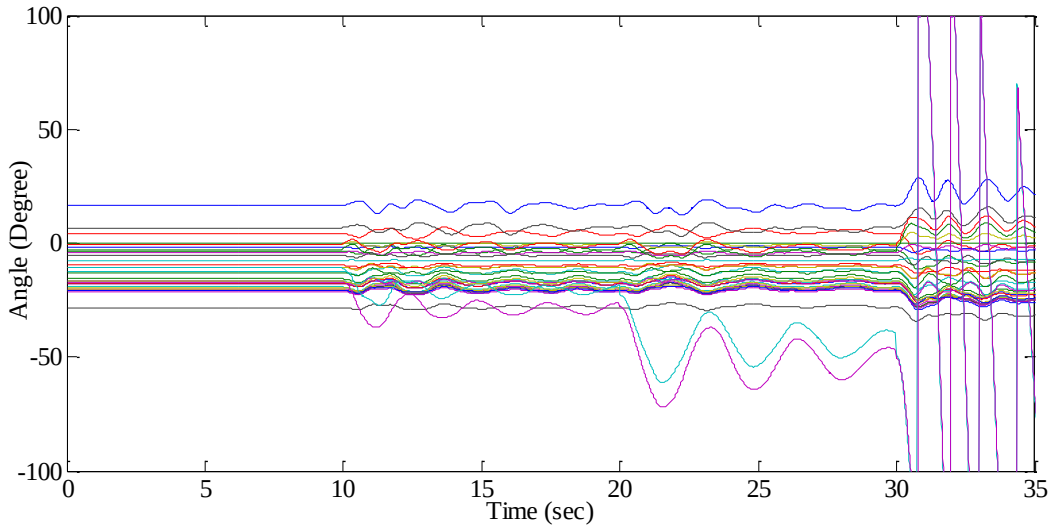

Figure 5.11 Voltage angle at PMU locations in case 2

Case 3: Figure 5.12 and Figure 5.13 show the voltage magnitude and phasor angles captured at PMU locations, respectively. The voltage drop within the islanded regions can result in UVLS units operations. The machine angles remain synchronize with the main grid, but experiences large oscillations. The SIP module detects region 3 to form an island at t= 30.2 sec.

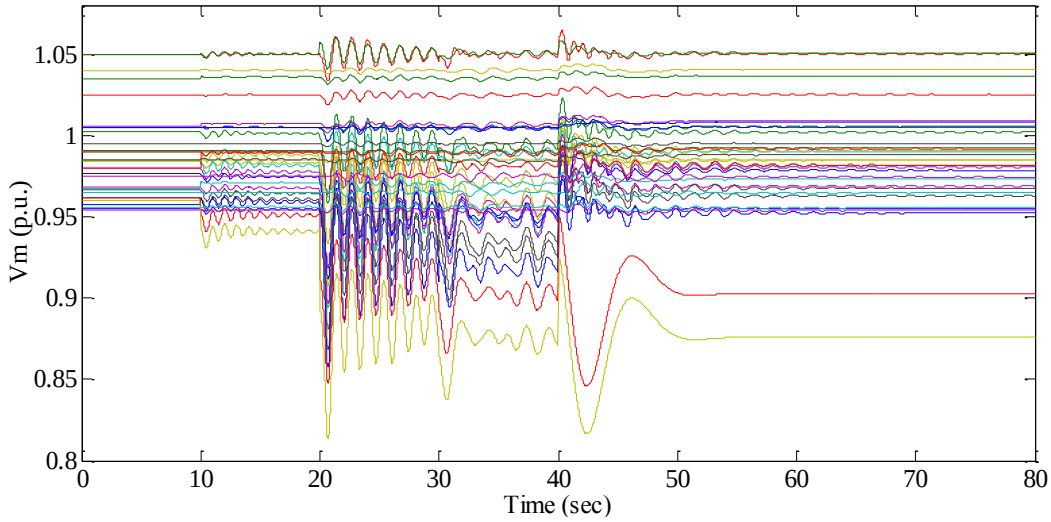

Figure 5.12 Voltage magnitude at PMU locations in case 3

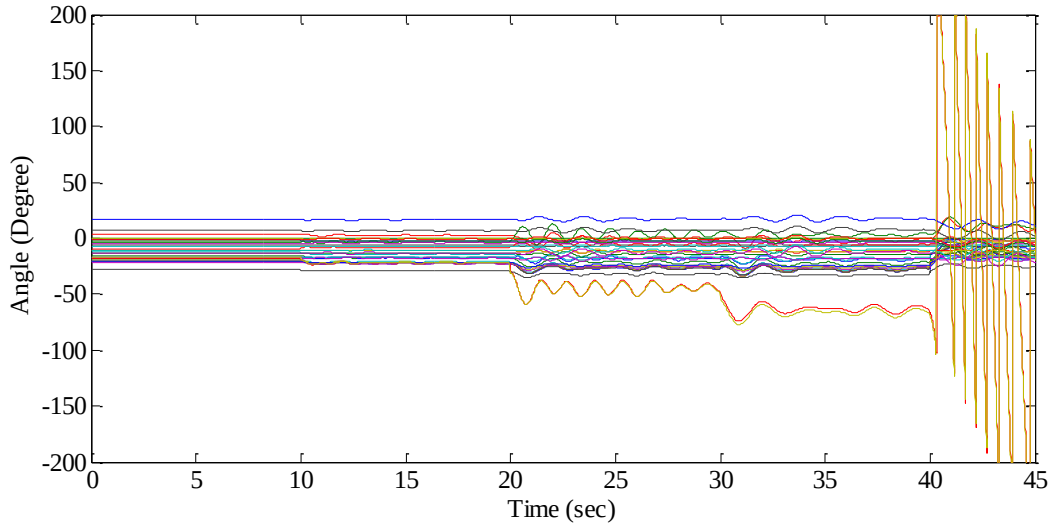

Figure 5.13 Voltage angle at PMU locations in case 3

Case 4: Figure 5.14 and Figure 5.15 show the voltage magnitude and phasor angles captured at PMU locations, respectively. The severe impact of outages can be seen on

voltage profiles especially after the fourth contingency. The islanded area remains stable after the contingency and the islanded machine angles go along with the main grid. The SIP module detects regions 1 and 3 to form an island at t= 42.3 sec.

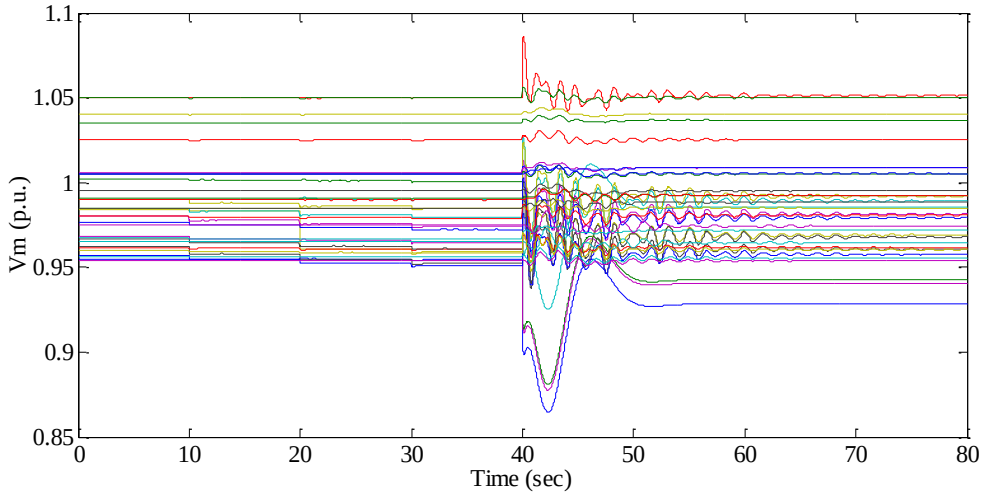

Figure 5.14 Voltage magnitude at PMU locations in case 4

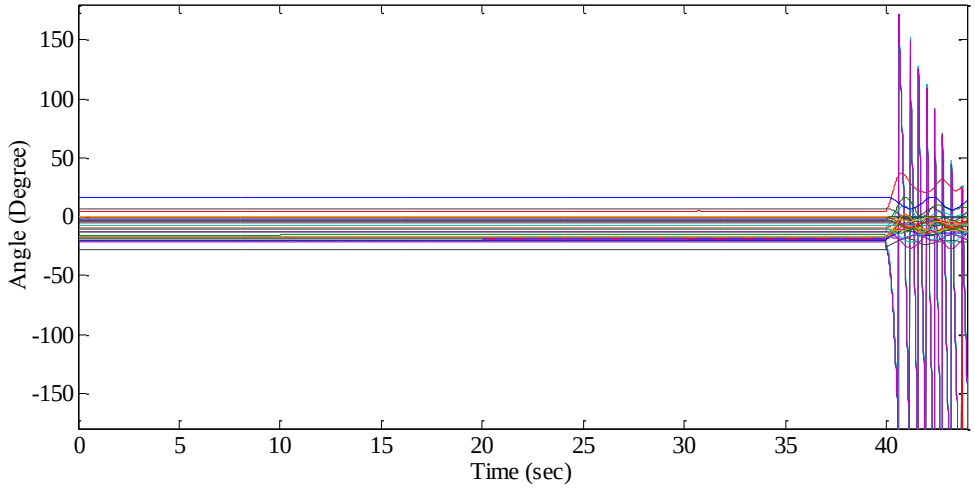

Figure 5.15 Voltage angle at PMU locations in case 4

5.5 Conclusion

In this section a two-step islanding prediction tool based on synchrophasor measurement has been proposed. The proposed SIP tool utilizes an efficient contingency creation algorithm to populate islanding scenarios. It then identifies unstable areas which are prone to creating un-wanted islands. Once such unstable areas are identified, the results may be used to trigger mitigation measures to prevent such isolations. This can prevent progression of cascading outages and possibly prevent a severe blackout.

6. INTEGRATED CONTROLLED ISLANDING TOOL[*]

6.1 Overview

Once several disturbances take place in the electric grid, the power system stability margin shrinks which eventually may lead to formation of un-wanted islands. The intentional islanding (also known as controlled islanding) of the grid during this stage of cascading outage can reduce or even eliminate possibility of major blackouts.

6.2 Background on Controlled Islanding

A number of severe blackouts have been reported in recent decades as the outcome of increasing electricity demand and power grid restructuring [112]. For example, on August 14th 2003, a devastating blackout hit the Northeastern US and Canada affecting 50 million people with an estimated total damage of 4-10 billion dollars [3].

In the slow progression stage of cascading outage, the overall performance of the system remains intact which can be resembled with steady state analysis. In this stage, utility operators may have enough time to evaluate the system condition, and take some control actions to prevent the possibility of further outages [113].

Various remedial and emergency actions including load and generator tripping, excitation controls and intentional islanding are deployed to prevent cascading blackouts [114]. Intentional islanding, also called controlled islanding, methods preserve stable areas

[*] Part of this section is reprinted with permission from "Prevention of power grid blackouts using intentional islanding scheme" by A. Esmaeilian and M. Kezunovic, Jan.-Feb. 2017. *IEEE Transactions on Industry Applications*, vol. 53, no. 1, pp. 622-629, ©2017 IEEE, with permission from IEEE.

from further outages, and expedite the restoration process by reducing transient stability problems during system re-connection [115]-[124].

The majority of controlled islanding schemes were classified as optimization problems. In [115]-[119], the slow coherency grouping of generators is utilized to split system into islands. In these studies, the coherent groups of generators are obtained by solving max-flow-min-cut optimization problem. However, due to highly nonlinear nature of the power system, the linearized electromechanical modeling, which is used in these methods may fail to obtain appropriate islanding solution.

Another controlled islanding scheme is obtained considering a graph search based method called ordered binary decision diagrams (OBDD) [120], [121]. In this method, the original power system is substituted with a simplified equivalent obtained using a graph based reduction algorithm. The solution space is narrowed down using OBDDs to fulfill the equality constraints. Then, power flow result is used to decide whether any of the islanding solutions satisfy inequality constraints or not. The major drawbacks of this method are the additional calculation burden required for simplification process and the risk that the superior optimal solutions may be lost due to simplification.

In recent years, several efforts were devoted to development of intentional islanding schemes based on clustering methods [122], [123]. In [122], a k-way spectral clustering method to split power systems into self-sustained islands considering minimum load-generation imbalance is presented. In [123], a multi-level kernel k-means algorithm to form islands based on minimum power flow disruption is proposed. The computational efficiency of these methods is good, but without dynamic constraints in the clustering

process, some of created islands may be divided into unstable sub-islands which eventually drive them to total blackouts.

In [124], authors proposed a controlled islanding scheme based on particle swarm optimization. The method uses minimal power imbalance criteria to form islands. In this method connection among sub-graphs are neglected to reduce computational burden, while it may increase possibility of isolated buses within the created islands.

6.3 Spectral Clustering

As previously shown in section 4, any electric grid can be represented using a graph where the vertices (nodes) and edges (links) of the graph stands for power system's buses and lines, respectively. To represent characteristics of the mapped power grid, edges of the graph can be weighted using different parameters such as admittance, active or reactive power flow.

In this dissertation, active power flow across transmission lines is used as the edge weight to determine cost of cutsets as will be presented later in this section. The edge weight matrix W is defined as:

$$W = \begin{cases} w_{ij} = \dfrac{|P_{ij}| + |P_{ji}|}{2} & i \neq j \\ w_{ij} = 0 & i = j \end{cases} \tag{6.1}$$

where P_{ij} and P_{ji} are the active power injected into the line from buses i and j, respectively. In (6.1), w_{ij} is calculated as the average power flow from two-end of the line to compensate power loss across the line. The edge weight matrix W is calculated based

on power flow which can represent the dynamic nature of power system as it alters according to system operating states.

The un-normalized Laplacian of the graph is defined as [125]:

$$L = \begin{cases} -w_{ij} & i \neq j \\ d_i = \sum_{j=1}^{n} w_{ij} & i = j \end{cases} \tag{6.2}$$

where w_{ij} is the element of edge weight matrix calculated in (6.1). The Laplacian matrix L can also be written as:

$$L = D - W \tag{6.3}$$

where D is the degree matrix with diagonal nonzero entries d_i. The normalized Laplacian matrix L_N is constructed using:

$$L_N = D^{-1/2}.L.D^{-1/2} \tag{6.4}$$

The distinct features of the Laplacian matrix of the graph *G* are explained in the next subsection. As depicted in Figure 6.1, a graph-cut problem is referred to the splitting of graph *G* into S_1 and S_2 by cutting the connecting edges between S_1 and S_2. The set of edges and the sum of their weights are known as *cutset* and *cut*, respectively.

$$cut(S_1, S_2) = \sum_{i \in S_1, j \in S_2} w_{ij} \tag{6.5}$$

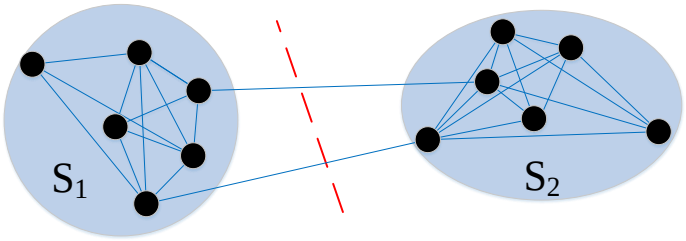

Figure 6.1 Solving graph-cut problem using spectral clustering

The graph-cut problem defined in (6.5) can be solved utilizing un-normalized spectral clustering method. It uses the two eigenvectors associated with the two smallest positive eigenvalues of the Laplacian matrix of *G* to form S_1 and S_2. The un-normalized spectral clustering method is defined using below steps [68]:

- Computing the two eigenvectors (v_1, v_2) of the Laplacian matrix *L* associated with the two smallest eigenvalues;
- Defining V as the matrix constructed using two columns of v_1 and v_2.
- Defining y_i as the i^{th} row of V;
- Applying a k-means or k-medoids clustering methods to cluster y_i into $S_1$and S_2.

Achieving a proper islanding solution using un-normalized spectral clustering of the power system graph might be infeasible as it splits power system into two islands without considering transient behavior of the system. Besides, it might also be necessary to divide the system into more than two islands to interrupt sequences of cascade outages.

In this dissertation, a controlled islanding scheme utilizing constrained spectral clustering to address above concerns is introduced. The proposed method introduces k-embedded clustering approach to allow splitting the system into several islands, if needed.

The proposed method considers generator coherency as an optimization constraint to avoid generators go out of synchronism and achieve stable islands.

6.4 Proposed Constraint Optimization Method

Once successive disturbances took place in the electric grid, its stability margin degrades, which eventually may lead to system separation and formation of un-wanted islands. The intentional islanding of the grid during the preliminary state of cascading outages progression can decrease or eliminate the possibility of severe blackouts. The controlled islanding concept is primarily introduced to work at the transmission level. The control islanding scheme can also expedite the restoration process of the power system.

To create an ideal self-sustained islanding solution, different constraints such as thermal limits, load-generation imbalance, generator coherency and transient stability should be taken into account [121]. Hence, a controlled islanding strategy is considered as a multi-constraint, multi-objective optimization problem in which it would rarely be possible to reach the best solution. So, a viable solution is to consider a sub-set of objectives and constraints to reduce the complexity of the problem. In this dissertation, the generator coherency is considered as a constraint to the minimization problem, while the power flow disruption between islands is defined as the objective function to be minimized.

6.4.1 Static Constraints

To attain a successful intentional islanding strategy, it is more influential to secure the transient stability rather than load-generation balance. An island with negative stability

index may ultimately become unstable even if the load-generation balance is satisfied within the island. There are two types of objective functions used in literature formulated as:

$$\underset{S_1,S_2 \subset G}{Min} \left(\left| \sum_{i \in S_1, j \in S_2} \left(\frac{|P_{ij} + P_{ji}|}{2} \right) \right| \right) \tag{6.6}$$

$$\underset{S_1,S_2 \subset G}{Min} \left(\left| \sum_{i \in S_1, j \in S_2} \left(\frac{|P_{ij}| + |P_{ji}|}{2} \right) \right| \right) \tag{6.7}$$

In (6.6), the objective function is defined to minimize the sum of active power flows between islands which is known as "power flow imbalance". Solving the optimization problem with this objective function secures islands with good load-generation balance. But, as shown in the example of Figure 6.2a, the solution may result in the switching of major transmission lines which transfer higher active power. Disconnection of such lines can cause transient stability problem at both intentional islanding and system restoration stages.

In (6.7), the objective function is defined to minimize the absolute value of the active power flow between islands, known as "power flow disruption". Solving the optimization problem with this objective function avoids the overloading of transmission lines within the islands. It can also facilitate reconnection of the islands in the restoration process due to the minimum power flow changes compared to the pre-disturbance condition (see Figure 6.2b).

In this dissertation, the objective function defined by (6.7) is selected to formulate the optimization problem.

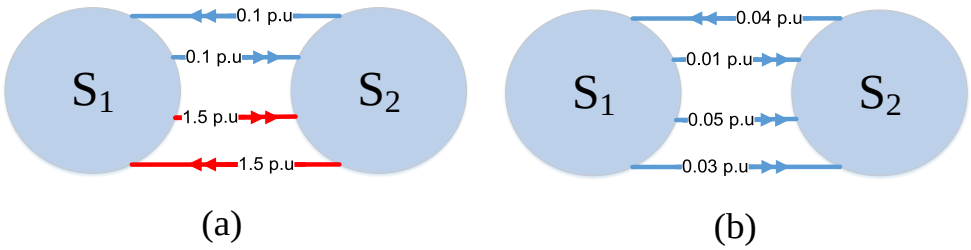

Figure 6.2 Two types of objective function using active power flow

6.4.2 Dynamic Constraints

A strong disturbance in an electric grid may trigger electromechanical wave oscillations which propagate through entire network and may result in generators going out-of-synchronism [91], [92]. The generators with stronger dynamic couplings remain synchronized with each other and are called coherent generators [126], [127]. Different approaches have been developed to determine coherent groups of generators [128], [129].

To achieve reliable islanding strategy, each group of the coherent generators must be kept in the same islands.

In this study, the generator coherency problem is determined using normalized spectral clustering. First, the dynamic graph of system L_D is defined as:

$$L_D = \begin{cases} \frac{\left|\partial P_{ij} / \partial \delta_{ij}\right| + \left|\partial P_{ji} / \partial \delta_{ji}\right|}{2} & i \neq j \\ -\sum_{l=1, l\neq i}^{n} L_D^{il} & i = j \end{cases} \tag{6.8}$$

By applying the four steps of spectral clustering method introduced in section 6.3, the generators are divided into two coherent groups S_{G1} and S_{G2}. Then, each group can be treated as a separate graph to perform recursive bisection spectral clustering till the desired number of coherent groups is achieved.

Once coherent generators are determined, it can be used as a constraint to k-embedded clustering method. Next, the constrained spectral k-embedded clustering method to achieve self-sustained islands will be discussed and formulated.

6.4.3 Constrained Spectral K-Embedded Clustering

Constrained spectral clustering is defined as a semi-supervised clustering method with the additional information converted in the form of pairwise constraints. This section describes how the generator coherency information is incorporated into constrained spectral clustering. The new constrained optimization formulation to solve controlled islanding problem is proposed.

In the constrained spectral clustering the terms Must Link (ML) and Cannot Link (CL) refer to vertices which must remain and be removed in the final solution, respectively [130], [131]. A ML-constraint ensures that the vertices which are connected through the ML remain within the same cluster. A CL-constraint ensures the vertices which are connected through the CL are grouped in different clusters. The constraint matrix *Q* is defined in (6.9):

$$Q = \begin{cases} -1 & if\ (x_i, x_j) \in CL \\ 1 & if\ (x_i, x_j) \in ML \\ 0 & else \end{cases} \tag{6.9}$$

The standard constrained clustering can only holds binary constraints for ML and CL. The following index is defined to verify satisfaction of constraints matrix Q.

$$u^T.Q.u = \Sigma_{i,j} u_i.u_j.q_{ij} \tag{6.10}$$

where $u \in \{-1,1\}^N$ is the indicator vector. The further extension is achieved when u and Q are relaxed.

$$u \in R^N \ , \ Q \in R^{N \times N} \tag{6.11}$$

If $Q_{ij} > 0$, then i and j are in the same cluster ; if $Q_{ij} < 0$, then i and j are in different clusters. As the value of $u^T.Q.u$ becomes higher the constraint matrix Q is more satisfied. The normalized form of constraint matrix Q is defined as follows.

$$Q_N = D^{-1/2}.Q.D^{-1/2} \tag{6.12}$$

where D is the degree matrix. The controlled islanding problem is defined as a constrained optimization problem with the following definition [131]:

$$\begin{aligned} &arg \ \ min \quad v^T.L_N.v \\ &s.t. \qquad v^T.Q.v > \beta \ , \quad v^T.v = \text{vol} \ , \ v \neq D^{1/2}.1 \end{aligned} \tag{6.13}$$

where $vol = \sum_1^N d_{ii}$ is the graph volume and β is the satisfaction threshold. $v^T.L_N.v$ is the cost of the cut, $v^T.v$ is defined to normalize v and $v \neq D^{1/2}.1$ is defined to avoid

trivial solutions. The Karush-Kuhn-Tucker Theorem [132] is used to solve the objective function in (6.13). After several mathematical steps [131], the solution of optimization equation in (6.13) can be attained by solving the generalized eigenvalue equation in (6.14).

$$L_N v = \lambda \left(Q_N - \frac{\beta}{vol} I \right) v \tag{6.14}$$

In summary, as shown in Figure 6.3, the step by step constrained spectral *k*-Embedded clustering algorithm is defined as follows.

- Determining k as the total number of clusters obtained from generator coherency grouping.
- Using graph representation of the power system to obtain edge weight matrix W and normalized Laplacian matrix L_N using (6.1) and (6.4), respectively.
- Building constraint matrix Q using (6.9).
- Solving generalized eigenvalue problem in (6.14)
- Disregarding eigenvectors related to non-positive eigenvalues.
- Eigenvectors normalization using: $v \longleftarrow \frac{v}{\|v\|}\sqrt{vol}$.
- Selecting k-1 eigenvectors ($v_1, \dots, v_{k-1}$) related to the k-1 lowest eigenvalues.
- Defining $V^* \leftarrow \arg\min V^T L_N V \; V^* \longleftarrow V^T . L_N . V$ where $V \in R^{n \times k-1}$ is the matrix built by vectors $v_1, \dots, v_{k-1}$ as columns [133].
- Applying k-medoids algorithm to obtain final islanding solution.

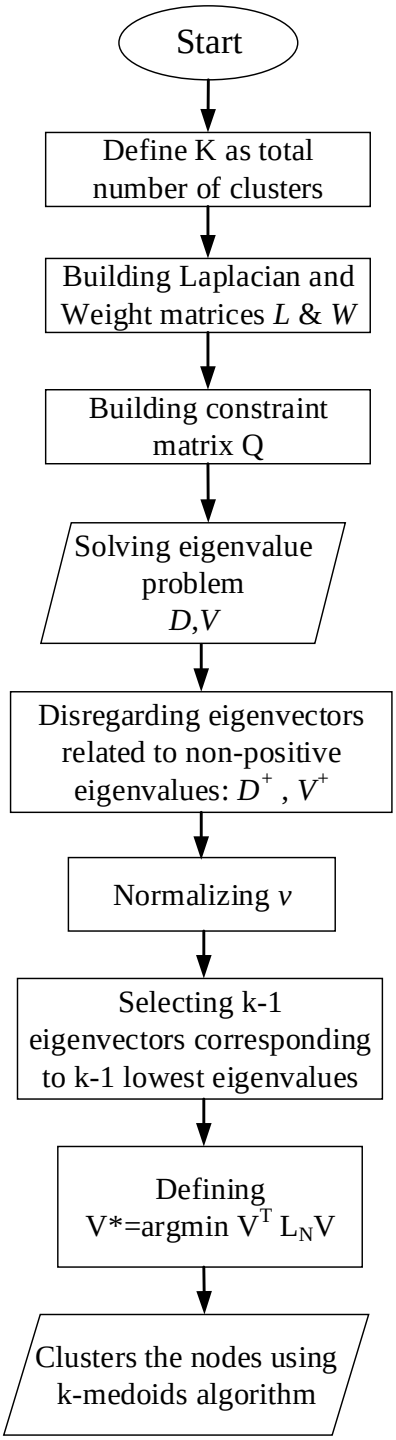

Figure 6.3 The proposed controlled islanding method

Comparing to bisection spectral clustering [134], the proposed k-embedded spectral clustering has higher flexibility in adjusting clusters and partitioning process. Despite k-means method which uses squared distances among data-points, the k-medoids method eliminates data anomalies and noises as it minimizes the sum of variances.

For instance, the proposed controlled islanding method is demonstrated using the simple IEEE 9-bus system with detail explanation of matrices formation. The generator coherency analysis results in separation of generators in two groups {G1} and {G2, G3} which can be seen in Figure 6.4. In this figure, the number attached to each line represents the per unit average active power flow across it. Figure 6.4 can be seen as a graph G where the lines and buses are edges and vertices, respectively. The weight of each edge is labeled next to it. Therefore, one can build the Laplacian matrix using (6.15).

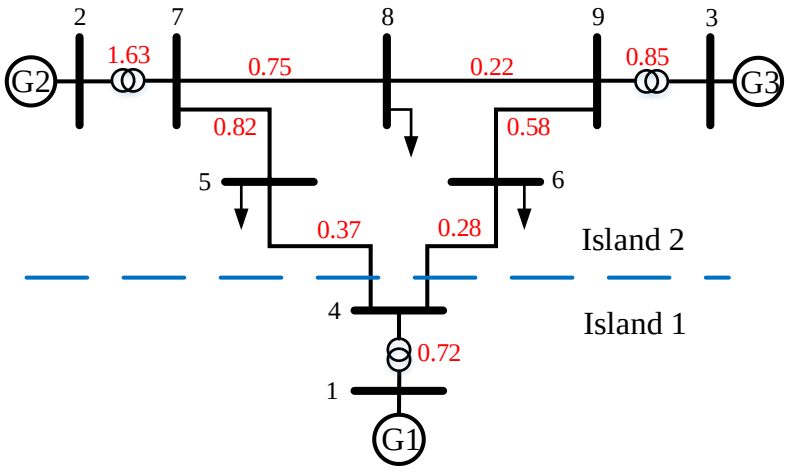

Figure 6.4 Verifying ICI tool using IEEE 9-bus

$$L = \begin{bmatrix} 0.72 & 0 & 0 & -0.72 & 0 & 0 & 0 & 0 & 0 \\ 0 & 1.63 & 0 & 0 & 0 & 0 & -1.63 & 0 & 0 \\ 0 & 0 & 0.85 & 0 & 0 & 0 & 0 & 0 & -0.85 \\ -0.72 & 0 & 0 & 1.37 & -0.37 & -0.28 & 0 & 0 & 0 \\ 0 & 0 & 0 & -0.37 & 1.19 & 0 & -0.82 & 0 & 0 \\ 0 & 0 & 0 & -0.28 & 0 & 0.86 & 0 & 0 & -0.58 \\ 0 & -1.63 & 0 & 0 & -0.82 & 0 & 3.2 & -0.75 & 0 \\ 0 & 0 & 0 & 0 & 0 & 0 & -0.75 & 0.97 & -0.22 \\ 0 & 0 & -0.85 & 0 & 0 & -0.58 & 0 & -0.22 & 1.65 \end{bmatrix} \quad (6.15)$$

The ML constraint between G2 and G3 are replaced by +1, and the CL constraint between G1 and {G2 and G3} are replaced by -1 to build matrix Q:

$$Q = \begin{bmatrix} 1 & -1 & -1 & 0 & 0 & 0 & 0 & 0 & 0 \\ -1 & 1 & 1 & 0 & 0 & 0 & 0 & 0 & 0 \\ -1 & 1 & 1 & 0 & 0 & 0 & 0 & 0 & 0 \\ 0 & 0 & 0 & 0 & 0 & 0 & 0 & 0 & 0 \\ 0 & 0 & 0 & 0 & 0 & 0 & 0 & 0 & 0 \\ 0 & 0 & 0 & 0 & 0 & 0 & 0 & 0 & 0 \\ 0 & 0 & 0 & 0 & 0 & 0 & 0 & 0 & 0 \\ 0 & 0 & 0 & 0 & 0 & 0 & 0 & 0 & 0 \\ 0 & 0 & 0 & 0 & 0 & 0 & 0 & 0 & 0 \end{bmatrix} \quad (6.16)$$

By calculating steps 4 to 9 in Figure 6.3, a single cutset is obtained as shown with dashed line in Figure 6.4. The cost of cut is the sum of average power flow across lines (4-5 and 4-6) and is equal to (0.28+0.37) = 0.65 p.u. The two islands include buses {1, 4} and {2, 3, 5, 6, 7, 8, 9}, respectively. Since {G1} is in the island1 and {G2, G3} are in the island2, the suggested islanding scheme guarantees generator coherency constraints, too.

6.5 Triggering Mechanism

The key to mitigate cascading outages is to trigger the intentional islanding method at the proper time. Prior studies on prevention of blackouts using controlled islanding [115]-[124] failed to introduce a triggering mechanism for their proposed methods.

In this dissertation, the SOVI, SOFI and SIP tools, defined in the previous sections, are combined to define a triggering mechanism for the intentional islanding module (see Figure 6.5). The triggering mechanism is defined based on thresholds for SOVI module along with disturbance data obtained from SOFI module and the output of SIP tool. The real time monitoring of a power system using the mentioned three modules allows the intentional islanding scheme to be deployed at the crucial time to interrupt the sequence of cascading outages. The proposed ICI method is defined using the following steps [135]-[137]:

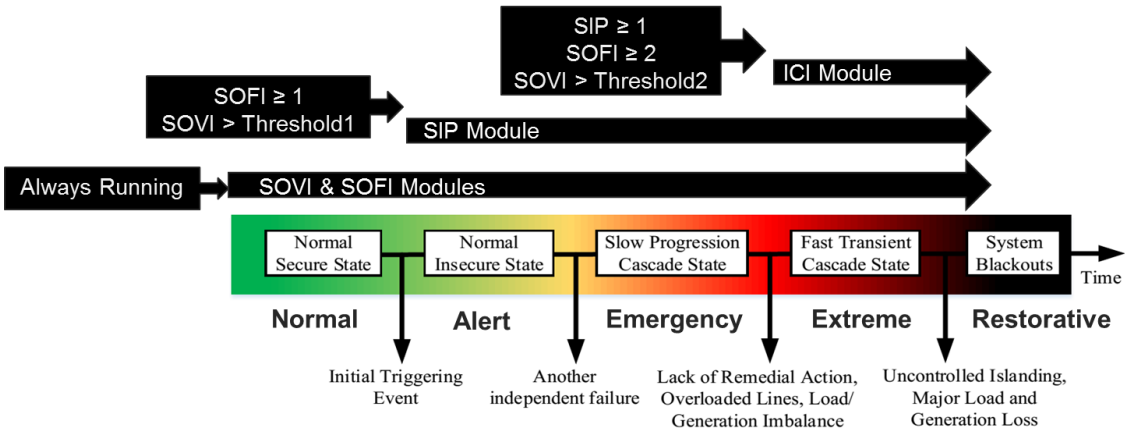

Figure 6.5 The proposed tools triggering mechanisms

- The graph G is defined to resemble the entire power system. In this modelling, buses, lines and average power flow across each line represent the graph's vertices, edges and edge weights, respectively.
- The graph G_D is defined to resemble the power system in dynamic time-scale. To obtain G_D, the Kron reduction method [138] is used to remove the buses without generators.
- Laplacian matrices L and L_D corresponding to the graphs G and G_D are calculated.
- The spectral clustering optimization problem is defined to determine the coherent groups of generators.
- The generator coherency result is used to define ML- and CL- constraints. A ML-constraint ensures that the vertices which are connected through the ML remain within the same cluster. A CL-constraint ensures the vertices which are connected through the CL are grouped in different clusters. The constraint matrix Q is defined based on ML- and CL- constraints.
- The constrained spectral clustering optimization method is used to find the islanding solution which results in islands with minimum power flow disruption across their boundaries while satisfies the constraint matrix Q.

6.6 Case Study

6.6.1 Cascade Outage Scenario Creation

From Figure 6.6, one can observe that IEEE118 bus test system consists of several areas which are loosely connected to each other. It is expected that following several consecutive outages, those areas might be disconnected from each other. In such cases, unless the generation capacity of each area matches amount of loads in that area, one or more areas may experience brownout or blackout.

Next, the sequence of events to create a hypothetical cascading event outage scenario is described, which will result in blackout. It should be noted that under-voltage load shedding is not considered in the scenario creation process to assist creating a system blackout, and 10 sec intervals are deliberately inserted between outages to help understanding of transient behavior after each step and assure readability of plots.

1. Parallel lines between buses (42–49) are tripped at t=10 sec due to inter-circuit fault.
2. Line between buses (37-38) is tripped at t=20 sec due to a phase to ground fault.
3. Line between buses (25-27) is tripped at t=30 sec due to another phase to ground fault.
4. Line between buses (17-30) is tripped at t=40 sec due to malfunction of distance relay caused by power swing.
5. Line between buses (4-5) is overloaded and a single phase fault occurs due to sagging of the line. The corresponding relays trip the line at t=50 sec.
6. Line between buses (5-11) is de-energized due to mis-operation of third zone relay under overload condition at t=60 sec.

7. Line between buses (5-6) is de-energized due to mis-operation of third zone relay under overload condition at t=70 sec.
8. Line between buses (23-25) is de-energized due to mis-operation of third zone relay under overload condition at t=80 sec. Following outage of the line (23-25) the voltage profile of the system collapses and blackout occurs.

Figure 6.7 shows the bus voltage, bus phase angle and frequency of the system in this cascade outage scenario. The first three events are considered as unstoppable outages (maintenance, faults, etc.) which may occur anytime in the system.

After the fourth event, voltage of buses (33 to 37 and 39 to 42) dropped below 0.8 pu, as the line (17-30) was the major route of transferring power from generators (10, 25 and 26) to that load area. Following this outage, redistribution of power flow caused overloads on lines (4-5, 5-6 and 5-11) which resulted in events 5 to 7.

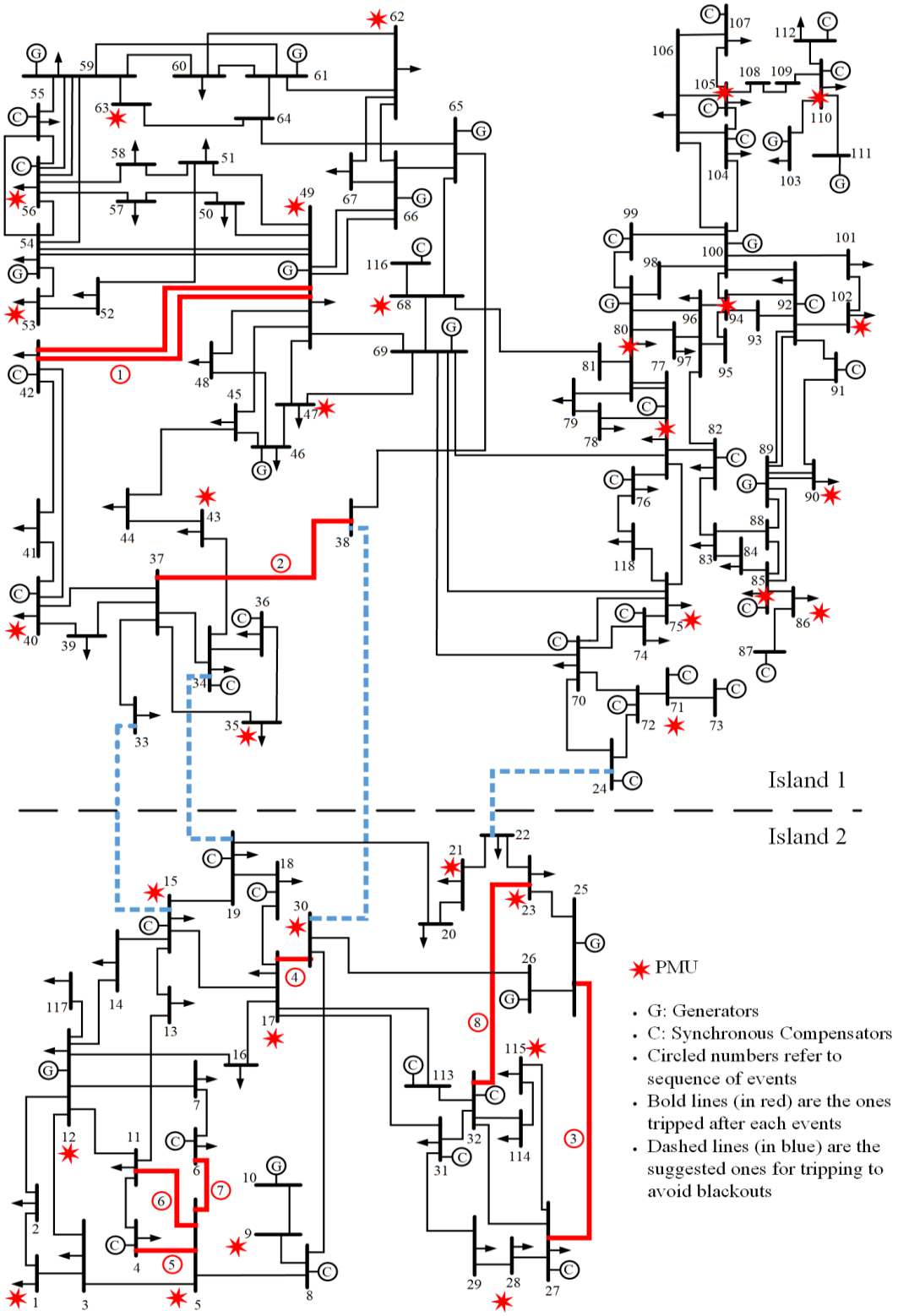

Figure 6.6 Testing ICI tool with IEEE 118-bus test system

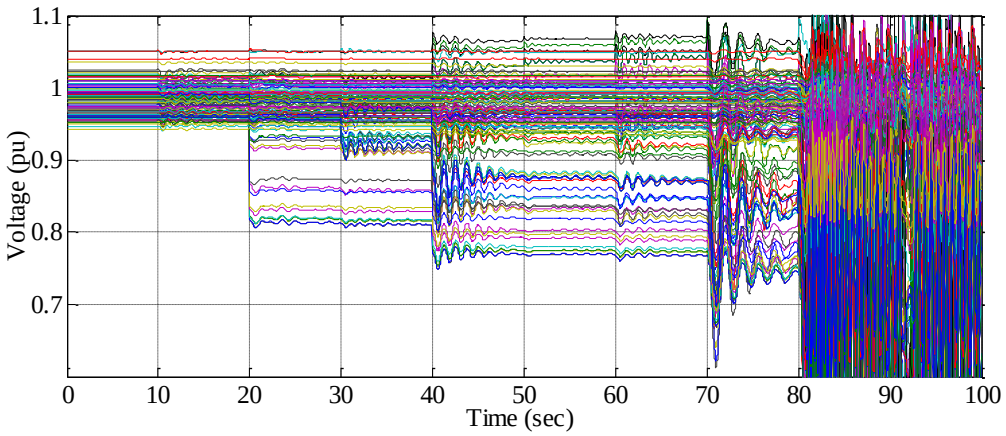

(a)

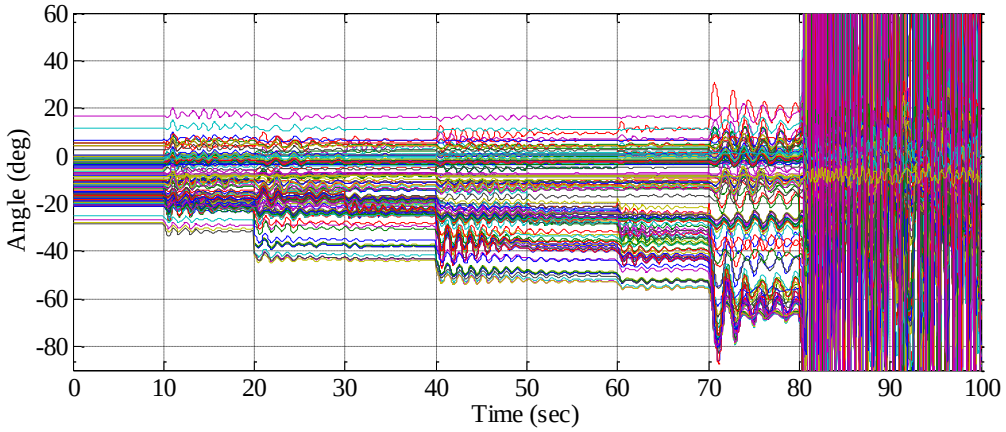

(b)

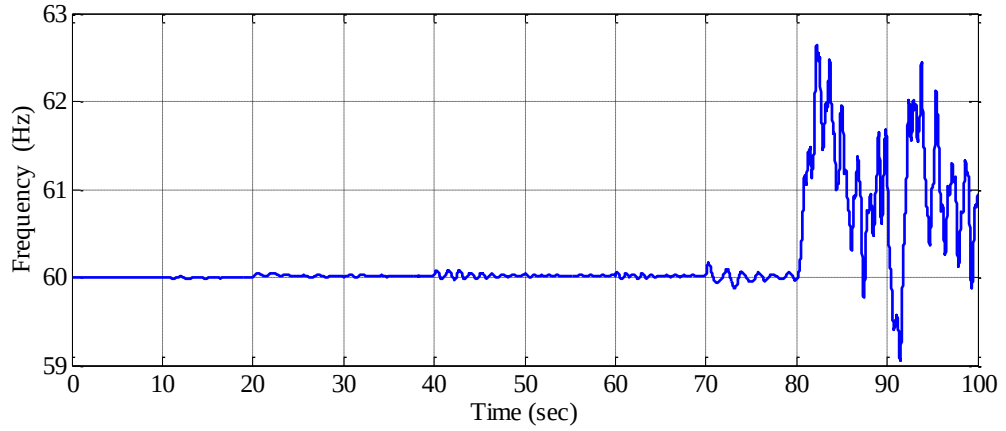

(c)

Figure 6.7 Bus voltage, bus angle and frequency of system during cascade outages-without controlled islanding scheme

6.6.2 Controlled Islanding Scheme

After several outages occurred, the controlled islanding scheme is triggered to determine the switching actions resulting in a self-sustained islanding solution. In this example, the islanding scheme is triggered after the third outage (line 25-27) occurred.

The generator coherency spectral clustering method determines that generators at buses (10, 12, 25, 26 and 31) form the first coherent group while other generators form the second group. The constraint matrix Q is built using the generator coherency information. The constrained spectral clustering algorithm suggests switching of lines (15-33, 19-34, 23-24 and 30-38) which divides the system into two islands as depicted in Figure 6.6.

Figure 6.8 shows the bus voltage, bus phase angle and frequency of IEEE 118-bus system under cascade outage scenario and following switching lines (15-33, 19-34, 23-24 and 30-38) at t=40 sec. The islanding solution prevents transferring power from island 2 to island 1 through line (38-30), and from island 1 to island 2 through lines (15-33 and 19-34) which avoids overloading of lines (4-5, 5-6, 5-11, 17-30 and 23-25). Comparing Figure 6.7 and Figure 6.8, it is obvious that the proposed islanding solution prevents cascade outages and conserves the system from blackout. In Figure 6.8, the voltage profile of buses 40, 41 and 42 are below 0.8 pu following separation of the system. Further studies prove that shedding load at bus 42 can increase the voltage profile of these buses above 0.8 pu threshold.

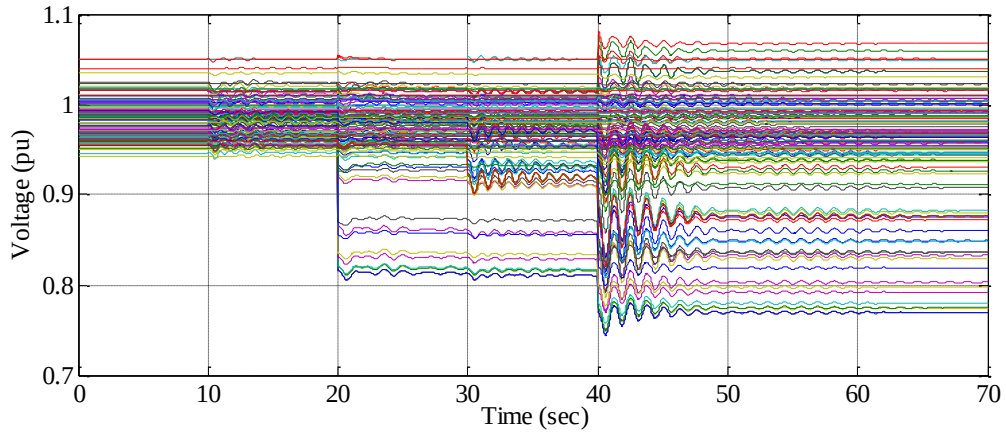

(a)

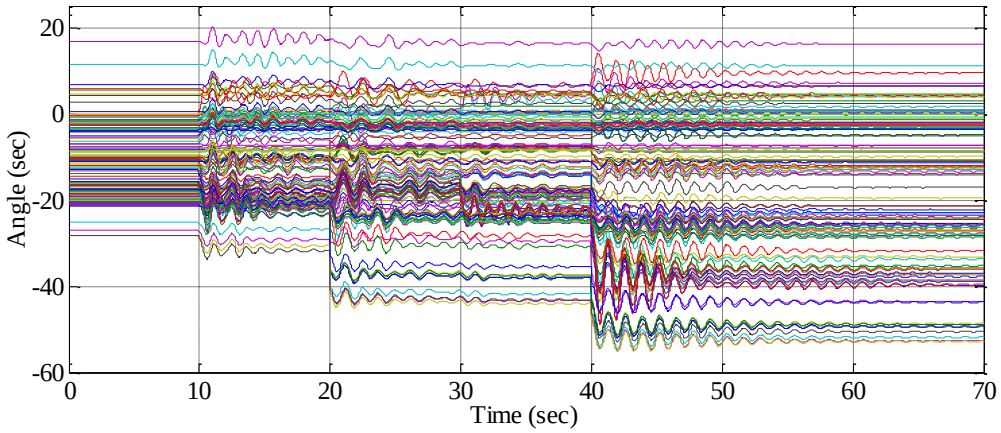

(b)

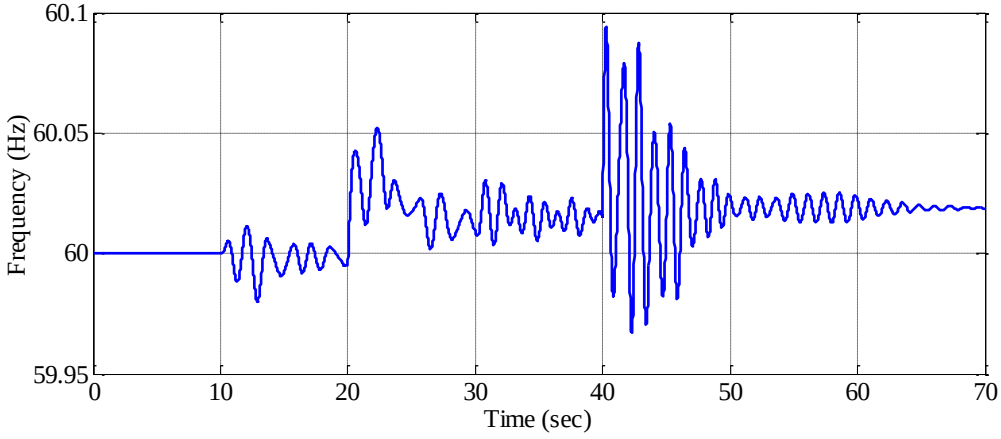

(c)

Figure 6.8 Bus voltage, bus angle and frequency of system equipped with controlled islanding scheme

The relatively small size of IEEE 118 bus system limited the scheme to a handful of scenarios. The additional test results using a real size system have been elaborated in section 7. Table 13 is a summary of results of deploying the proposed scheme for all created scenarios. The amount of load shedding (to maintain voltage profile above 0.8 pu) is much lower than when the controlled islanding scheme is deployed, which verifies the effectiveness of the scheme in preventing blackouts.

TABLE 13 SUMMARY OF SIMULATED CASCADE OUTAGE SCENARIOS

	Scenario_1	**Scenario_2**	**Scenario_3**	**Scenario_4**
Number of islands	2	2	3	3
Switched lines	15-33, 19-34 23-24, 30-38	68-81, 69-77 75-77, 76-77	15-33, 17-31, 19-20 19-34, 23-24 26-30, 30-38	15-33, 19-34, 23-24 30-38, 68-81, 69-77 75-118, 76-77
Load shedding w/o scheme	4242 MW	4242 MW	4242 MW	4242 MW
Load shedding w scheme	96 MW	0 MW	71 MW	33 MW

6.6.3 Computational Efficiency

A successful intentional islanding scheme must be computationally efficient to be applicable to a real size system. Utilizing minimal power imbalance results in Non-deterministic Polynomial-time hard (NP-hard) problems. The computational solution time of NP-hard problems grows in an exponential order [139]. In the proposed method, minimal power flow disruption is used as objective function, which can be solved in polynomial time order [139], [140]. The required run time of the presented scheme using

MATLAB R2016b for the two test systems are shown in Table 14. Simulations are executed using Windows 7, Intel(R) Xeon(R) 3.2GHz CPU, 12GB RAM PC.

TABLE 14 PROPOSED METHOD EXECUTION TIME

Test Systems	**IEEE 9-bus system**	**IEEE 118-bus system**
Execution Time (s)	<0.001	0.073

6.7 Conclusion

In this section, a constrained spectral k-embedded clustering method [136], [137] to obtain a viable solution for intentional (controlled) islanding problem is proposed. The proposed tool can reduce time and complexity of islanding re-connection process, create stable islands using generator coherency data and minimize the amount of load shedding by minimizing power flow disruption across islands' boundaries. The tool has been tested using few cascading outage scenarios and its fast and accurate performance has been verified. The tool, if utilized by the operators controlling the power system, could be a last resort to rescue power system from state of blackouts.

7. TESTING METHODOLOGY USING LARGE NETWORK

7.1 Test System

In this section a cascading outage scenario is studied on the 1354-buses European transmission system [141], [142] as shown in Figure 7.1. This system accurately represents part of the European high voltage transmission network. The network contains 1354-buses, 260 generators, and 1,991 branches and it operates at 380 and 220 kV.

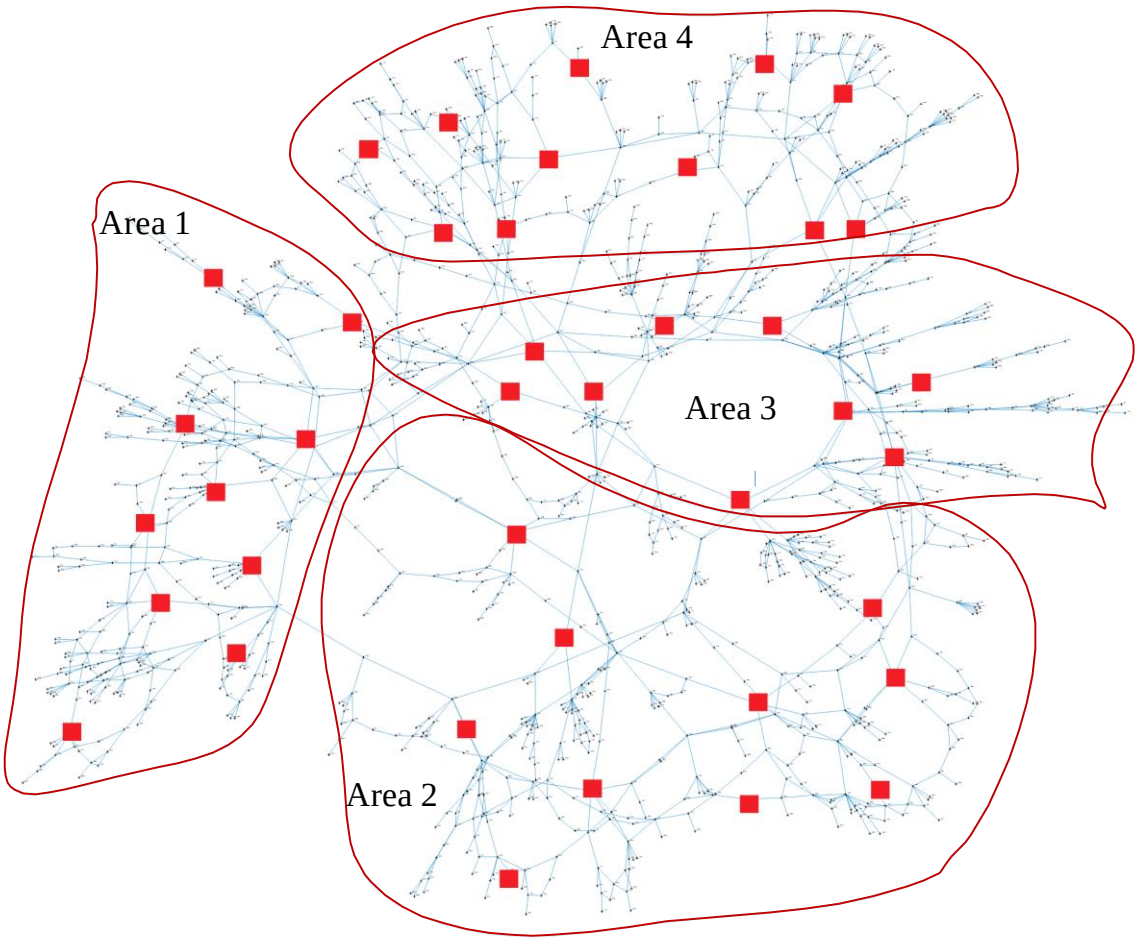

Figure 7.1 1354-bus European high voltage transmission network

The data stems from the Pan European Grid Advanced Simulation and State Estimation (PEGASE) project, part of the 7th Framework Program of the European Union [143]. In this study, 40 PMUs are placed in the system as shown in Figure 7.1.

7.2 Full Scale Synchrophasor Testbed

Figure 7.2 shows the TAMU synchrophasor testbed environment used to perform the testing. The power system is modeled in RT-LAB and events are simulated in OPAL-RT simulator. PMU measurements from 40 locations as shown in Figure 7.1 are transferred through substation PDCs and communication channels to the control center PDC. The measurements are archived in PI historian server. GE software solution is used to visualize the measurements. A cascading outage scenario has been studied next.

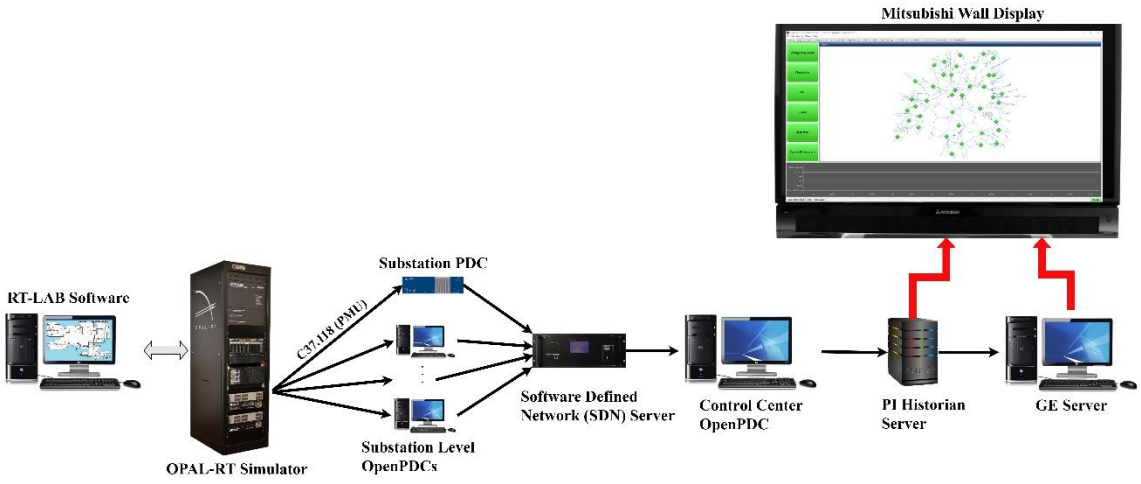

Figure 7.2 TAMU synchrophasor testbed

7.3 Test Results Before Utilization of the Proposed Tools

Figures 7.3 to 7.6 show the voltage profile captured by PMU units in four areas of the system defined in Figure 7.1. The cascading events started with several independent outages that has occurred between t=20 sec to t=40 sec. As a result, the security margin of the system has decreased. Several lines overloaded in the boundaries of area 1 and 2 due to load-generation imbalance and change of power flow paths. In the time span of t=40 sec to t=140 sec, several overloaded lines were tripped one after each other making the in-service ones more overloaded until areas 1 and 2 are islanded from the rest of the system. In area 1, load-generation balance along with reactive generation reserve prevents voltage collapse, however power swings and small oscillations continues up to 50 sec after separation of area 1 from the main island (see Figure 7.3).

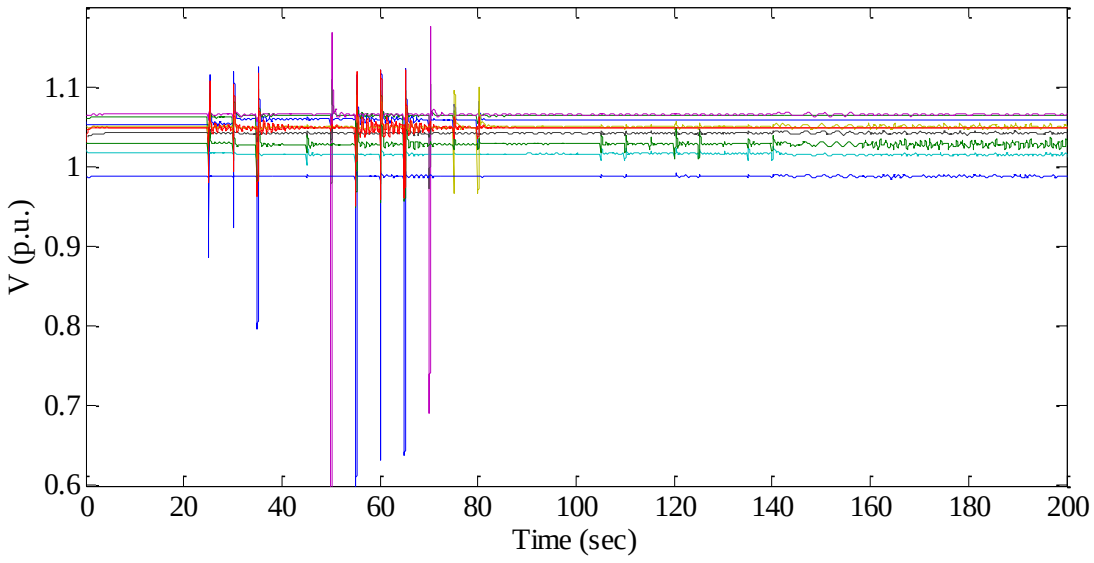

Figure 7.3 Voltage profile of area 1 without proposed tools

Due to excessive loads in area 2, once they are separated from the system, generators in area 2 become over-excited until the over-excitation protective units operate and disconnect several generators. As shown in Figure 7.4, area 2 collapses at around t=160 sec.

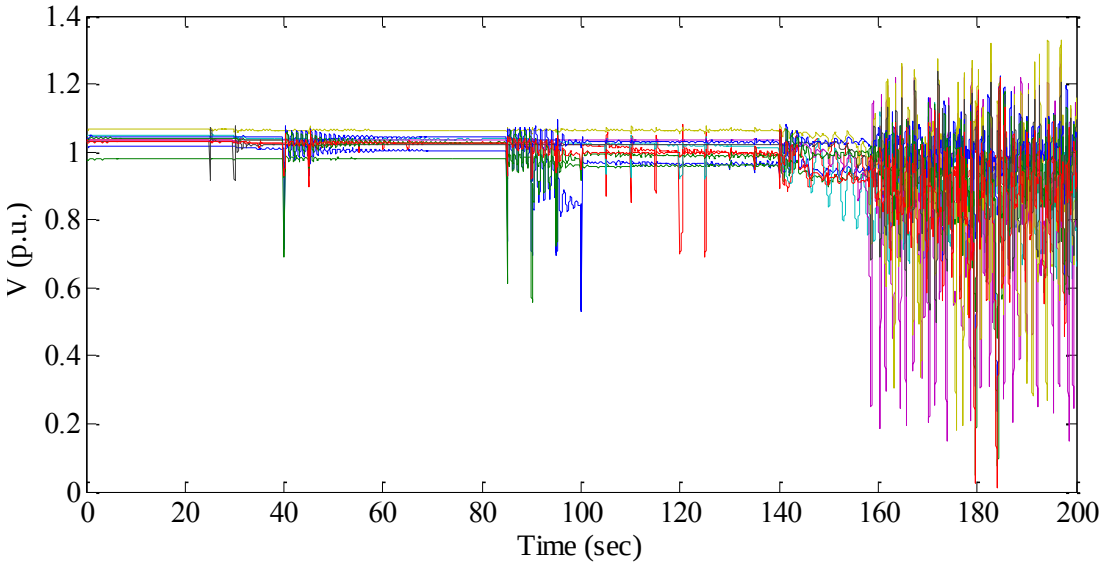

Figure 7.4 Voltage profile of area 2 without proposed tools

Area 3 and 4 remains connected to each other, but experience a non-decaying swing after separation from area 1 and 2 which can be seen in Figure 7.5 and Figure 7.6.

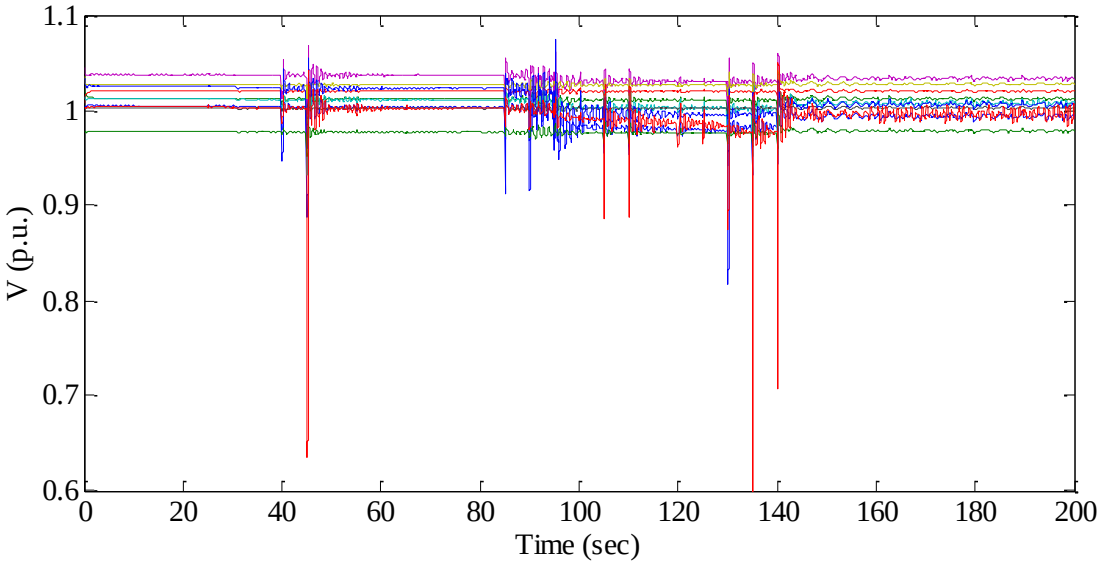

Figure 7.5 Voltage profile of area 3 without proposed tools

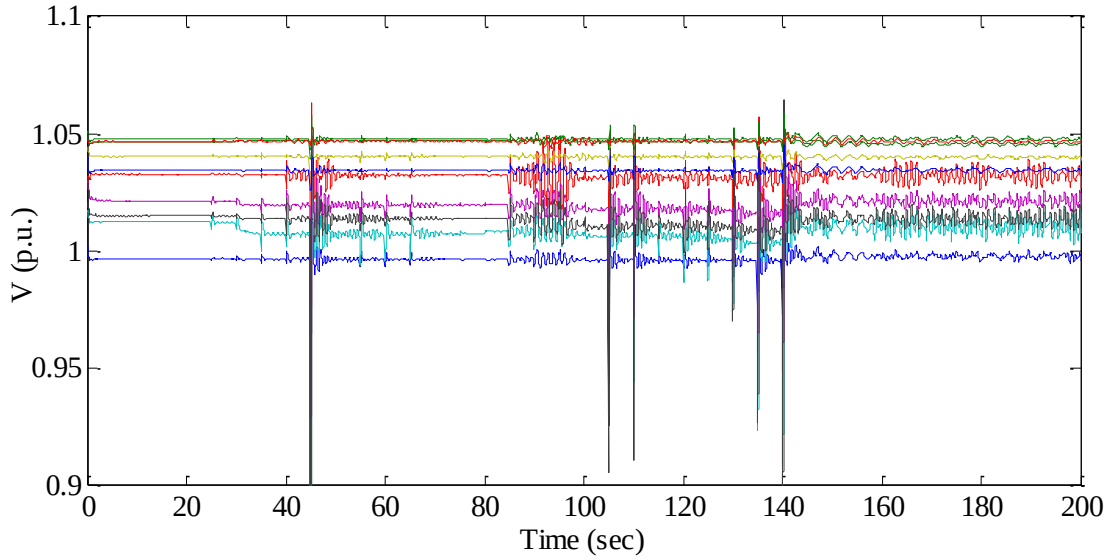

Figure 7.6 Voltage profile of area 4 without proposed tools

7.4 Test Results After Utilization of the Proposed Tools

Figure 7.7 to Figure 7.10 show the voltage profile captured by PMU units in the four areas under the same scenario with deployment of proposed tools. The proposed monitoring tools triggers the ICI tool at t=85 sec.

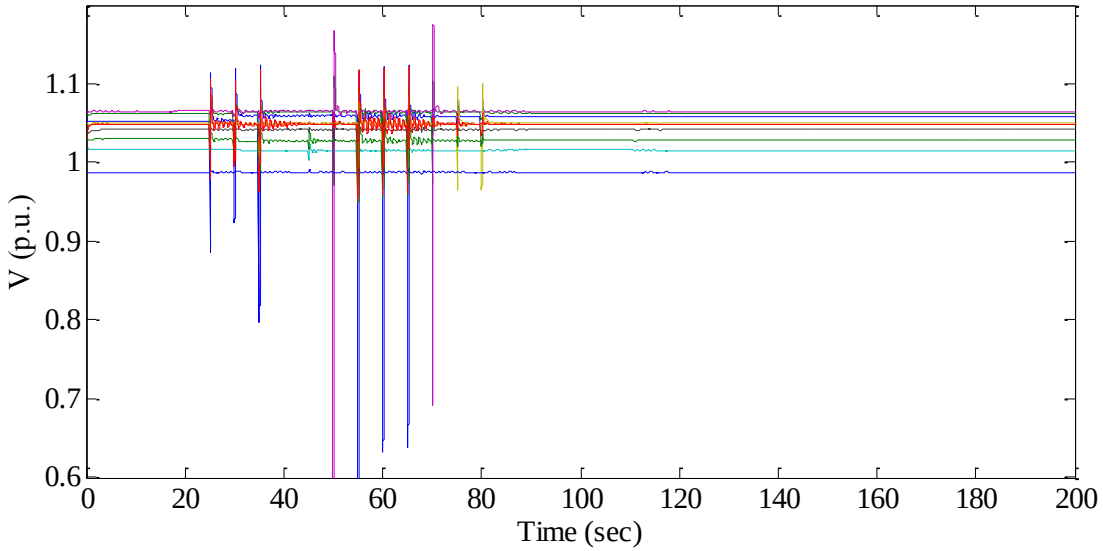

Figure 7.7 Voltage profile of area 1 with proposed tools

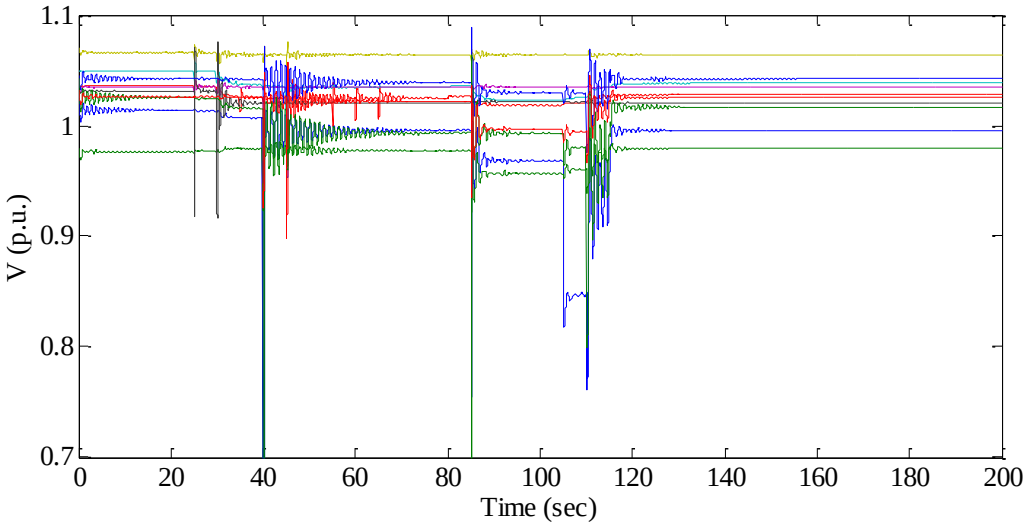

Figure 7.8 Voltage profile of area 2 with proposed tools

Once ICI tool is triggered, several lines are selected to be switched out to create intentional islands. The intentional island includes area 2 and lower part of area 1 in Figure 7.1. Deployment of proposed tools resulted in prevention of cascading outages and area 2 black out. It can be seen from Figure 7.8 that the system oscillations die down after t=160 sec.

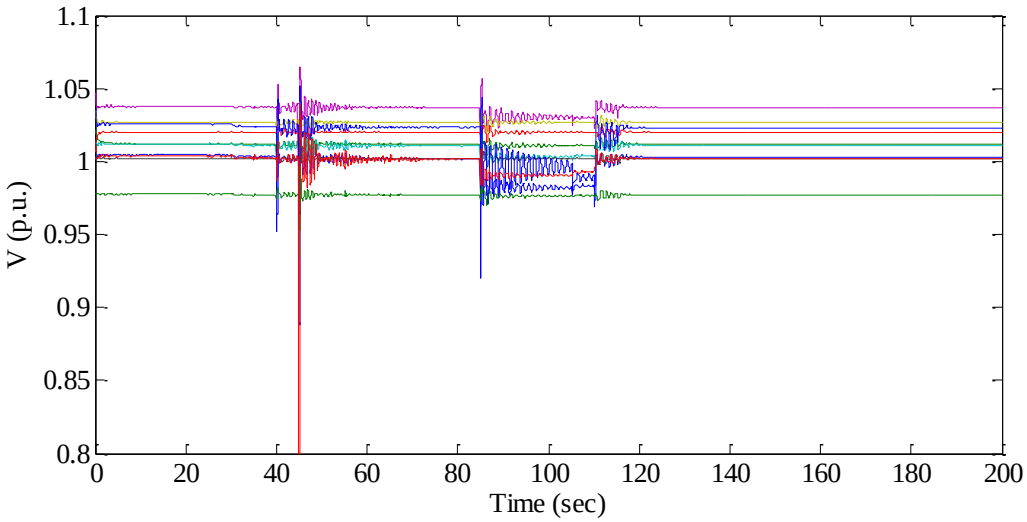

Figure 7.9 Voltage profile of area 3 with proposed tools

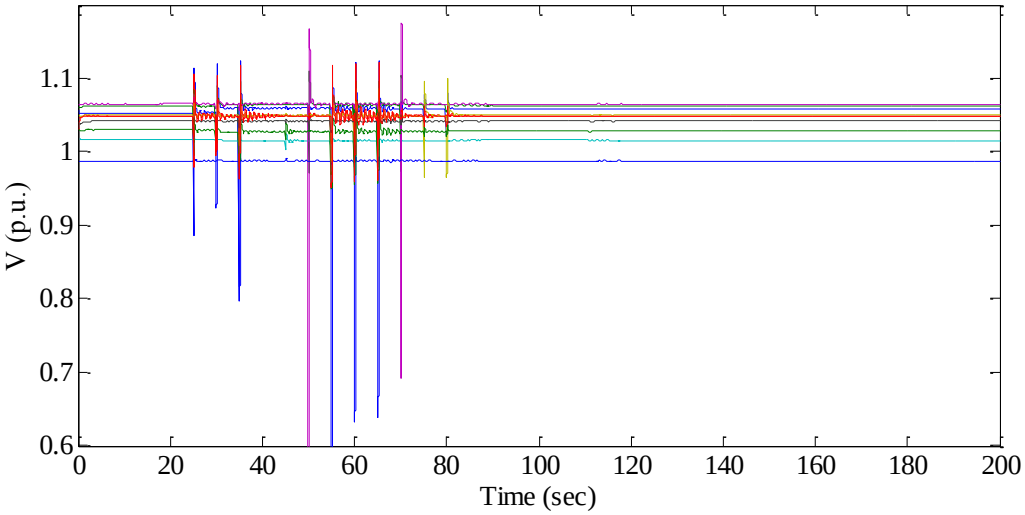

Figure 7.10 Voltage profile of area 4 with proposed tools

7.5 Conclusion

In this section, a real size system has been modeled using the full scale synchrophasor testbed. A realistic cascade outage scenario has been simulated and the system condition has been investigated before and after utilization of the proposed tools. The test results further proved the accuracy and effectiveness of the proposed tools.

The integrated scheme, if utilized in a real power system, could provide powerful means to help operators monitor and arrest cascade outages at early stages and rescue power system from severe blackouts.

8. CONCLUSIONS

The power system cascading outages are complex. Studies have revealed the devastating impacts of cascading outages on economic and social life. Many researchers tried to find a feasible way to detect, prevent and mitigate them. Synchrophasor systems can provide a unique opportunity to detect, prevent and mitigate cascading outages.

In this dissertation several major blackouts in recent decades have been explored to understand mechanisms of cascading outages, their causes and consequences. A set of tools for fast detection and mitigation of cascading outages in power system based on availability of synchrophasor system has been developed and presented.

8.1 Contributions

The main contributions of this dissertation are summarized as follows:

- *Formulation of the mechanism of cascading outages*. This dissertation explored several major cascading blackouts in the world. By investigating the mechanism of cascading outages, it can be concluded that most cascading outages have a few typical stages: normal and alert stages, emergency stage (slow progression of cascade outages) and in extremis stage (fast progression of cascade outages). The normal, alert and emergency stages operators may have enough time to evaluate the system condition, identify some vulnerable contingencies, take some control to increase the security level and prevent the possible cascading blackouts. The in extremis stage requires tools for automated actions since the transient stability collapse needs to be prevented extremely quickly.

- *Development of the online synchrophasor based vulnerability analysis and fault identification methods*. The proposed Synchrophasor based Online Vulnerability Index (SOVI) tool is aimed at providing a comprehensive evaluation for individual components as well as system-wide security situation under different conditions. The importance of each bus and transmission line is taken into account by calculating the vertex and edge betweenness centrality. The Synchrophasor based Online Fault Identification (SOFI) tool is aimed at providing real time information regarding contingencies in the system, which can be used by operator and maintenance crews to expedite the restoration process. These tools can operate together to alarm operator at the early stage of cascading outage.
- *Development of the synchrophasor based islanding prediction method to identify areas prone to formation of un-wanted islands.* The proposed Synchrophasor based Islanding Prediction (SIP) tool consists of an offline part of islanding database creation and ANN training, and an online part where the SIP tool uses the SOVI's outputs and the trained ANN module to predict possibility of islanding cases. A depth of observability method is used to create a reasonable and realistic islanding scenario database. A neural network is trained using MATLAB toolbox to *recognize* areas prone to be separated from the system.
- *Development of the controlled islanding mitigation tool as the last resort to prevent the system blackouts*. The proposed Integrated Controlled Islanding (ICI) tool reduced the complexity and time of re-connection process due to the nature of objective function used in formulations. Definition of objective function based on

minimal power flow disruption also resulted in more stabilized islands. The slow coherency information used as the constraint in optimization process ensure that non-coherent generators are not in the same islands. The spectral k-embedded clustering provides flexibility in the clustering process. Unlike prior studies, this dissertation defined an integrated real time triggering mechanism obtained from several proposed synchrophasor based monitoring modules (SOVI, SOFI and SIP) to enable the ICI mitigation tool at the proper time.

8.2 Advantages of the Proposed Methods

Compared to prior work, the main advantages of this study are:

- The integrated scheme detects disturbances, and provides immediate topology update. So the error caused by divergence of conventional state estimator under some contingency scenarios could be avoided (Alert/Emergency Stages);
- The integrated scheme monitors the system at local and system-wide levels and identifies system vulnerability as indices to be used to automate triggering of SIP and ICI modules at the proper time (Alert/Emergency Stages);
- The integrated scheme identifies unstable areas which are prone to create un-wanted islands, and automatically triggers RAS to prevent such isolations (Emergency Stage);
- The integrated scheme prevents the propagation of cascading outages by intentional separation of the system to minimize the amount of load shedding and to increase transient stability of the created islands (Extreme Stage);

- Due to minimization of power flow across boundaries of intentionally created islands, the integrated scheme allows faster and less complex restoration process (Restoration Stage).

8.3 Suggestion for Future Research

The research described in this dissertation may be continued in the future in the following directions:

- A (hybrid) PMU based state estimation method can be developed to work along with the tools to provide an accurate topology model of the system in real time. With an online state estimation, all states of the system could be available with high accuracy which allows the SOVI tool to be implemented for all buses, lines and generators rather than only the ones equipped with PMUs.
- Other intelligent methods such as the decision tree method can be used instead of the proposed ANN method to explore possibility of performance improvement for the SIP tool. The decision tree analysis has been widely used for different power system applications.
- In this study, depth of observability is used as the constraint to reduce the size of islanding database. Other graph search methods can be explored in order to reduce the computation burden and speed up the offline process.
- All the proposed methods are programmed in MATLAB. They need to be converted to highly efficient programming code using different programming language if the field test is to be applied in the future.

REFERENCES

[1] H. Song, The detection, prevention and mitigation of cascading outages in the power system, College Station: Ph.D. dissertation, Dept. Electrical and Computer Engineering, Texas A&M University, 2006.

[2] C. Pang, Fast detection and mitigation of cascading outages in the power system, College Station: Ph.D. dissertation, Dept. Electrical and Computer Engineering, Texas A&M University, 2011.

[3] U.S.-Canada Power System Outage Task Force, "Final report on the August 14, 2003 blackout in the United States and Canada: Causes and recommendations," [Online] Available: http://www.nerc.com, April 5, 2004.

[4] [Online]. Available: http://www.nerc.com/pa/Stand/Pages/default.aspx.

[5] "Real Power Balancing Control Performance," North American Electric Reliability Corporation (NERC).

[6] "Voltage and Reactive Control," North American Electric Reliability Corporation (NERC).

[7] "Transmission Operations," North American Electric Reliability Corporation (NERC).

[8] "Steady-State and Dynamic System Model Validation," North American Electric Reliability Corporation (NERC).

[9] "System Protection Coordination," North American Electric Reliability Corporation (NERC).

[10] "Transmission System Planning Performance Requirements," North American Electric Reliability Corporation (NERC).

[11] "Emergency Operations," North American Electric Reliability Corporation (NERC).

[12] S. Deng, S. Meliopoulos and T. Mount, "Modeling market signals for transmission adequacy issues: Valuation of transmission facilities and load

participation contracts in restructured electric power systems," Power Systems Engineering Research Center, Feb. 2007.

[13] L. Milli, Q. Qiu and A. G. Phadke, "Risk assessment of catastrophic failures in electric power systems," *International Journal of Critical Infrastructures,* vol. 1, no. 1, pp. 38-63, 2004.

[14] M. Amin and P. F. Schewe, "Preventing Blackouts," *Scientific American Magazine,* pp. 60-61, May 2007.

[15] B. A. Carreras, V. E. Lynch, I. Dobson and D. E. Newman, "Complex dynamics of blackouts in power transmission systems," *Chaos,* vol. 14, no. 3, pp. 643-652, Sept. 2004.

[16] I. Dobson, B. A. Carreras, V. E. Lynch and D. E. Newman, "An initial model for complex dynamics in electric power system blackouts," in *34th Hawaii International Conference on System Sciences (HICSS 2001),* , Maui, Hawaii, 3-6 Jan. 2001.

[17] B. A. Carreras, V. E. Lynch, M. L. Sachtjen, I. Dobson and D. E. Newman, "Modeling blackout dynamics in power transmission networks with simple structure," in *34th Hawaii International Conference on System Sciences (HICSS 2001),* Maui, Hawaii, 3-6 Jan. 2001.

[18] B. A. Carreras, V. E. Lynch, I. Dobson and D. E. Newman, "Dynamics, criticality and self-organization in a model for blackouts in power transmission systems," in *35th Hawaii International Conference on System Sciences(HICSS 2002),* Hawaii, 7-10 Jan. 2002.

[19] B. A. Carreras, V. E. Lynch and I. Dobson, "Dynamical and probabilistic approaches to the study of blackout vulnerability of the power transmission grid," in *37th Annual Hawaii International Conference on System Sciences (HICSS 2004),* Hawaii, 5-8 Jan. 2004.

[20] I. Dobson, B. A. Carreras and D. E. Newman, "A loading-dependent model of probabilistic cascading failure," *Probability in the Engineering and Informational Sciences,* vol. 19, no. 1, pp. 15-32, Jan. 2005.

[21] I. Dobson, B. A. Carreras and D. E. Newman, "A branching process approximation to cascading load-dependent system failure," in *37th Hawaii International Conference on System Sciences (HICSS 2004),* Hawaii, 5-8 Jan. 2004.

[22] H. Ren and I. Dobson, "Using transmission line outage data to estimate cascading failure propagation in an electric power system," *IEEE Transactions on Circuits and Systems Part II,* vol. 55, no. 9, pp. 927-931, Sept. 2008.

[23] I. Dobson, J. Kim and K. R. Wierzbicki, "Testing branching process estimators of cascading failure with data from a simulation of transmission line outages," *Risk Analysis,* vol. 30, no. 4, pp. 650-662, Feb. 2010.

[24] X. Yu and C. Singh, "A practical approach for integrated power system vulnerability analysis with protection failures," *IEEE Transactions on Power Systems,* vol. 19, no. 4, pp. 1811-1820, Nov. 2004.

[25] X. Yu and C. Singh, "Power system reliability analysis considering protection failures," in *IEEE PES Summer Meeting*, Chicago, USA, 21-25 Jul. 2002.

[26] A. G. Phadke, "Hidden failures in electric power systems," *International Journal of Critical Infrastructures,* vol. 1, no. 1, pp. 64-75, 2004.

[27] A. G. Phadke and J. S. Thorp, "Expose hidden failures to prevent cascading outages," *IEEE Computer Applications in Power,* vol. 9, no. 3, pp. 20-23, 1996.

[28] D. C. Elizondo, J. D. L. Ree, A. G. Phadke and S. Horowitz, "Hidden failures in protection systems and their impact on wide-area disturbances," in *IEEE Power Engineering Society Winter Meeting*, Jan./Feb. 2001.

[29] J. Chen, J. S. Thorp and I. Dobson, "Cascading dynamics and mitigation assessment in power system disturbances via a hidden failure model," *International Journal of Electric Power Energy System,* vol. 27, no. 4, pp. 318-326, May 2005.

[30] J. C. Tan, P. A. Crossley and P. G. McLaren, "Application of a wide area backup protection expert system to prevent cascading outages," *IEEE Transactions on Power Delivery,* vol. 17, no. 2, pp. 375-380, Apr. 2002.

[31] Q. Chen, K. Zhu and J. D. McCalley, "Dynamic decision-event trees for rapid response to unfolding events in bulk transmission systems," in *IEEE Porto Power Tech Proceedings*, Porto, Portugal, 10-13 Sept. 2001.

[32] C. C. Liu, "Learning to recognize the vulnerable patterns of cascaded events," EPRI Technical Report, 2007.

[33] C. W. Taylor, D. C. Erickson, K. E. Martin, R. E. Wilson, V. Venkatasubramanian and e. al., "WACS-wide-area stability and voltage control

system: R&D and online demonstration," *Proceedings of the IEEE,* vol. 93, no. 5, pp. 892-906, May 2005.

[34] M. Zima, M. Larsson, P. Korba, C. Rehtanz and G. Andersson, "Design aspects for wide-area monitoring and control systems," *Proceedings of the IEEE,* vol. 93, no. 5, pp. 980-996, May 2005.

[35] J. Bertsch, C. Carnal, D. Karlson, J. McDaniel and K. Vu, "Wide-area protection and power system utilization," *Proceedings of the IEEE,* vol. 93, no. 5, pp. 997-1003, May 2005.

[36] W. R. Lachs, "Area-wide system protection scheme against extreme contingencies," *Proceedings of the IEEE,* vol. 93, no. 5, pp. 1004-1027, May 2005.

[37] I. W. G. C6, "Wide Area Protection and Emergency Control," Technical Report, [Online] Available: http://www.pes-psrc.org, 2002.

[38] M. Begovic, D. Novosel, D. Karlsson, C. Henville, G. Michel and e. al., "Wide area protection and emergency control," *Proceedings of the IEEE,* vol. 93, no. 5, pp. 876-891, May 2005.

[39] F. Hashiesh, H. E. Mostafa, A. Khatib, I. Helal and M. M. Mansour, "An intelligent wide area synchrophasor based system for predicting and mitigating transient instabilities," *IEEE Transactions on Smart Grid,* vol. 3, no. 2, Jun. 2012.

[40] J. Y. Zhang and C. M. Bush, "PMU based islanding detection to improve system operation," in *IEEE Power and Energy Society General Meeting (PESGM)*, Boston, USA, 17-21 Jul. 2016.

[41] T. Xu and T. Overbye, "Real-time event detection and feature extraction using PMU measurement data," in *IEEE International Conference on Smart Grid Communications,* Miami, USA, 2-5 Nov. 2015.

[42] I. Kamwa, R. Grondin and Y. Hebert, "Wide-area measurement based stabilizing control of large power systems-a decentralized/hierarchical approach," *IEEE Transactions Power Systems,* vol. 16, no. 1, pp. 136-153, Feb. 2001.

[43] A. Darvishi and I. Dobson, "Threshold-based monitoring of multiple outages with PMU measurements of area angle," *IEEE Transactions on Power Systems*, vol. 31, no. 3, May 2016.

[44] PSerc Project S29 Final Report- Part I, "Detection, prevention and mitigation of cascading events," PSerc Publication [Online] Available: http://www.pserc.org, Sept. 2008.

[45] PSerc Project S26 Final Report, "Risk of Cascading Outages," PSerc Publication, [Online] Available: http://www.pserc.org, Feb. 2008.

[46] K. Sun and Z. Han, "Analysis and comparison on several kinds of models of cascading failure in power system," in *IEEE/PES Transmission and Distribution Conference and Exposition: Asia and Pacific*, Dalian, China, 14-18 Aug 2005.

[47] P. Hines, J. Apt and S. Talukdar, "Large blackouts in North America: Historical trends and policy implications," *Energy Policy*, vol. 37, no. 12, pp. 5249-5259, Dec. 2009.

[48] M. Amin, "North America's electricity infrastructure: are we ready for more perfect storms?," *IEEE Security & Privacy*, pp. 19-25, Sept./Oct. 2003.

[49] B. Carreras, D. E. Newman, I. Dobson and A. B. Poole, "Initial evidence for self-organized criticality in electric power blackouts," in *33rd Hawaii International Conference on System Sciences*, Maui, Hawaii, Jan. 2000.

[50] B. Carreras, D. Newman, I. Dobson and A. Poole, "Evidence for self organized criticality in a time series of electric power system blackouts," *IEEE Trans. Circuits & Systems I*, vol. 51, no. 9, pp. 1733-1740, Sept. 2004.

[51] J. Simonoff, C. Restrepo and R. Zimmerman, "Risk-management and risk-analysis-based decision tools for attacks on electric power," *Risk Analysis*, vol. 27, no. 3, pp. 547-570, 2007.

[52] R. Weron and I. Simonsen, Blackouts, risk, and fat-tailed distributions, in Practical Fruits of Econophysics, Springer-Tokyo, 2005.

[53] I. T. Force, " on Understanding, Prediction, Mitigation and Restoration of Cascading Failures, "Risk assessment of cascading outages: Part I – Overview of methodologies," in *IEEE Power and Energy Society General Meeting*, Detroit, MI, USA, July 2011.

[54] X. Weng, Y. Hong, A. Xue and S. Mei, "Failure analysis on China power grid based on power law," *Journal of Control Theory and Applications,* vol. 4, no. 3, pp. 235-238, Aug. 2006.

[55] A. J. Holmgren and S. Molin, "Using disturbance data to assess vulnerability of electric power delivery systems," *Journal of Infrastructure Systems,* vol. 12, no. 4, pp. 243-251, Dec. 2006.

[56] J. Bakke, A. Hansen and J. Kertesz, "Failures and avalanches in complex networks," *Europhysics Letters,* vol. 76, no. 4, pp. 717-723, 2006.

[57] Q. Chen, Risk Management of Cascading Failure in Composite Reliability of a Deregulated Power System with Microgrids, Falls Church, Virginia: Virginia Polytechnic Institute and State University, Dec. 2013.

[58] "Report on the Grid Disturbances on 30th July and 31st July 2012," Central Electricity Regulatory Commission India, India, 2012.

[59] "Arizona-Southern California Outages on Spetember 8, 2011 - Causes and Recommendations," Federal Energy Regulatory Commission and North American Electric Reliability Corporation, 2012.

[60] Y. Wang, Security of Electric Power Systems: Cascading Outage Analysis, Interdiction Model and Resilience to Natural Disasters, Texas, USA: The University of Texas at Austin, 2015.

[61] "Report of the National Grid Investigation into the Frequency Deviation and Automatic Demand Disconnection that occured on the 27th May 2008.," National Grid, UK, 2009.

[62] "Final Report on System Disturbance on 4 November 2006.," UCTE, 2007.

[63] E. Johansson, K. Uhlen, A. Nybø, G. Kjølle and O. Gjerde, "Extraordinary events: Understanding sequence, causes, and remedies," in *European Safety and Reliability Conference (ESREL),* , 5-9 Sept. 2010.

[64] P. Henneaux, J. Song and E. Cotilla-Sanchez, "Enhancing test power systems for dynamic cascading outage simulations," in *2nd IEEE Conference on Technologies for Sustainability (SusTech),* 2014.

[65] F. Aminifar, M. Fotuhi-Firuzabad, A. Safdarian, A. Davoudi and M. Shahidehpour, "Synchrophasor Measurement Technology in Power Systems: Panorama and State-of-the-Art," *IEEE Access*, vol. 2, pp. 1607-1628, 2014.

[66] "north american synchrophasor initiative," [Online]. Available: www.naspi.org.

[67] M. Vaiman, P. Hines, J. Jiang, S. Norris, M. Papic, A. Pitto, Y. Wang and G. Zweigle, "Mitigation and prevention of cascading outages: Methodologies and practical applications," in *IEEE Power and Energy Society General Meeting*, Vancouver, Canada, July 2013.

[68] J. H. Chow, Time-Scale Modeling of Dynamic Networks with Applications to Power Systems, New York: Springer- Verlag, 1982.

[69] J. Zhu, Power system applications of graph theory, New York: Nova Science Publishers, Inc., 2009.

[70] D. Fay, H. Haddadi, A. Thomason, A. W. Moore, R. Mortier, A. Jamakovic, S. Uhlig and M. Rio, "Weighted spectral distribution for internet topology analysis: theory and applications," *IEEE/ACM Transactions on Networking*, vol. 18, no. 1, pp. 164-176, Feb. 2010.

[71] S. Pemmaraju and S. Skiena, Computational Discrete Mathematics: Combinatorics and Graph Theory with Mathematica, New York: Cambridge Univ. Press, 2003.

[72] X. L. Huang and B. Bensaou, "On max-min fairness and scheduling in wireless ad-hoc networks: analytical framework and implementation," in *In Proceedings of the 2nd ACM international symposium on Mobile ad hoc networking & computing*, New York, NY, USA, 2001.

[73] J. R. Bettman, "A graph theory approach to comparing consumer information processing models," *Management Science*, vol. 18, pp. 114-128, 1971.

[74] J. A. Barnes, "Graph theory and social networks: A technical comment on connectedeness and connectivity," *Sociology*, vol. 3, no. 2, pp. 215-232, 1969.

[75] S. M. Wagner and N. Neshat, "Assessing the vulnerability of supply chains using graph theory," *International Journal of Production Economics*, vol. 126, no. 1, pp. 121-129, July 2010.

[76] L. H. Hsu and C. K. Lin, Graph Theory and Interconnection Networks, RC PR Inc, 2008.

[77] T. H. Lee, D. H. Thorne and E. F. Hill, "A transportation method for economic dispatching - application and comparison," *IEEE Transactions on Power Apparatus and Systems,* Vols. PAS-99, no. 6, pp. 2373-2385, Nov. 1980.

[78] P. Hines and S. Blumsack, "A centrality measure for electrical networks," in *41st Hawaii International Conference on System Sciences*, Hawaii, Jan. 2008.

[79] A. E. Motter and Y.-C. Lai, "Cascade-based attacks on complex networks," *Physical Review E,* vol. 66, 2002.

[80] G. N. Korres and P. Katsikas, "A hybrid method for observability analysis using a reduced network graph theory," *IEEE Transactions on Power Systems,* vol. 18, no. 1, pp. 295-304, Feb. 2003.

[81] N. Liu, J. Zhang, H. Zhang and W. Liu, "Security assessment for communication networks of power control systems using attack graph and MCDM," *IEEE Transactions on Power Delivery,* vol. 25, no. 3, pp. 1492-1500, July 2010.

[82] D. Dustegor, S. V. Poroseva, M. Y. Hussaini and S. Woodruff, "Automated graph-based methodology for fault detection and location in power systems," *IEEE Transactions on Power Delivery,* vol. 25, no. 2, pp. 638-646, April 2010.

[83] L. C. Freeman, "A set of measures of centrality based on betweenness," *Sociometry,* vol. 40, pp. 35-41, 1977.

[84] T. Athay, R. Podmore and S. Virmani, "A Practical Method for the Direct Analysis of Transient Stability," *IEEE Transactions on Power Apparatus and Systems,* Vols. PAS-98, no. 2, pp. 573-584, March/April 1979.

[85] R. D. Zimmerman, C. E. Murillo-Sanchez and R. J. Thomas, "MATPOWER: Steady-State Operations, Planning and Analysis Tools for Power Systems Research and Education," *IEEE Transactions on Power Systems,* vol. 26, no. 1, pp. 12-19, Feb. 2011.

[86] J. S. Thorp and e. al., "Electromechanical wave propagation in large electric power systems," *IEEE Transactions on Circuits and Systems I: Fundamental Theory and Applications,* vol. 45, pp. 614-622, 1998.

[87] A. Semlyen, "Analysis of disturbance propagation in power systems based on a homogeneous dynamic model," *IEEE Transactions on Power Apparatus and Systems,* Vols. PAS-93, pp. 676-684, 1974.

[88] A. J. Arana, Analysis of electromechanical phenomena in the power-angle domain, Blacksburg, Virginia, USA: Ph.D. dissertation, Virginia Polytechnic Institute and State University, Dec. 2009.

[89] M. Parashar and e. al., "Continuum modeling of electromechanical dynamics in large-scale power systems," *IEEE Transactions on Circuits and Systems I: Regular Papers,* vol. 51, pp. 1848-1858, 2004.

[90] A. Esmaeilian and M. Kezunovic, "Testbed study of electromechanical wave propagation impacts on protective devices," in *International Conference on Power Systems Transients (IPST 2015)*, Croatia, Jun. 15-18 2015.

[91] A. Esmaeilian and M. Kezunovic, "Impact of electro-mechanical wave oscillations propagation on protection schemes," *Electric Power System Research,* vol. 138, pp. 85-91, Sept. 2016.

[92] A. Esmaeilian and M. Kezunovic, "Fault location using sparse synchrophasor measurement of electromechanical wave oscillations," *IEEE Transactions on Power Delivery,* vol. 31, no. 4, pp. 1787-1796, Aug. 2016.

[93] E. W. Dijkstra, "A note on two problems in connexion with graphs," *Numerische Mathematik,* vol. 1, no. 1, pp. 269-271, Dec. 1959.

[94] U. Rudez and R. Mihalic, "A Method of Detecting the Time of Arrival for an Electromechanical Wave in Large Power Systems," in *2013 IEEE PowerTech (POWERTECH)*, Grenoble, 16-20 June 2013.

[95] U. Rudez and R. Mihalic, "Understanding the Electromechanical Wave Propagation Speed," in *2013 IREP Symposium-Bulk Power System Dynamics and Control –IX (IREP*, Rethymnon, Greece, August 25-30, 2013.

[96] D. K. Ranaweera, "Comparison of neural network models for fault diagnosis of power systems," *Electric Power Systems Research,* vol. 29, pp. 99-104, 1994.

[97] A. Abdullah and e. al., "Test Bed for Cascading Failure Scenarios Evaluation," in *IPST 2013*, Vancouver, Canada, Jul 2013.

[98] R. Christie, " Power System Test Archive," Aug. 1999. [Online]. Available: http://www.ee.washington.edu/research/pstca.

[99] S. Azizi, A. Dobakhshari, A. N. Sarmadi and A. M. Ranjbar, "Optimal PMU Placement by an Equivalent Linear Formulation for Exhaustive Search," *IEEE Transactions on Smart Grid,* vol. 3, no. 1, Mar. 2012.

[100] R. Sun, "Wide Area Power System Islanding Detection, Classification and State Evaluation Algorithm," irginia Polytechnic Institute and State University, Blacksburg, Virginia, 2012.

[101] M. Zhou, V. A. Centeno, A. G. Phadke, Y. Hu, D. Novosel and H. Volskis, "A preprocessing method for effective PMU placement studies," in *Third International Conference on Electric Utility Deregulation and Restructuring andPower Technologies*, April 2008.

[102] A. Galushkin, Neural Network Theory, New York: Springer, 2007.

[103] M. Delimar, I. Pavic and Z. Hebel, "Artificial neural networks in power system topology recognition," in *Computer as a Tool in EUROCON*, 2003.

[104] N. Amjady and M. Ehsan, "Evaluation of power systems reliability by an artificial," *IEEE Transactions on Power Systems,* vol. 14, no. 1, pp. 287-292, 1999.

[105] M. Wu and P. Rastgoufard, "Optimum decision by artificial neural networks for reactive power control equipment to enhance power system stability and security performance," in *IEEE Power Engineering Society General Meeting*, 2004.

[106] M. Oleskovicz, D. V. Coury and A. C. d. Carvalho, "Artificial neural network applied to power system protection," in *5th Brazilian Symposium on Neural Networks*, 1998.

[107] A. S. Bretas and A. G. Phadke, "Artificial neural networks in power system," *IEEE Transactions on Power Delivery,* vol. 18, no. 4, pp. 1181-1186, 2003.

[108] D. Wenjin and W. Ping, "Application of Pattern Recognition and Artificial Neural Network to Load Forecasting in Electric Power System," in *Third International Conference on Natural Computation*, 2007.

[109] Z. Qin, J. Davidson and A. A. Fouad, "Application of artificial neural networks in power system security and vulnerability assessment," *IEEE Transactions on Power Systems,* vol. 9, no. 1, pp. 525-532, 1994.

[110] C. Jensen, M. El-Sharkawi and R. Marks, "Power System Security Assessment Using Neural Networks: Feature Selection Using Fisher Discrimination," *IEEE Power Engineering Review,* vol. 21, no. 10, 2001.

[111] [Online]. Available: https://www.opal-rt.com/.

[112] A. Atputharajah and T. K. Saha, "Power system blackouts - literature review," in *International Conference on Industrial and Information Systems (ICIIS)*, Sri Lanka, 28-31 Dec. 2009.

[113] H. Song and M. Kezunovic, "A new analysis method for early detection and prevention of cascading events," *Electric Power Systems Research,* vol. 77, no. 2, pp. 1132-1142, 2007.

[114] R. Baldick, B. Chowdhury, I. Dobson, D. Zhaoyang, G. Bei, D. Hawkins and e. al., "Initial review of methods for cascading failure analysis in electric power transmission systems," in *in: Proceedings of the IEEE PES General Meeting*, Pittsburgh, PA, USA, Jul. 2008.

[115] B. Yang, V. Vittal and G. T. Heydt, "Slow-Coherency-Based Controlled Islanding-A Demonstration of the Approach on the August 14, 2003 Blackout Scenario," *IEEE Transactions on Power Systems,* vol. 21, no. 4, pp. 1840-1847, Nov. 2006.

[116] V. Vittal, W. Kliemann, Y. Ni, D. G. Chapman, A. D. Silk and D. J. Sobajic, "Determination of generator groupings for an islanding scheme in the Manitoba hydro system using the method of normal forms," *IEEE Transactions on Power Systems,* vol. 13, no. 4, pp. 1345-1351, Nov. 1998.

[117] J. Jung, C. C. Liu, S. L. Tanimoto and V. Vittal, "Adaptation in load shedding under vulnerable operating conditions," *IEEE Transactions on Power Systems,* vol. 17, no. 4, pp. 1199-1205, Nov. 2002.

[118] H. You, V. Vittal and Z. Yang, "Self-healing in power systems: an approach using islanding and rate of frequency decline-based load shedding," *IEEE Transactions on Power Systems,* vol. 18, no. 1, pp. 174-181, Feb. 2003.

[119] H. You, V. Vittal and X. Wang, "Slow coherency-based islanding," *IEEE Transactions on Power Systems,* vol. 19, no. 1, pp. 483-491, Feb. 2004.

[120] K. Sun, D. Zheng and Q. Lu, "Splitting strategies for islanding operation of large-scale power systems using OBDD-based methods," *IEEE Transactions on Power Systems,* vol. 18, no. 2, pp. 912-923, May 2003.

[121] Q. Zhao, K. Sun, D. Zheng, J. Ma and Q. Lu, "A study of system splitting strategies for island operation of power system: a two-phase method based on OBDDs," *IEEE Transactions on Power Systems,* vol. 18, no. 4, pp. 1556-1565, Nov. 2003.

[122] H. Li, G. W. Rosenwald, J. Jung and C.-C. Liu, "Strategic Power Infrastructure Defense," *Proceedings of the IEEE,* vol. 93, pp. 918-933, 2005.

[123] A. Peiravi and R. Ildarabadi, "A Fast Algorithm for Intentional Islanding of Power Systems Using the Multilevel Kernel k-Means Approach," *Journal of Applied Sciences,* vol. 9, pp. 2247-2255, 2009.

[124] L. Liu, W. Liu, D. A. Cartes and I. Y. Chung, "Slow coherency and angle modulated particle swarm optimization based islanding of large-scale power systems," *Advanced Engineering Informatics,* vol. 23, no. 1, pp. 45-56, 2009.

[125] [Online]. Available: https://en.wikipedia.org/wiki/Laplacian_matrix .

[126] M. A. M. Ariff and B. C. Pal, "Coherency identification in interconnected power system -An independent component analysis approach," *IEEE Transactions on Power Systems,* vol. 28, no. 2, May 2013.

[127] C. Juarez, A. R. Messina, R. Castellanos and G. Espinosa-Perez, "Characterization of multi-Machine system behavior using a hierarchical trajectory cluster analysis," *IEEE Transactions on Power Systems,* vol. 26, no. 3, pp. 972-981, Aug. 2011.

[128] J. H. C. R. A. Date, "Aggregation properties of linearized two-time-scale power networks," *IEEE Transactions on Circuits and Systems,* vol. 38, no. 7, pp. 720-730, July, 1991.

[129] e. a. W. Price, "Improved dynamic equivalencing software," GE Power Systems Engineering, EPRITR-105 919 Project 2447-02, Dec. 1995.

[130] X. Wang and I. Davidson, "Flexible constrained spectral clustering," in *16th ACM SIGKDD International Conference on Knowledge Discovery and Data Mining*, Washington DC, USA, 2010.

[131] X. Wang, B. Qian and I. Davidson, "On constrained spectral clustering and its applications," *Data Mining and Knowledge Discovery*, pp. 1-29, Sep. 2012.

[132] H. Kuhn and A. Tucker, "Nonlinear programming," *ACM SIGMAP Bulletin*, pp. 6-18, 1982.

[133] [Online]. Available: http://www.mathworks.com/help/stats/kmedoids.html.

[134] L. Ding, F. M. Gonzalez-Longatt, P. Wall and V. Terzija, "Two-step spectral clustering controlled islanding algorithm," *IEEE Transactions on Power Systems*, vol. 28, no. 2, May 2013.

[135] A. Esmaeilian and M. Kezunovic, "Prevention of cascading outages using sparse wide area synchrophasor measurements," in *IEEE PES Innovative Smart Grid Technologies*, Ljubljana, Sloveni, Oct. 2016.

[136] A. Esmaeilian and M. Kezunovic, "Controlled islanding to prevent cascade outages using constrained spectral k-embedded clustering," in *19th Power Systems Computation Conference (PSCC 2016)*, Genoa, Italy, Jun. 2016.

[137] A. Esmaeilian and M. Kezunovic, "Prevention of power grid blackouts using intentional islanding scheme," *IEEE Transactions on Industry Applications*, vol. 53, no. 1, pp. 622 - 629, 2017.

[138] F. Dorfler and F. Bullo, "Kron Reduction of Graphs with Applications to Electrical Networks," *IEEE Transactions on Circuits and Systems*, vol. 60, no. 1, 2013.

[139] A. Sen, P. Ghosh, V. Vittal and B. Yang, "A new min-cut problem with application to electric power network partitioning," *Europian Transactions on Electrical Power* , vol. 19, no. 6, p. 778–797, 2009.

[140] U. V. Luxburg, "A tutorial on spectral clustering," *Statistical Computation*, vol. 17, no. 4, p. 395–416, Dec. 2007.

[141] C. Josz, S. Fliscounakis, J. Maeght and P. Panciatici, "AC power flow data in MATPOWER and QCQP format: iTesla, RTE snapshots, and PEGASE," March 2016. [Online]. Available: arxiv.org/abs/1603.01533.

[142] S. Fliscounakis, P. Panciatici, F. Capitanescu and L. Wehenkel, "Contingency ranking with respect to overloads in very large power systems taking into account uncertainty, preventive and corrective actions," *IEEE Transactions on Power Systems,* vol. 28, no. 4, pp. 4909-4917, 2013.

[143] [Online]. Available: http://www.fp7-pegase.com/.

APPENDIX A - PUBLICATIONS

Journals:

A. Esmaeilian, M. Kezunovic, "Prevention of power grid blackouts using intentional islanding scheme," *IEEE Transactions on Industry Applications*, vol. 53, no. 1, Jan.-Feb. 2017.

A. Esmaeilian, M. Kezunovic, "Impact of electromechanical wave oscillations propagation on protection schemes," *Electric Power Systems Research*, vol. 138, pp. 85-91, Sept. 2016.

A. Esmaeilian, M. Kezunovic, "Fault Location Using Sparse Synchrophasor Measurement of Electromechanical-Wave Oscillations," *IEEE Transactions on Power Delivery*, vol. 31, no. 4, pp. 1787-1796, Aug. 2016.

A. Esmaeilian, T. Popovic, M. Kezunovic, "Transmission line relay mis-operation detection based on time-synchronized field data," *Electric Power Systems Research*, vol. 125, pp.174-183, Aug. 2015.

P. Dutta, A. Esmaeilian, M. Kezunovic, "Transmission-Line Fault Analysis Using Synchronized Sampling," *IEEE Transactions on Power Delivery*, vol. 29, no. 2, Apr. 2014.

Conferences:

M. Kezunovic, A. Esmaeilian, G. Manimaran, A. Mehrizi-Sani, "The use of system in the loop, hardware in the loop, and co-modeling of cyber-physical systems in developing and evaluating smart grid solutions," *50th Hawaii International Conference on System Science (HICCS2017)*, Hawaii, 4-7 Jan. 2017.

M. Kezunovic, A. Esmaeilian, T. Becejac, P. Dehghanian, C. Qian, "Life cycle management tools for synchrophasor systems: Why we need them and what they should entail," *Workshop on Control of Transmission and Distribution Smart Grids (CTDSG 2016)*, Prague, Czech Republic, Oct. 2016.

A. Esmaeilian, M. Kezunovic, "Prevention of cascading outages using sparse wide area synchrophasor measurements," *IEEE PES Innovative Smart Grid Technologies*, Europe (ISGT), Ljubljana, Slovenia, Oct. 2016.

A. Esmaeilian, M. Kezunovic, "Controlled islanding to prevent cascade outages using constrained spectral k-embedded clustering," *19th Power Systems Computation Conference (PSCC 2016)*, Genoa, Italy, Jun. 2016.

M. Kezunovic, P.-C. Chen, A. Esmaeilian, M. Tasdighi, "Hierarchically Coordinated Protection: An Integrated Concept of Corrective, Predictive, and Inherently Adaptive Protection," *CIGRE International Conference on Actual Trends in Development of Power System Relay Protection and Automation*, Sochi, Russia, Jun. 2015.

A. Esmaeilian, M. Kezunovic, "Testbed study of electromechanical wave propagation impacts on protective devices," *International Conference on Power Systems Transients (IPST 2015)*, Croatia, Jun. 15-18 2015.

A. Esmaeilian, M. Kezunovic, "Evaluation of fault analysis tool under power swing and out-of-step conditions," *46th North American Power Symposium (NAPS 2014)*, Pullman, WA, USA, 7-9 Sept. 2014.

M. Kezunovic, T. Popovic, G. Gurrala, P. Dehghanian, A. Esmaeilian, M. Tasdighi, "Reliable implementation of robust adaptive topology control," *47th Hawaii International Conference on System Science (HICSS 2014)*, Hawaii, 6-9 Jan. 2014.

A. Esmaeilian, M. Kezunovic, "An Impedance Based Fault Location Algorithm for Tapped Lines Using Local Measurements," *45th North American Power Symposium (NAPS2013)*, Manhattan, KS, USA, 22-24 Sept. 2013.

A. Abdullah, A. Esmaeilian, G. Gurrala, P. Dutta, T. Popovic, M. Kezunovic, "Test Bed for Cascading Failure Scenarios Evaluation," *International Conference on Power System Transients (IPST 2013)*, Vancouver, Canada, 18-20 Jul. 2013.